Modelling the dynamic behaviour of a rotor nacelle assembly during the installation using a floating vessel
P.H. Bastiaanssen
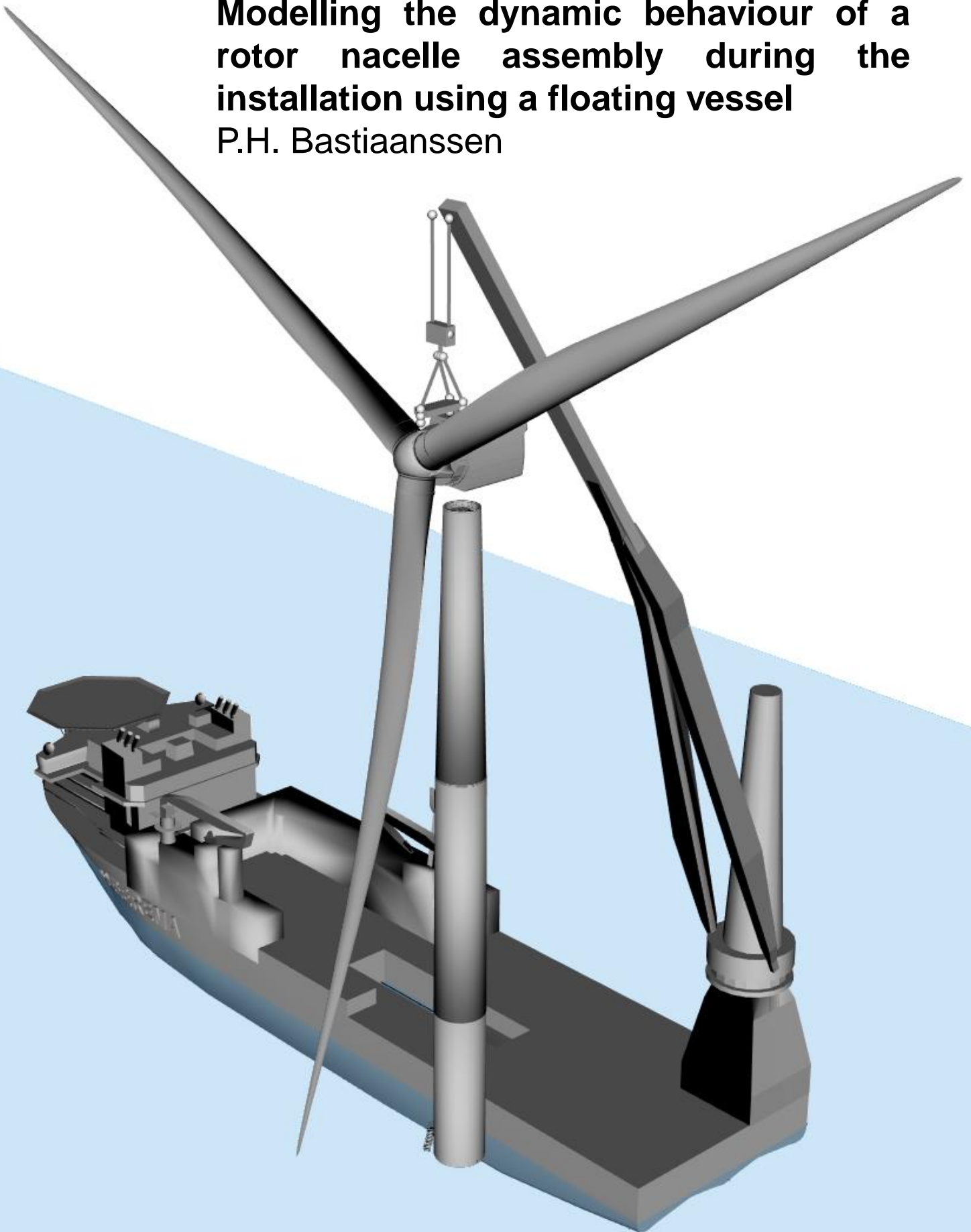
This page is intentionally left blank.

Modelling the dynamic behaviour of a rotor nacelle assembly during installation using a floating vessel

by

P.H. Bastiaanssen

to obtain the degrees

Master of Science
in Offshore and Dredging Engineering
at Delft University of Technology

Master of Science
in Technology - Wind Energy
at Norwegian University of Science and Technology

to be defended on September 23, 2020 at 15.00 h.

Student number:	4373413 (TU Delft)	517527 (NTNU)
Supervision:	Prof. dr. A.V. Metrikine	TU Delft (Chairman)
	Prof. dr. ir. Z. Gao	NTNU
	Dr. ir. B.C. Ummels	TU Delft
	ir. G. Meskers	Heerema Marine Contractors

An electronic version of this thesis is available at `http://repository.tudelft.nl/`.
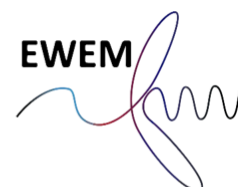
Summary

The offshore wind energy industry has been developing rapidly due to the increasing demand for renewable energy. As a result, offshore wind turbines are increasing in mass and height and are installed at larger water depths and further away from shore. Jack-up vessels can lift themselves above the water, eliminating the influence of the waves on the vessel motions, but are limited by water depth, soil conditions and crane capacity. A floating vessel on the other hand, is not limited by this, but is sensitive to wave-induced motions. Heerema Marine Contractors (HMC) developed a new installation method using a floating vessel, where the rotor nacelle assembly (RNA) of a wind turbine is assembled on an assembly tower on deck and is installed in one lift. In this way the number of critical lifts is changed to one lift, being it a challenging one.

The research objective is to gain a better understanding of the dynamic behaviour of a rotor nacelle assembly, particularly due to the wind, focusing on the horizontal motions of the RNA, when it is hanging in the crane above the tower. To examine the dynamic behaviour of the RNA, separate models are made to assess the effect of the wind and waves individually. This is done to identify which motions are due to the wind, and which motions are due to the waves. Finally, the wind and waves are coupled to gain insight in the coupled response. Furthermore, a case study is performed to prove its applicability for implementing and assessing the effect of using tugger lines on mitigating horizontal motions.

Model 1 − Wind only is performed in OrcaFlex using time domain simulations, in which the effect of wind turbine blade pitch angle, length of the hoist wires and wind speed and wind direction on the RNA response is examined. It is concluded that a 0 deg blade pitch and a short as possible pendulum, result in the smallest motions. The main responses are a pendulum motion in the direction of the wind and a slow yaw motion. Moreover, the RNA responses are significant and can limit the operation. In *Model 2 − Waves only*, frequency domain analyses are performed in Liftdyn to observe the influence of wave conditions and crane configuration on the RNA response. It is shown that head sea and crane pointing to port side yield the smallest motions, while the optimal crane tip height depends on the wave peak period. The main response of the RNA due to waves is a sideward pendulum (in the direction of the waves) coupled with vessel pitch motion. The magnitude of the pendulum motion increases with wave peak period and is significantly larger than wind. In *Model 3 − Wind & Waves* the wind and waves are coupled, performed in OrcaFlex using time domain simulations. It is concluded that wave-induced motions are governing. For short wave peak periods, the vessel pitch and crane tip responses are small and as a result, the RNA sideward pendulum motion as well. For long wave peak periods, the vessel pitch response is excited and thus the crane tip motion is large. Therefore, the RNA sideward pendulum motion is large as well. For both short and long wave peak periods, the horizontal motions have to be mitigated to install the RNA.

In the case study, constraints that represent tugger lines, are implemented to examine the effect on the RNA motions and to assess if the model can be used for developing concepts to reduce the motions. It is shown that providing stiffness in the horizontal plane helps to reduce the sideward pendulum. However, a roll motion of the RNA is still excited. Hence, roll stiffness is added. For long peak periods, the RNA motion has to follow the opposing motion of the crane tip. More research is required to develop a concept that can follow the crane tip for short peak periods and oppose the motion of the crane tip for long wave peak periods, to ultimately reduce the RNA response.

Preface

This master thesis report serves as the final deliverable to complete the European Wind Energy Master and to obtain a degree in Offshore and Dredging Engineering at Delft University of Technology (TU Delt) and Technology - Wind Energy (NTNU) at Norwegian University of Science and Technology. The master thesis was carried out in cooperation with Heerema Marine Contractors.

It has been an amazing journey to get where I am and I would like to thank a number of people that helped me to achieve this. First of all, from TU Delft, the chairman of my graduation committee, Andrei Metrikine, for guiding me to successfully complete this project. Furthermore, I would like to thank my supervisor, Bart Ummels, for our regular meetings and helping me throughout the project. I particularly liked the informal way of our conversations.

From NTNU, I would like to express my sincere gratitude to Zhen Gao. You have guided me from the start of the literature research in Trondheim and you continued helping me out all the way to the end. I especially appreciate your commitment to continue our regular meetings and your support, even though I went back to the Netherlands.

From Heerema Marine Contractors, I want to thank Geert Meskers for providing me the support and guidance to keep me on track. Countless times you have pointed me in the right direction and I enjoyed our discussions. Furthermore, I would like to thank Rieno Graveland for your expertise and advice. I had a great time at the office.

I would like to thank my friends, family and roommates for keeping me motivated, especially during the time we had to work from home and last but not least, I want to thank my fellow students from EWEM for the amazing time and unforgettable trips we made in Copenhagen, Delft and Trondheim.

Piet Bastiaanssen
Rotterdam, September 2020

Contents

List of Tables

List of Figures

List of Symbols

Symbol	Description	Unit
C_d	Drag coefficient	[-]
c	Chord length	[m]
C_l	Lift coefficient	[-]
C_M	Added mass coefficient	[-]
D	Drag, diameter	[kN], [m]
E	Young's modulus	[kN/mm^2]
f	Frequency	[Hz]
f_n	Natural frequency	[Hz]
g	Gravitational acceleration	[m/s^2]
H, h	Height	[m]
H_s	Significant wave height	[m]
I	Mass moment of inertia	[kg·m^2]
L	Lift, length	[kN], [m]
T_n	Natural period	[s]
V_w, V_0, U	Wind speed	[m/s]
α	Angle of attack	[deg]
α	Exponent vertical wind profile	[-]
θ	Inflow angle	[deg]
λ	Wave length	[m]
ρ	Density	[kg/m^3]
φ	Mode shape	[-]
ω	Frequency	[rad/s]

List of Abbreviations

Symbol	Description
CoG	Center of gravity
DP	Dynamic Positioning
DoF	Degree of freedom
HMC	Heerema Marine Contractors
MSL	Mean Sea Level
PSD	Power Spectral Density
RAO	Response Amplitude Operator
RNA	Rotor nacelle assembly
SDA	Significant Double Amplitude
SWL	Safe working load
WTG	Wind Turbine Generator
X (Uppercase)	Global coordinate, Global translational response
RX (Uppercase)	Global rotational response
x (Lowercase)	Local coordinate, Local translational response
Rx (Lowercase)	Local rotational response

<div align="right">1</div>

Introduction

This chapter provides an introduction to the thesis topic that is focusing on modelling the response of a rotor nacelle assembly (RNA) during lifting using a floating vessel and analysing the dynamic behaviour. First, the current offshore wind industry and installation strategies are discussed in sections 1.1 and 1.2. Then, the problem is formulated in section 1.3 and a literature review is performed in section 1.4 to look into the feasibility of using floating vessels to install wind turbine components and how control of the load while lifting is established. Finally, based on this research, the research objective and questions are established and the approach and outline are defined in sections 1.5, 1.6 and 1.7.

1.1. Background

The offshore wind energy industry has been developing rapidly the last decades due to the ever increasing demand for renewable energy. At the end of 2019, Europa has a total installed offshore wind capacity of 22.0 GW, which has increased by seven times the past ten years, as can be seen in Figure 1.1.
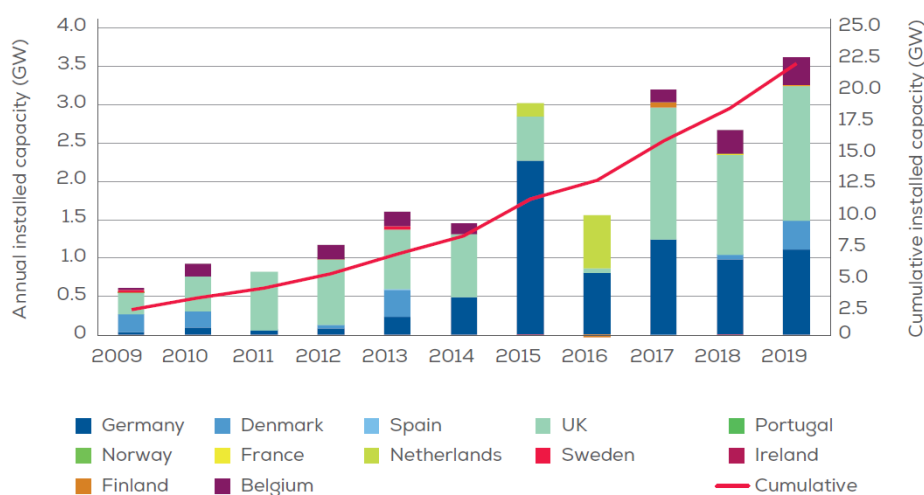
Figure 1.1: Annual offshore wind installations in Europe by country and cumulative capacity (Wind Europe, 2020)

With the increasing installed capacity of offshore wind, the level of technology also advances. This
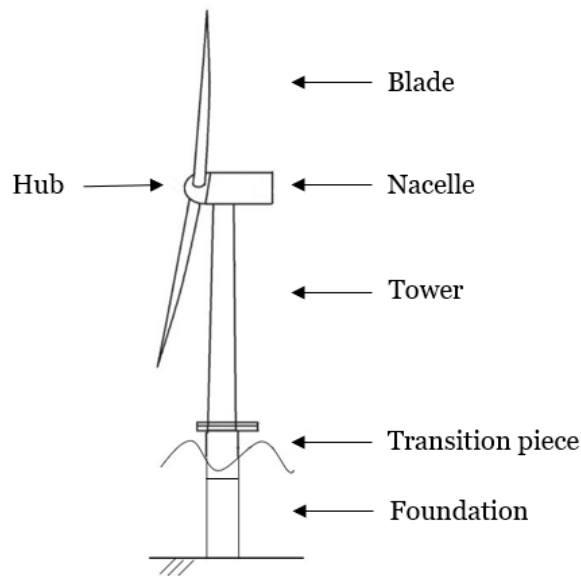
Figure 1.2: Offshore wind turbine components.

results in larger turbines with higher power capacity at larger hub heights. The average installed turbine capacity has increased significantly the last few years, from 3 MW in 2015 to 7.8 MW in 2019 (Wind Europe, 2020). As a consequence of this turbine size increase, along with the increase in turbine height, the foundation increases in size and mass. Furthermore, due to the growing offshore wind projects, these offshore wind farms tend to be located further from shore at larger water depths, where higher and steadier wind speeds prevail, increasing the WTG's size and mass as well. This challenges the industry to design structures capable of withstanding the loads during its lifetime, while still having a cost-efficient design.

1.2. Offshore wind turbine installation

A critical phase during the life cycle of an offshore wind turbine is the transport and installation, which can be up to 20% of the capital expenditures (CapEx) with bottom-founded substructure (Stehly et al., 2016). This is mainly due to the complex operation and harsh environmental offshore conditions. Additionally, with the increasing size and mass of the structure that have to be placed at larger water depths, this challenges the industry even more. It requires installation vessels with larger crane capacity that are able to lift to higher heights. Therefore, a significant cost reduction can be achieved for offshore wind energy by finding innovative solutions. Innovations can be sought in two aspects of offshore installation, the lifting configuration and installation vessel and is discussed in this section.

1.2.1. Lifting configuration

An offshore wind turbine consists of the following main components: nacelle, hub, blades, tower, foundation and, in most designs, the transition piece. These are depicted in Figure 1.2. During installation, these components have to be treated carefully to ensure the structural integrity. A broad spectrum of installation methods exist in the industry to install the turbines that vary in the method of transporting and lifting of the rotor and nacelle. Four methods are briefly described below.

The first and most common method is lifting all components individually. This has the most num-

ber of lifts to be performed, but the lifts are relatively easy. Furthermore, these components can be stacked efficiently on the deck of the installation or feeder vessel, as shown in Figure 1.3. The blades can be installed in different orientations, horizontal and tilted.

The second method is the full rotor lift, where the three blades and hub are pre-assembled on-shore. In this way the number of lifts is reduced and fewer components have to be assembled in the harsh offshore environment, decreasing the installation time. However, this also makes the lift more complicated and fewer components can be transported, as they take up more space, as shown in Figure 1.4.

The third method is the bunny-ear configuration, where the nacelle, hub and two blades are pre-assembled. The nacelle can then be placed on deck, with the two blades pointing upwards, resembling a bunny's head. The third blade is installed in the final lift. This method has not been used over the last years − the last time was during the installation of the prototype of the Haliade 6 MW turbine in 2013 (Fred. Olsen Windcarrier, 2013).

The final method of installing WTG (Wind Turbine Generator) is new and is not considered yet to be feasible for large wind projects. With this method a fully assembled WTG is installed, rotor, nacelle and tower, in one lift, as shown in Figures 1.5 and 1.6. So far this method has only been used for a few demonstration projects. It is not yet feasible because the workability of the operation is expected to be low and not commercially attractive.

Figure 1.3: Bold Tern from Fred. Olsen Wind Carrier (jack-up vessel) with single components (Fred. Olsen Windcarrier).

Figure 1.4: Victoria Matthias from MPI Offshore (jack-up vessel) with pre-assembled rotors on the main deck (Eurogate).

1.2.2. Installation vessel

Currently, a jack-up vessel is the most used vessel to install WTG. It is capable to lift itself out of the sea by putting its legs on the sea bed, eliminating the influence of the waves on the motion of the vessel. This however, is time consuming when it has to move between the foundations. Furthermore, it is susceptible to the environmental conditions when the ship is lifted or lowered, it is limited by soil conditions and water depth (most vessels up to 40-50 m) and it has a limited deck space. Therefore, a jack-up vessel may become less suitable for offshore wind projects in deeper waters.

A floating vessel on the other hand, is not limited by water depth or soil conditions and can quickly move from one foundation to another, showing its logistical flexibility. Furthermore, floating vessels can weather vane continuously in order to reduce the motion. It is however, limited by its responses due to wave-induced motions, which have to be minimised during lifting operations, since high accuracy is required when installation wind turbine components, considering that these components have fragile connection interfaces. Floating vessels use dynamic positioning (DP) or a mooring sys-

tem for station keeping and stability.

Essentially, two floating vessel types exist that can be used in the offshore wind industry, a semi-submersible and a monohull, shown in Figures 1.5 and 1.6, respectively. They both have different hydrodynamic properties, in which the semi-submersible has better stability in waves, while the monohull has an improved sailing speed. Therefore, the semi-submersible would need a feeder system to bring wind turbine components from a feeder vessel when the wind farm is located further offshore, while a monohull can optionally sail back and forth.
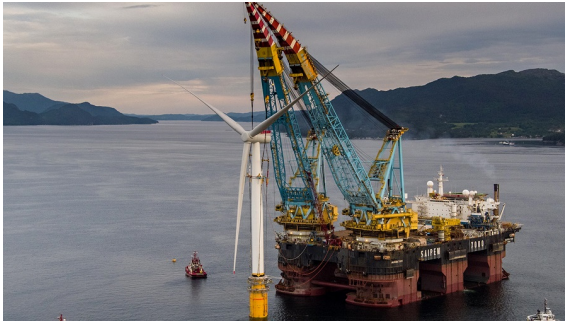
Figure 1.5: Saipem 7000 from Saipem S.p.A. (semi-submersible) installing the Hywind, a floating wind turbine (Timperley, 2017).

Figure 1.6: Aegir from Heerema Marine Contractors (monohull) installing the DOT offshore wind turbine (HMC).

1.3. Problem formulation

With the perspective of the offshore wind energy market, where larger and heavier wind turbines will be placed in deeper waters, floating vessels can play a fundamental role in installing these turbines. By making use of the versatile properties of floating vessels and new installation methods, the installation costs and ultimately the levelised cost of offshore wind can be reduced. This is where Heerema Marine Contractors (HMC) comes into play.

HMC developed a new installation concept, by assembling the nacelle, hub and rotor blades of the WTG on top of a assembly tower that is placed on the deck of the installation vessel. The tower of the WTG is already installed on the foundation. By first placing the nacelle on the assembly tower and then installing the blades one by one, the relative motions between blade and assembly tower are reduced as they are both fixed to the vessel, making the lift significantly less complex. This requires only one more lift to install the full WTG, on top of the lifts required for the tower, comparing to five lifts in case when the components are installed individually on the WTG tower. The lift of the rotor nacelle assembly (RNA) is visualised in Figure 1.7.

With this method, the components can be transported individually and thus the blades can be stacked on top of each other, resulting in efficient use of space. These components can be brought to the offshore site by using barges or the installation vessel itself. This installation method allows for a quick and efficient way to install WTG and can further bring down the cost of installing WTGs.

The RNA lift from the assembly tower to the WTG tower is a complex one. With next generation WTG reaching rotor diameters of up to 220 m, the responses due to environmental conditions can be significant. The crane tip is moving due to the wave-induced motions of the floating vessel, while the wind is acting on the blades. These motions have to be controlled in order to install the RNA without sustaining damage, in a short as possible time frame, while safety is maintained.

Before a clear problem and objective of the thesis can be defined, important aspects that are related to the installation of the RNA are described. Using this description, the scope and approach can be

Figure 1.7: Lifting the RNA from the assembly tower on deck of the installation vessel to the already installed tower.

defined as well.

The RNA that is hanging in the crane, will move due to wind and waves. The important motions of the RNA when placing it on top of a tower are the RNA rigid body motions. These are translations in x, y and z (surge, sway and heave) and rotations around x, y and z (pitch, roll and yaw). Some motions require more attention than others when installing the RNA. The magnitude of the maximum allowed motion depends on the guide and bumper system that is used for the installation. This system provides safe guidance of the RNA by constraining degrees of freedom, eliminating residual motions and providing bolt-hole alignment. Before the RNA is placed on top of the tower, the motions of the RNA need to be monitored first. During this monitoring phase, the RNA is hanging approximately 2.5 m above the tower and as soon as the motions are within the predefined limits, the RNA is lowered onto the tower.

The motions in x and y determine the position of the RNA above the tower in the horizontal plane, while the motion in z determines the vertical position. The pitch and roll angle ensure that the RNA is hanging horizontally sufficiently. Finally, the yaw angle determines the heading control of the RNA and this control should be very accurate, as can be seen in Figure 1.8, where alignment of the bolts and holes must be obtained.

Optimal control of the motions is essential during the installation of the RNA. Therefore, motion compensation is required. For this purpose, different systems are used for compensation of motions

in difference directions and are explained below.

A heave compensation system is used to control the heave motion of the load. The RNA will move in z-direction, due to the wave-induced motions of the vessel. A heave compensation system is able to control the winch of the hoist wire to pay in or pay out the wire to keep the load at a certain position.

The remaining motions (surge, sway, yaw, pitch and roll) are to be controlled, where a pendulum motion in x or y also induces the RNA to pitch and roll, depending on what kind of motions are excited by the vessel and wind.

Figure 1.8: Bolt-hole alignment of the nacelle and tower (Fred. Olsen Wind Carrier, 2017).

1.4. Literature review

Prior to performing this research, a literature study has been conducted to review the current knowledge and research in the field of offshore wind turbine installation with focus on blade installation and installation by floating vessels. The findings from this study are summarised below.

Floating vessels have great potential to be used to install turbines. However, the wave-induced motions of the suspended load can form a problem during lifting operations. Zhao et al. (2019) performed a feasibility study on installing offshore wind turbine blades by floating vessels. In this study both a semi-submersible and monohull's performance are compared to installations by jack-up vessels and it was concluded that it is feasible to use floating vessels to install offshore wind turbines blades, based on vessel performance. It is required however, that the dynamic positioning system mitigates the slowly varying horizontal motions of the vessel due to waves. The feasibility of the installation depends on site specific conditions and vessel parameters and a higher feasibility can be obtained with vessels that respond to small wave frequencies. The semi-submersible has overall better performance than the monohull, because its natural period is well above the upper limit of typical wave periods, caused by the geometry and size of the vessel.

Zhao (2019) established a coupled method to simulate the response of a single blade in the mating phase during installation using floating vessels due to wind and waves. Furthermore, the operational limits during this installation are assessed, taking into account both motion response and structural integrity at the root of the blade. The author concluded that a monohull can install single blades with a wave peak period of up to 7 s, while it is possible for a semi-submersible with a wave peak period of 8 s. Furthermore, the aerodynamic damping of the blade due to its own motion is important for the dynamic response of the blade.

Almost all literature about the installation of wind turbine blades only focuses on single blade installation, not on the lifts of full rotor or bunny ear configuration. Even though the approach taken to model the motions during single blade lifts can also be applied to the modelling of other lifting configurations, there is a big difference. First of all, the mass increases significantly with more blades, the hub and nacelle attached, changing the dynamic behaviour of the load suspended from the crane. Secondly, with more blades the aerodynamic loading increases, leading to different motions due to wind. Finally, when lifting a single blade, the blade is clamped at the centre of gravity (cog), with the centroid of the aerodynamic loading distribution reasonably close to this position, depending on the blade orientation. When lifting a full rotor, the hook is attached at the hub. Hence, this creates large arms to the centroid of the lift and drag distribution of the blades, resulting in large moments. These differences make the lift more complex and have to be accounted for.

Different approaches can be used to model the aerodynamic loading on the blades. The cross-flow principle (Hoerner, 1985) can be used to determine this loading. Zhao (2019) used the cross-flow principle, but also notes that even though this principle provides a good estimation of aerodynamic loads, this is not the case for large yawed inflow angles, based on comparison with CFD analyses. Gaunaa et al. (2014) proposed a simple engineering model that focuses on the first-order aerodynamic and aeroelastic behaviour of a single blade during installation using the cross-flow principle. An improvement is made by Gaunaa et al. (2016) on this first-order model by correcting the aerodynamic loading for large blade pitch and yaw angles using CFD analysis. Kuijken (2015) looked into the aerodynamic loading of single blade installation using a jack-up vessel in extreme wind conditions (high wind speeds, large inflow angles). The main focus on the aforementioned studies is the response of the blade due to wind only and thus is the method on how to determine the aerodynamic loading more complex compared to studies where a coupled analysis from wind and waves is performed, such as in Zhao (2019).

Tugger lines are used to control motions in the horizontal plane. They are attached between the crane boom and the load that is suspended from the crane. The lines run on tugger winches and these winches control the tension of the tugger line and thus can be used to control the motion of the load. Pre-tension is applied to avoid slack lines. De Leeuw (2019) looked into using passive control of tugger lines during single blade installation with a jack-up vessel and concluded that by increasing the tugger line tension, the stiffness of the system increases and thus natural frequencies as well, resulting in smaller motions of the blade root during the mating phase. The downside however, is that the tugger winches need to be able to handle larger loads, requiring an expensive tugger winch system. Furthermore, the attachment points of the tugger lines have influence on the dynamics of the system and increasing the restoring arm can lead to better motion control.

Controlling the motions of the load using tugger lines can also be done by active control. Ren et al. (2018) developed a closed loop algorithm for single blade installation to reduce the motions by actively controlling the tension in the two tugger lines and it effectively reduces the motion of the blade root in the wind direction during the alignment phase.

1.5. Research objective and questions

The objective of this research is to gain a better understanding of the dynamic behaviour of a rotor nacelle assembly, particularly due to the wind, focusing on the horizontal motions of the RNA, when it is hanging in the crane above the tower. In order to accomplish this research objective, the following research questions are established:

1. How can the responses of a rotor nacelle assembly hanging in the crane of a floating vessel be modelled accurately?

2. What are the horizontal motions of a rotor nacelle assembly hanging in the crane due to wind and due to waves?

3. What are critical parameters, in addition to environmental conditions, affecting the response of a rotor nacelle assembly hanging in the crane?

4. For which environmental conditions does the response of a rotor nacelle assembly keep within the workability limits?

5. Can the developed model be used to implement tugger line control to effectively reduce the rotor nacelle assembly motions??

1.6. Scope and approach

With the research objective and questions being defined for this thesis, the scope and approach of this thesis is described below.

A critical phase before the RNA is being aligned with the tower, is the monitoring phase, where the motions of the RNA are monitored and have to be within the predefined limits. The focus of this research is how the aerodynamic loading on the blades, hydrodynamic loading on the vessel and the lifting configuration influence the dynamics of the RNA suspended from the crane.

The motion of the RNA is evaluated when it is hanging 2.5 m above the tower. This vertical distance is chosen, because it is large enough to taken into account the heave-induced motions of the RNA due to vessel motions. Hence, the lift-off from the assembly tower and lifting it to hub height is not considered in this research. The tower that is already installed is also subjected to wind and waves and thus also moves. Properties of the installation vessel and WTG are provided by HMC and even though the influence of these properties on the dynamic behaviour of the RNA is examined, the design is not reviewed and improvements are not made.

A fully coupled method is developed for numerical modelling and analysis of the RNA responses. Using this model, time and frequency domain simulations are ran to identify the characteristics of the dynamic RNA behaviour and based on this analysis, governing motions of the RNA are identified. Finally, a case study is performed to assess if the model can be used for implementation of tugger line control.

1.7. Thesis outline

The approach that is taken during this research to answer the research questions stated above can divided into three main steps: the input parameters, the model and the output of the model – the responses of the RNA.

In the first step the input parameters of the model are defined, such as properties of the installation vessel and WTG, environmental conditions and rigging configuration.

In the next step the models are built that simulate the RNA response due to wind and waves. This is done in three different models, which are *Model 1 − Wind only*, *Model 2 − Waves only* and *Model 3 − Wind & Waves*. The reason that effect of wind and waves on the dynamics of the system is performed separately is because it is essential to understand where motions of the RNA originate from, wind or waves. Wind-induced motion of the RNA originates from the rotor blades and thus compensation have to be applied directly on the RNA, while waves cause motions of the vessel and crane and in turn the RNA that is suspended from the crane. Therefore, to compensate wave-induced motion, motion compensation is not required directly on the RNA, but can also be applied in the crane

boom or crane tip. In all three models, the environmental conditions are varied to assess the effect of different wind and wave conditions on the response of the RNA to gain a better understanding on the behaviour of the RNA.

Model 1 – Wind only is performed in OrcaFlex using time domain simulations, while *Model 2 – Waves only* is performed in Liftdyn, which is in-house frequency domain tool. The coupled *Model 3 – Wind & Waves* is an extension of the first model, where the vessel is added and is thus in OrcaFlex, again with time domain simulations.

In addition to analysing the dynamic behaviour of the RNA, the influence of parameters that affect the RNA responses are examined as well, such as pitch angle of the blades, crane slew angle and crane radius and heading of the vessel and RNA with respect to the wind or waves.

In the final step a case study is performed in which tugger lines are used to constrain the motion of the RNA. The tugger lines are used based on the analysis on what the governing motions are to eliminate excessive responses. Again, environmental conditions are varied to evaluate the effect on the RNA responses.

In Figure 1.9 the approach and steps that are taken during this research are visualised in a flow chart.
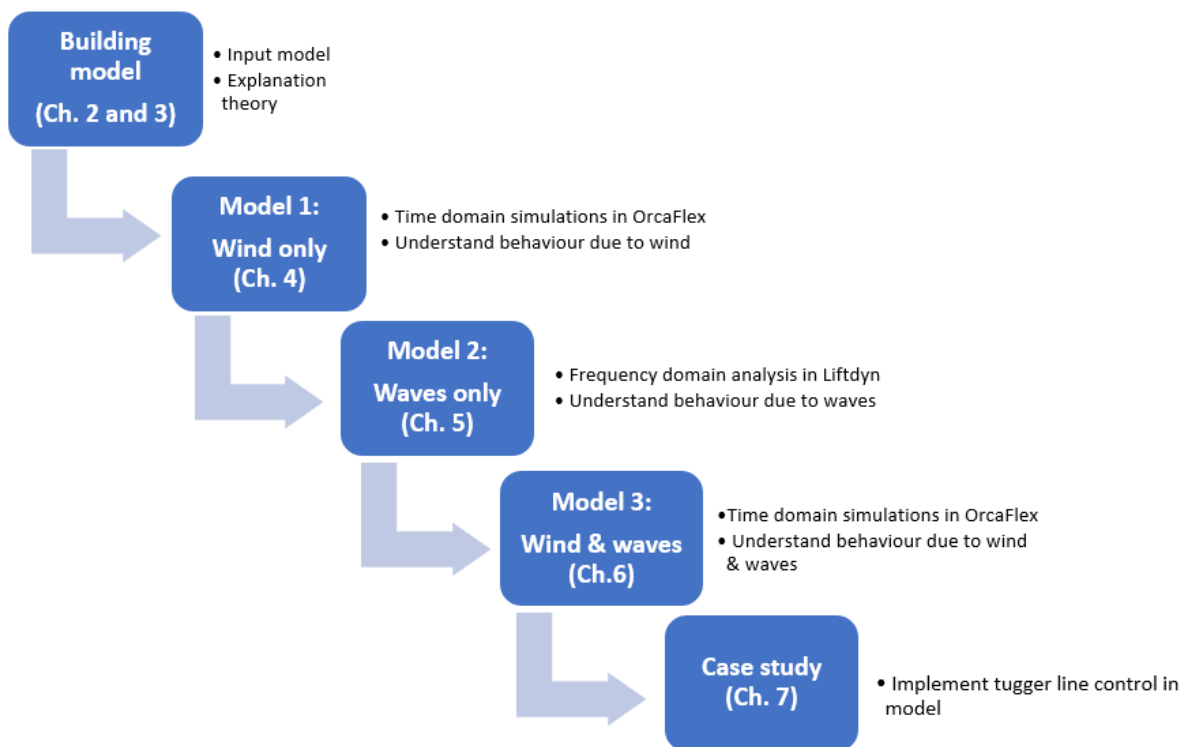
Figure 1.9: Flowchart of the approach during the thesis research.

<div align="right">

2

</div>

System Overview

This chapter provides an overview of the complete installation of a rotor nacelle assembly. First, the installation concept is described in more detail in section 2.1, consisting of the procedure that is followed and the steps that need to be taken. Then, the WTG and installation vessel that are used during this research are described in sections 2.2 and 2.3. Next, the equipment used during the lifting operation is discussed in section 2.4, which also serves as input for the model.

2.1. The installation concept

Assembling an offshore wind farm is a complex logistic procedure. All WTG components have to be brought to the offshore location and be installed under harsh environmental conditions. A number of blades, towers and nacelles can be brought on deck of the installation vessel. From there, the tower is installed first on the foundation. Next, the nacelle is placed on top of the assembly tower, that is fixed to the vessel. Then, the blades can be stabbed horizontally in the hub and finally, the complete RNA can be lifted from the assembly tower and installed on the WTG tower, as shown in Figure 2.1.

A key advantage of this installation methodology is the controlled installation of the blades, which has been identified as the most critical part of a WTG installation, due to the high precision required, fragile components and sensitivity for motions due to the environment. By installing the blades on to the assembly tower, which is fixed to the vessel, there is good control over the blade motions, because only small relative motions exist between the nacelle and blade.

2.2. Wind turbine

During this research, a turbine has to be chosen as input for the model. The selected WTG is the General Electric Haliade-X 12 MW offshore wind turbine, belonging to the next-generation WTGs. This direct-drive WTG has a rotor diameter of 220 m, resulting in blades of 107 m long. With these blades a capacity factor of 63% can be reached.

The reason that this WTG is chosen is because the motions during lifting the RNA are expected to be larger for larger turbines. Longer blades capture more wind and hence larger aerodynamic loads are generated. Furthermore, with a hub height of 138 m, the wind speeds are also more extreme, as the wind speed increases with height.

A result of the increasing hub height, is that the cranes of the installation vessels need to reach

Figure 2.1: Lifting the RNA from the assembly tower to the WTG tower.

larger altitudes, which might form problems for these vessels. The offshore wind industry is rapidly changing and the installation vessels need to be adapted accordingly – in both crane height and capacity.

Turbine manufacturers are not eager to share detailed properties of the WTG blades, especially the aerodynamic properties. Therefore, some assumptions and estimations have to be made to be able to model the blade. Recently, NREL has released a new reference wind turbine, which serves as a basic model for industry and researchers to help developing and designing the next-generation WTGs (NREL, 2020). This open source model features a 15 MW WTG with a rotor diameter of 240 m with detailed properties available to the public domain.

From this model, the aerodynamic properties of the blades are derived and used as input for the GE WTG, by scaling down the rotor diameter to 220 m. The blade is divided into 200 segments and each segment has geometrical properties, as listed below. The properties for all segments of the blade are presented in Appendix A.

- Chord length: this is the length of the airfoil, which is defined between the leading edge and trailing edge.

- Aerodynamic twist: this defines the twist of the airfoil with respect to the blade root. Because the rotational speed at the tip is larger than at the root, the velocity triangle (the ratio between rotational speed and incoming wind speed) changes at each blade segment. Therefore, by twisting the airfoil at each segment, this allows for optimal aerodynamic loads during operation of the WTG.

- Thickness-to-chord ratio: this ratio defines the between the maximum thickness of the airfoil and the chord length.

- Aerodynamic centre: this defines the location in the airfoil where the resulting lift, drag and moment are applied.

- Airfoil: over the length of the blade, 8 different airfoils are defined. Each airfoil contains data for the C_L-α, C_D-α and C_M-α curves, the lift, drag and moment coefficients versus angle of

attack, respectively. This determines the coefficients for the lift, drag and moment generated by each segment for each angle of attack and these coefficients are used to calculate aerodynamic loads. Each airfoil has a thickness-to-chord ratio and with the thickness-to-chord ratio from each blade segment, interpolation is used between the two airfoils to determine the correct aerodynamic properties.

The mass, centre of gravity (CoG) and radii of gyration of the nacelle, hub and blades is provided by GE and thus no assumptions have to be made. The total mass of the RNA is 866 mT, consisting of nacelle (495 mT), blades (3·60 mT) and hub (190 mT).

Finally, the lift points are also provided by the turbine manufacturer. These points are used to lift the nacelle individually. It is assumed that the same lift points can be used to lift the RNA. The difference is that the CoG is shifted forward, due to the weight of the rotor and thus distribution of weight per lift point is different. The locations of the CoG of the RNA and lift points are shown in Figure 2.2. More properties of the nacelle, hub and rotor is provided in Appendix A.

The WTG to be installed is featured by a monopile substructure. The reason for this is because in addition of properties of the NREL 15 MW reference turbine, they also provide initial dimensions for a monopile substructure. Hence, these dimensions can be used in the analysis of the hub deflection of the tower in Chapter 3.
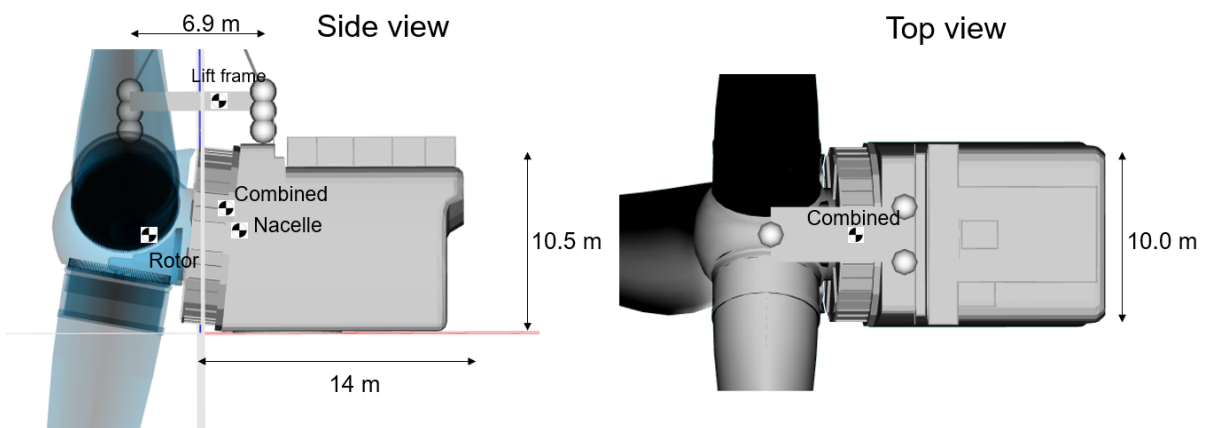
Figure 2.2: Top and side view of the GE 12 MW RNA, showing CoGs, dimensions and lift points.

2.3. Installation vessel

Two types of floating vessels exist that are used in the offshore industry – monohulls and semi-submersibles – and they have different properties, since their geometry differs considerably. A monohull vessel is more sensitive to wave-induced motions, but has better sailing speed and can thus sail back and forth to pick up WTG components, while a semi-submersible would need to lift components on deck from a barge offshore.

In this research a monohull vessel is chosen, since this type of vessel will result in the largest motions of the RNA that is hanging in the crane due to waves and hence makes the modelling and understanding the dynamic behaviour more relevant. In the vessel fleet of HMC there is in addition to three semi-submersible vessels, also one monohull vessel, Aegir and this vessel is used during this research. Aegir is shown in Figure 2.3. This heavy lift vessel was originally built to install deep water infrastructure, but is currently updated to adapt to the competitive and fast changing offshore energy industry. An important feature of this 210 m vessel is the crane placed at the stern, port side

Table 2.1: Stiffness and damping values used to model the DP system of the vessel.

	Stiffness		Damping	
Surge	100	kN/m	2596	kN.s/m
Sway	100	kN/m	2596	kN.s/m
Yaw	3491	kNm/deg	$15.34 \cdot 10^3$	kNm.s/deg

of the vessel, capable of lifting 4000 mT at 40 m radius.

Moreover, the vessel has a DP class 3 system that is used for station keeping. The class DP3 system of the vessel is modelled as spring and dampers applied at the CoG of the vessel and provides stiffness and damping in surge, sway and yaw and is used as stationkeeping of the vessel. The damping value is chosen to be 50% of the critical damping for each DoF, using a vessel mass of $67.4 \cdot 10^3$ mT, including ballasting water. The values are presented in Table 2.1.

Additionally, roll viscous damping is also applied to the vessel at the CoG. The value depends on the type of operation the vessel is carrying out. For critical installation work the allowable roll limit of the vessel is smaller than for general construction work on the vessel. Since lifting and installing a RNA is a complex lift, the allowable roll of the vessel is limited and as a result a recommended value of $15.18 \cdot 10^3$ kNm.s/deg is used.

An important note to make is that the current crane of Aegir is not capable of installing the GE 12 MW WTG, due to a lack of crane capacity and lifting height. In stead, a non-existing crane upgrade is used by fixing a fly jib to the crane boom, extending its reach and lifting capacity considerably.

Figure 2.3: Aegir, a monohull floating vessel from HMC.

2.4. Installation equipment

Two essential features for this research are discussed, the WTG and installation vessel. However, more equipment is necessary to install WTGs and that is discussed in this section, consisting of the crane block, lift frame, hoist wires, slings. First, all equipment is explained and finally an overview
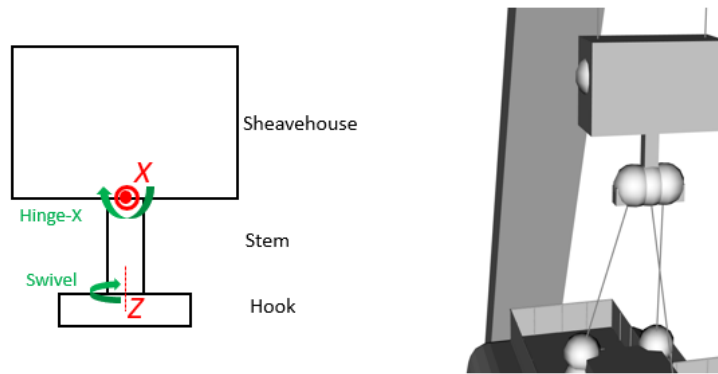
Figure 2.4: The 1000 mT auxiliary crane block, indicating the hinge and swivel of the crane block.

is given with properties.

2.4.1. Crane block

From the main winch located in the crane on deck, hoist wires are connected to the crane block. These hoist wires are part of the reeving system, meaning they run between sheaves and drums back and forth. As a result, the crane block, which is suspended from the crane, is connected multiple times to the same crane wire and thus increasing the stiffness. The reeving required for the lifting operation depends on the weight that has to be lifted.

The crane block used during this research is shown in Figure 2.4, which is an auxiliary crane block with a safe working load (SWL) of 1000 mT and mass of 50 mT. The crane block can be divided into three bodies, the sheavehouse, stem and hook. The hoist wires are connected to the hoist points in the sheavehouse, this is where the sheaves are located for reeving of the hoist wires. Below the sheavehouse is the stem, which is connected to the sheavehouse with a hinge and can rotate freely around X, as visualised in the drawing. Then, the hook is connected to the stem and the hook can swivel freely in yaw around the stem. The prongs are located on the hook, this is where the slings are hooked on and the slings connect the crane block with the load that is being lifted.

2.4.2. Lift frame

A lift frame is used between the crane block and RNA for a better distribution of the loads through the slings. Furthermore, limitations exist for the angle at which the slings are connected to the lift points on the nacelle. Depending on the turbine manufacturer, the lift points can deal with a maximum amount of horizontal loads. If no lift frame would be used, the slings between the crane block and nacelle must be significantly longer to have vertical slings connected to the lift points on the nacelle.

The mass of the lift frame is 80 mT. The width and length of the lift frame match the width and length between the lift points on the nacelle. The height of the lift frame is 1.0 m. The lift frame is rigidly connected to the nacelle, to decrease the number of DoFs in the system.

Figure 2.5: Rigging arrangement for installing the RNA using three slings from crane block to lift frame. The lift frame is rigidly connected to the RNA. The nacelle is modelled as one body and the rotor as another body that is rigidly connected to the nacelle

2.4.3. Slings

Three slings are used to connect the nacelle to the crane block, from each lift point on the lift frame, which is located exactly above the lift points of the nacelle, to the prongs on the hook. Each sling of the two lift points located at the back are connected to each side of the prong, while the sling of the front lift point is connected to the middle of the hook. In reality, this sling would be two slings, with each going to one prong. However, to simplify the model, this is modelled as one sling. As a result, the stiffness of this sling is multiplied by 2. The slings in aft have an angle of 66 deg with respect to the horizontal plane, while this angle of the front sling is 61 deg. As a result, the lengths of the slings are around 8.0 m.

The mass of the slings is not taken into account in this research. The maximum mass of the rigging arrangement can be approximated to be 3% of the mass that is lifted (HMC), assuming steel slings. In practice, the percentage is much lower. By adding the mass of the slings, the complexity of the system is increased, while the effect on the dynamics of the system is negligible. Therefore, the mass of the slings is not considered.

The sling properties are as follows: Young's modulus E is 20 kN/mm^2, the diameter D is 160 mm, resulting in $EA = 40.2 \cdot 10^3$ kN.

2.4.4. Hoist wires

The hoist wires connect the crane block to the crane boom. In reality the wires are connected to main winches and runs via sheaves from the crane boom back to deck. As explained earlier, the crane wires run multiple times between the winch and crane block. In the model, two crane wires are modelled. For this type of lifting operation, a reeving of 2 x 4 is used. Hence, one crane wire represents four crane wires in reality.

The hoist wire properties are as follows: Young's modulus E is 41.5 kN/mm^2, the diameter D is 72 mm, resulting in $EA = 676 \cdot 10^3$ kN, using the defined reeving.

Theoretical Background

In this chapter the methods are explained how the motions of the RNA due to the wind and waves can be determined. This includes aerodynamic and hydrodynamic theory to obtain the loads on the blade, the vessel and WTG substructure and how from these loads, the motions are calculated in sections 3.2 and 3.4. Furthermore, wind and wave conditions are explained in sections 3.1 and 3.3. Moreover, the software used throughout this research is discussed in section 3.5. Finally, an analysis is performed in section 3.6 regarding the deflection of the hub.

3.1. Wind conditions

This section discusses the wind climate that is used throughout this research, consisting of the wind profile and wind spectrum. The wind direction and wind speed determine the magnitude of the aerodynamic load distribution of the blades. To model the response due to the wind, a wind field has to be generated.

The vertical variation, being the wind speed varying over height, gives a significant difference in the magnitude of the wind speed at 10 m and at hub height. DNV (2010) provides different methods to determine how the wind speed varies over height, assuming that the terrain conditions and atmospheric stability conditions are not complex. In this study the power law profile is used and is presented in Equation 3.1.

$$U(z) = U(h) \left(\frac{z}{H} \right)^{\alpha} \tag{3.1}$$

Where $U(h)$ is the 10-minute mean wind speed at the reference height h of 10 m and α is the power-law exponent. This exponent depends on the terrain considered, which in this case is an open sea with waves. According to DNV (2010), this value is 0.12.

As a result of this wind profile, with a wind speed of 10 m/s at 10 m height, at hub height a wind speed of 13.7 m/s is experienced. Since the aerodynamic loading scales with the wind speed squared, this yields a significant difference for the magnitude of the lift and drag depending on the height of the blade. Time series of the wind speed at 10 m and 138 m are presented in Figure 3.1.

Furthermore, a wind spectrum has to be defined in the model, which describes how the wind speed fluctuates around the mean wind speed. DNV (2010) recommends to use the Frøya wind spectrum, as shown in Equations 3.2 and 3.3, for wind over water and is originally developed for neutral con-
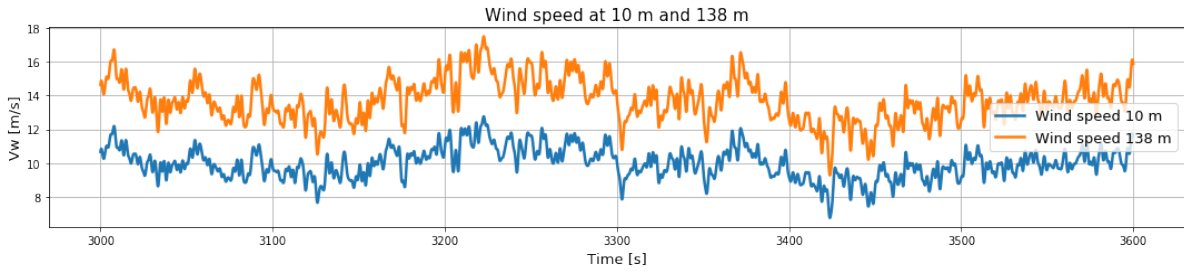
Figure 3.1: Time series of a mean wind speed of 10 m/s at 10 m and the resulting wind speed at 138 m height. A vertical wind profile is defined using a power law profile in the model with an exponent of 0.12.

ditions over water in the Norwegian Sea. In regimes where stability effects are of importance, it is not advised to choose this wind spectrum.

$$S_U(f) = 320 \cdot \frac{\left(\frac{U_0}{10}\right)^2 \left(\frac{z}{10}\right)^{0.45}}{\left(1 + \tilde{f}^n\right)^{\frac{5}{3n}}} \tag{3.2}$$

$$\tilde{f} = 172 \cdot f \cdot \left(\frac{U_0}{10}\right)^{-0.75} \tag{3.3}$$

Where $n = 0.468$ and U_0 is the 1-hour mean wind speed at 10 m height. In Figure 3.2 the Frøya wind spectrum is presented.

Gusts are characterised as brief increases in wind speed of less than 20 seconds and can occur as part of natural fluctuations around the mean wind speed at local positions in the wind field. These local maxima cannot be modelled in OrcaFlex, only a global increase in wind speed due to the wind spectrum in the field. Furthermore, the direction of the wind in the whole wind field is the same – at local scale the wind direction is the same as the global wind direction, which is given as input in the model.
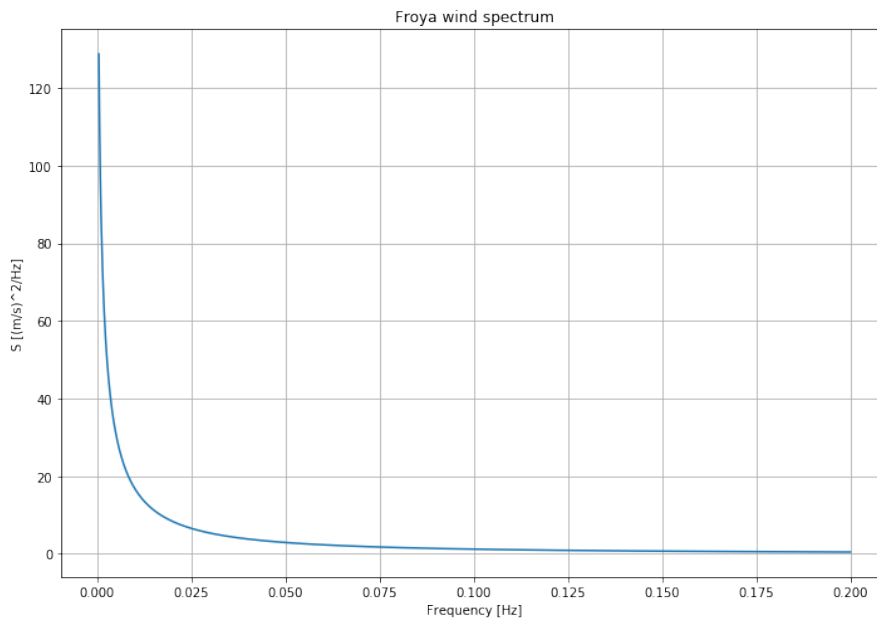
Figure 3.2: Frøya wind spectrum for a wind speed of 10 m/s at 10 m height.

3.2. Aerodynamic theory

To understand the dynamic behaviour of the RNA due to the wind, some aerodynamic theory is explained first on how aerodynamic loads are generated. Note that only the wind on the rotor is taken into account and not wind on the vessel, crane or nacelle. The aerodynamic loads on the rotor are computed in OrcaFlex. First, some basic principles on lift and drag is explained.

3.2.1. Lift and drag

In Figure 3.3 an airfoil of a wind turbine blade is shown with an incoming wind flow with angle of attack α. Due to the air pressure difference between the top and bottom of the airfoil, lift is generated and is always perpendicular to the incoming wind direction. The drag force is always parallel to the incoming wind and defined positive against the wind. Depending on the angle of attack, the 2D lift and drag coefficients C_l and C_d change and define the magnitude of the lift l_i and drag load d_i of a 2D airfoil, as determined in Equations 3.4 and 3.5. By integrating the load distribution over the length of the blade, taking into account the width of each segment, the total lift and drag force can be calculated. The moment at the root due to aerodynamic loading can be determined by multiplying the load distribution with the distance to the root and integrating over the length of the blade.

$$l_i = C_{l_i} \frac{1}{2} \rho_{\text{air}} V_0^2 c_i \tag{3.4}$$

$$d_i = C_{d_i} \frac{1}{2} \rho_{\text{air}} V_0^2 c_i \tag{3.5}$$

Where i is a subscript representing the blade segment, ρ_{air} is the air density, V_0 is the incoming wind speed and c is the chord length of the airfoil.
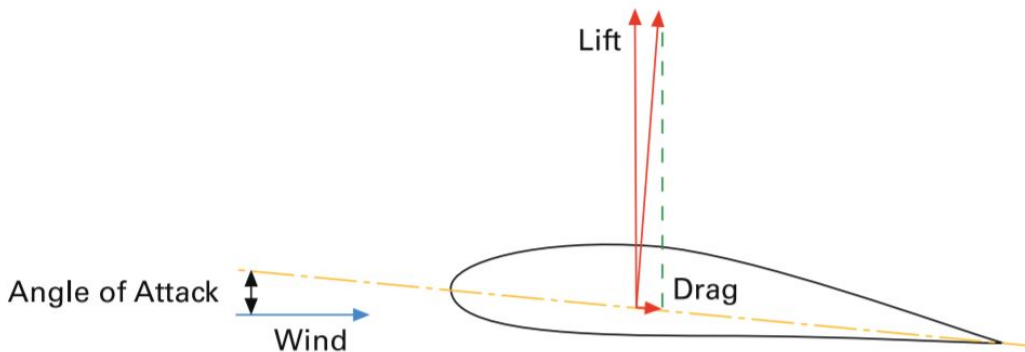
Figure 3.3: Incoming wind flow with an angle of attack on a cross-section of a wind turbine blade.

The aerodynamic loads of a WTG in operation or at standstill differs significantly. This is because for an operating WTG, there is an additional incoming wind velocity component, the wind speed experiences by the airfoil, because the blades are rotating. Because the rotational speed experiences by the blade segment increases when going from root to blade, the blades are twisted to still have optimal angle of attack. This has been accounted for in the model. The lift and drag distribution of the blade during standstill is presented in Figure 3.4 for varying pitch angles of the blade. The differences in magnitude of the load distribution is due to the aerodynamic twist at each segment and the chord length. The pitch of the blade can be changed during operation to control the power

output of the turbine and significantly influences the magnitude of the lift and drag generated by the blades. It effectively changes the local angle of attack at each segment, changing the C_l and C_d values. The influence of the blade pitch angle can clearly be seen in the figure, not only in magnitude of the load, but also the distribution. Hence, it is important to look into the response of the blades for different pitch angles.
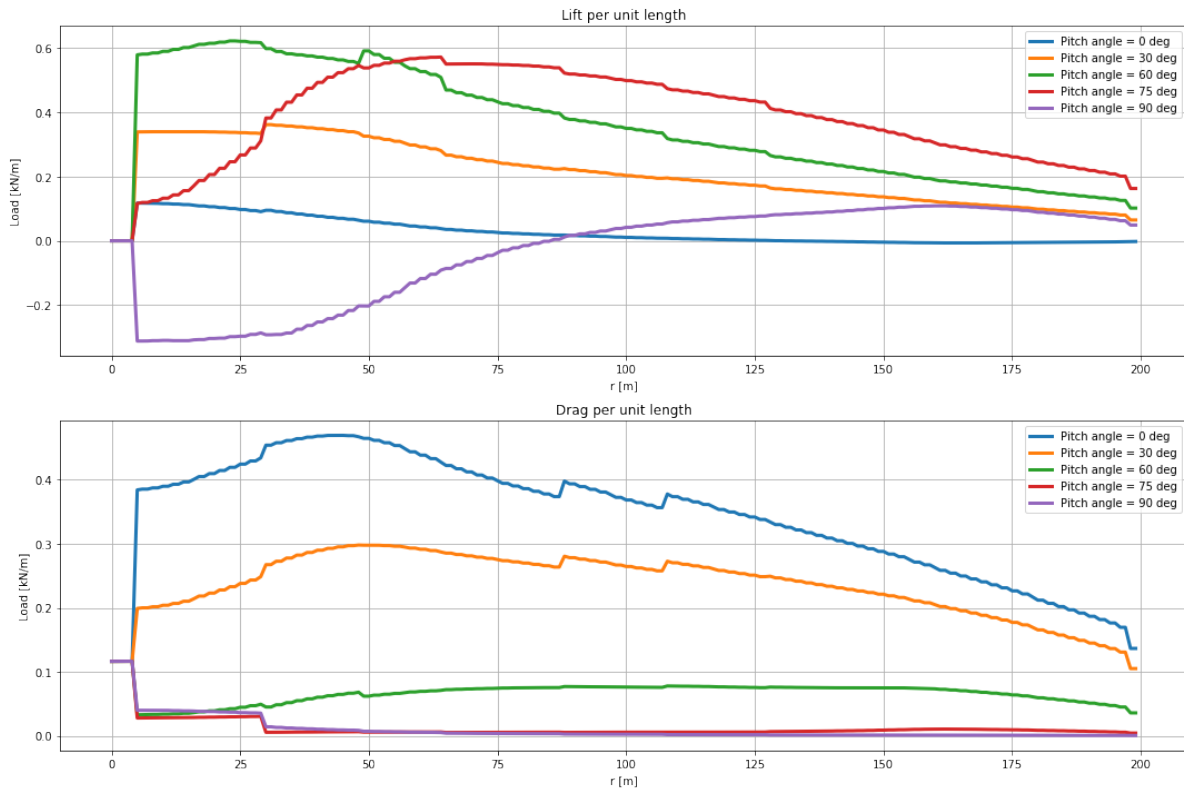
Figure 3.4: Lift and drag distribution over the length of the blade for varying blade pitch angles.

3.2.2. Cross-flow principle

Hoerner (1985) presented a method to determine drag forces with lines that have an inclination with respect to the incoming airflow, the cross-flow principle. This principle states that for incoming wind on a 2D structure, the spanwise velocity component of the wind can be neglected, resulting in a very practical method to determine aerodynamic forces on a segment. For a straight, horizontal single blade, this means that both the lift and drag scale with $\cos^2 \theta$, with θ being the inflow angle of the wind. Prebend of the blades, which accounts for the deflection at the tip during operation, is not considered in this research and are thus assumed to be straight.

As discussed in the literature review in section 1.4, the validity of the cross-flow principle is questioned for large inflow angles. Studies are performed regarding this subject, in which is concluded that corrections can be applied, based on CFD analyses for single blade installation. However, this is an assumptions that has to be made, as in OrcaFlex the calculation of the aerodynamic loads cannot be changed.

It is important to note that the effect of the cross-flow principle differs depending on the orientation of the blade. If only wind is considered in the horizontal plane, X and Y, so only wind velocity components in global X and Y, this means that the wind direction has no influence in case of blades that are completely vertical, e.g. pointing upwards or downwards, because there is no spanwise flow

over the blade, which would be neglected according to the cross-flow principle. This is shown in Figure 3.5. Note that for varying wind directions, the angle of attack on the blade differs and thus according to the airfoil data, the forces change as well.

For a horizontal blade on the other hand, as shown in Figure 3.6, the resultant aerodynamic forces differs significantly per wind direction. If the wind comes blows towards the global X direction, no velocity would be neglected. However, if the wind direction is towards global Y, all wind flows in the spanwise direction of the blade and hence no aerodynamic force is generated.

Each blade is divided into 200 of segments, resulting in each segment having a 0.535 m width and at each segment the loads are determined. These are then summed together to obtain the total aerodynamic forces and moments in and around x, y and z.
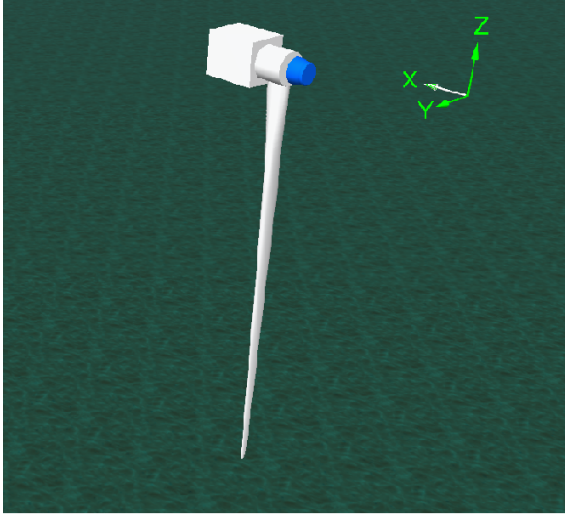
Figure 3.5: For a vertically orientated blade, the cross-flow principle does not neglect a wind component for a certain wind direction.
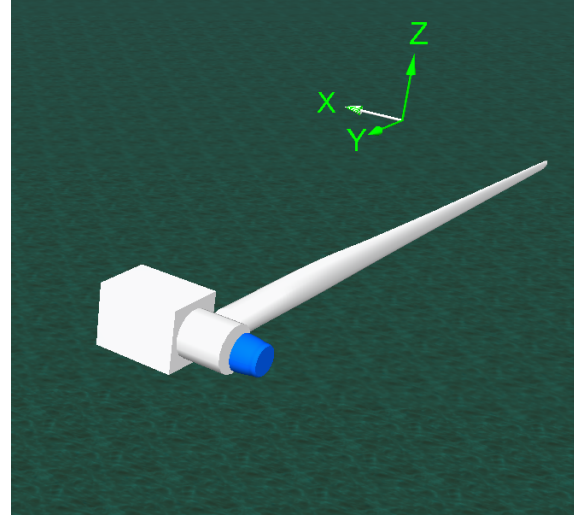
Figure 3.6: For a horizontally orientated blade, the cross-flow principle has effect on the magnitude of the aerodynamic loads, depending on the wind direction.

3.3. Wave conditions

This section describes the wave climate that is used throughout this research. Basically, two types of waves exist, regular and irregular waves. Regular waves have a constant wave height and period and form perfect oscillations. This is referred to as Airy waves. A real sea state consists of irregular random waves. These can be modelled as a summation of sinusoidal linear wave components.

The JONSWAP spectrum, as shown in Equation 3.6, is a spectrum that describes wind seas very well (DNV, 2010) and is used as spectrum to model the waves.

$$S_J(f) = \frac{\alpha g^2}{16\pi^4} f^{-5} \exp\left[-\frac{5}{4}\left(\frac{f}{f_m}\right)^{-4}\right] \gamma^b \tag{3.6}$$

$$b = \exp\left(-\frac{1}{2\sigma^2}\left(\frac{f}{f_m}-1\right)^2\right) \tag{3.7}$$

$$\sigma = \begin{cases} 0.07 \rightarrow f \le f_m \\ 0.09 \rightarrow f > f_m \end{cases} \tag{3.8}$$

Where α is a data item and is 0.00987, g is the gravitational acceleration, $f_m = \frac{1}{T_p}$ is the peak fre-

quency, γ is the peak enhancement factor, which is determined using Equation 3.9.

$$\gamma = \begin{cases} 5 & \rightarrow \quad \frac{T_p}{\sqrt{H_s}} \leq 3.6 \\ \exp\left(5.75 - 1.15\frac{T_p}{\sqrt{H_s}}\right) & \rightarrow \quad 3.6 < \frac{T_p}{\sqrt{H_s}} < 5 \\ 1 & \rightarrow \quad 5 \leq \frac{T_p}{\sqrt{H_s}} \end{cases} \tag{3.9}$$

Moreover, wave spreading is used to simulate a more realistic sea state. A monohull vessel is susceptible to roll and if the waves are all perfect head waves for the vessel, the roll motion of the vessel is not excited, hence simulating a non-realistic response of a load hanging in the crane. Spreading of the waves is modelled by using a directional spreading spectrum S_D, which is expressed in Equation 3.10. During this research a spreading exponent of $n = 2$ is used, which is a typical value. The direction range $-\frac{\pi}{2} \leq \theta - \theta_p \leq \frac{\pi}{2}$ is discretised into a number of wave directions, which is set to 11 wave directions.

$$S_D(\theta) = K(n)\cos^n(\theta - \theta_p) \qquad\qquad \text{for} -\frac{\pi}{2} \leq \theta - \theta_p \leq \frac{\pi}{2} \tag{3.10}$$

$$K(n) = \frac{\Gamma(\frac{n}{2} + 1)}{\sqrt{\pi}\Gamma(\frac{n}{2} + \frac{1}{2})} \tag{3.11}$$

Where n is the spreading exponent, θ is the wave direction, θ_p is the principle wave direction and $K(n)$ is a normalising constant.

Finally, the total spectrum of the waves is thus a combination of the wave frequency spectrum S_J and directional spectrum S_D.

$$S(f,\theta) = S_J(f,\theta) \cdot S_D\theta \tag{3.12}$$

Wheeler stretching is used to predict the wave particle velocity and acceleration above the mean water level. This is required, because the kinematics of particles that are above the water are not known and thus a theory is necessary to stretch the theory of the water particle kinematics.

3.4. Hydrodynamics

In addition of the response of the RNA due to the wind, it will also move due to wave-induced motion of the vessel. Moreover, the monopile is subjected to waves and thus the monopile and tower are excited by waves as well. To understand the behaviour of the vessel and substructure, some hydrodynamic theory is explained that is used in this research. The theory that is explained in this section is also used in both OrcaFlex and Liftdyn.

Wave loads on offshore structures can essentially be divided into two categories: one for structures with relatively small cross-section and the other for large volume structures. For the former, free surface effects are not as dominant as the oscillatory drag due to separation, leading to the Morison equation. This can thus be applied for slender structures, such as the wind turbine's foundation. Diffraction and radiation forces are prevailing when a large volume structure is considered − the installation vessel. In this case, the potential flow theory is more accurate, since it takes free-surface effects into account. The hydrodynamic loads on the vessel and monopile are explained in more detail in this section.

3.4.1. Hydrodynamic loads on the vessel

Linear theory is able to describe the wave-induced motion and loads on the installation vessel. In this theory it is assumed that the waves are regular, with small wave steepness and not breaking. Furthermore, the wave-induced motion and load amplitudes on the vessel due to these waves are linearly proportional to the wave elevation. Non-linear effects also exist, but they are of greater importance in non-linear sea states.

On the sea the vessel is subjected to incident waves with an irregular nature. According to Faltinsen (1990), the response due to irregular waves can be obtained by superimposing the response due to linear waves.

Essentially, the loads can be divided into two categories – diffraction and radiation forces, as illustrated in Figure 3.7. Diffraction forces are the forces on the vessel when the vessel is fixed, while it is subjected to incident regular waves. Even though the vessel is stationary, the wave field will be affected due to its presence of the vessel. These hydrodynamic loads can be referred to as wave excitation loads.

The radiation forces on the other hand, are the forces on the vessel that occur when the vessel is forced to oscillate at the wave frequency in its six degrees of freedom, while there are no waves. The generated hydrodynamic loads can be described as added mass, damping and restoring terms.
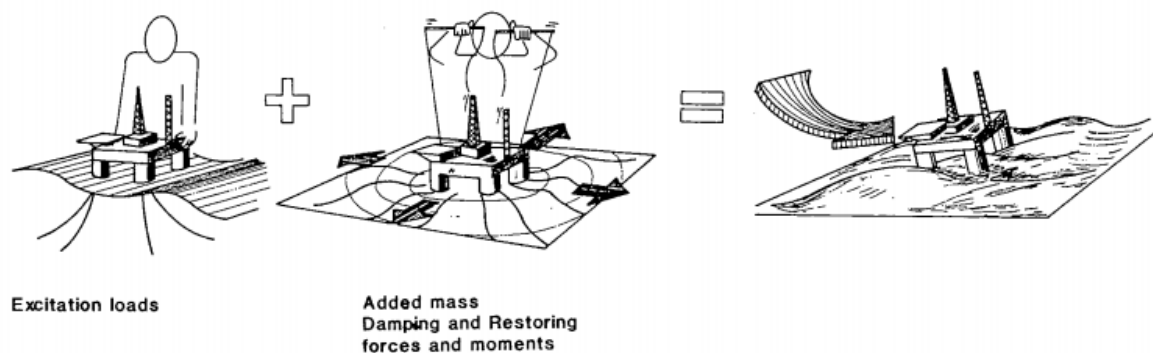
Figure 3.7: Superposition of wave excitation, added mass, damping and restoring loads (Faltinsen, 1990).

3.4.2. Hydrodynamic loads on the monopile

The Morison equation, described by Morison et al. (1950), can be used for slender structures, which yields the resultant force per unit length for a fixed vertical pile in an oscillatory flow. It is valid when the wave length is larger than five timer the diameter, e.g. $\lambda > 5D$ (DNV, 2010). The Morison equation is an ideal approach for calculating the hydrodynamic loads on a monopile exposed to regular linear waves. It is a superposition of two separate phenomena at a given value of z:

- A drag force caused by the flow velocity.

- An inertial force caused by the horizontal acceleration of the wave particles, consisting of a hydrodynamic mass force and the Froude-Krylov force.

The hydrodynamic mass force is the force required to accelerate the water following the motion of the structure, while the Froude-Krylov force is the force due to the pressure gradient of the outer flow. The Morison equation is expressed in Equation 3.13 in case of a cylindrical structure, as this is relevant for the case considered during this literature review.

$$\mathrm{d}F = \underbrace{C_D \frac{1}{2}\rho D\,\mathrm{d}z|u|u}_{\text{Drag force}} + \underbrace{\rho \frac{\pi D^2}{4}\mathrm{d}z C_m \dot{u}}_{\text{Hydrodynamic mass force}} + \underbrace{\rho \frac{\pi D^2}{4}\mathrm{d}z \dot{u}}_{\text{Froude-Krylov force}} \tag{3.13}$$

It is often written as:

$$\mathrm{d}F = C_D \frac{1}{2}\rho D\,\mathrm{d}z|u|u + \rho \frac{\pi D^2}{4}\,\mathrm{d}z C_M \dot{u} \tag{3.14}$$

Where ρ is the density of the fluid, D is the diameter, u and $\dot{u}$ are the horizontal velocity and acceleration of the particle at the midpoint of the strip and C_M (= $C_m + 1$) and C_D are the added mass and drag coefficients. Generally, the added mass and drag coefficient are around 2.0 and 1.0, respectively. The exact values are determined empirically and depend on several parameters, such as the Reynolds number, the surface roughness of the structure and the Keulegan-Carpenter number. More information on how to obtain these parameters can be found in DNV (2010).

Note that, when considering the Morison equation as a function of time, that the drag and inertia term are 90 deg out of phase of each other due to the phase shift between the wave particle velocity and acceleration. Depending on the diameter of the structure, the inertia or drag term is dominant. This depends on the ratio of the diameter D over the wavelength λ of the incident wave. As explained earlier, the inertia term is due to the presence of a structure in a wave field. If the size of the structure is small compared to the incoming wave (small D/λ), the inertia term is dominant. With increasing diameter while having the same incoming wave, the drag term will be prevailing.

As a result of the structure exposed to waves, it will be put in motion, creating a relative velocity between the wave particles and the structure. Hence, the hydrodynamic loads will be slightly larger or smaller, depending whether the structure oscillates forwards or backwards. This can be accounted for by using relative velocities and accelerations. Also, the current velocity can be added in this way. The derivation of relative velocity formulation of the Morison equation is shown in DNV (2010).

3.5. Modelling of RNA and vessel response in software

This section describes the approaches used to model the responses of the vessel and RNA. This is explained for time domain simulations in OrcaFlex and frequency domain analyses in Liftdyn.

3.5.1. OrcaFlex – Time domain

Time domain analyses are required to model the RNA response due to wind. Even though a frequency domain analysis allows for a quick method to look into the dynamic behaviour of the system, this method cannot be used when examining how the blades generate aerodynamic forces from the wind for different wind directions and blade pitch angles. Furthermore, in the coupled model of wind and waves, frequency domain analyses cannot be performed as well.

RNA
In OrcaFlex, the aerodynamic loads on the blades due to the wind are computed as explained in section 3.2. The blade is divided into a number of segments and at each segment, the load is determined, using the geometrical blade properties, lift, drag and moment coefficients. The relative velocity between the wind speed and the velocity of the blade is taken into account.

Vessel
The motion of the vessel due to waves in OrcaFlex is defined using load RAOs, representing the load

(forces and moments) on the vessel. The amplitude of the RAO is the magnitude of the force for surge, sway and heave, and moment for roll, pitch and yaw. Furthermore, the RAO defines a phase, which describes the motion of the vessel with the incoming waves. From the loads that act on the vessel, the motion can be derived using the vessel's mass and inertia and possible any other external loads from the equation of motion.

The load RAOs are imported from WAMIT, which is a diffraction analysis software that determines the forces and moments in the frequency domain. Therefore, the load RAOs are frequency dependent and are determined for frequencies between 0.025 and 2.0 rad/s, with steps of 0.025 rad/s. Moreover, this analysis is performed for all wave directions, from 0 to 345 deg with steps of 15 deg. OrcaFlex linearly interpolates between wave directions and frequencies to obtain the forces and moments of incoming waves.

Solving equation of motion
OrcaFlex solves the equation of motion in the time domain as follows:

$$\mathbf{M}(p,a) + \mathbf{C}(p,v) + \mathbf{K}(p) = F(p,v,t) \tag{3.15}$$

Where $\mathbf{M}(p,a)$ is the system inertia load, $\mathbf{C}(p,v)$ is the system damping load, $\mathbf{K}(p)$ is the system stiffness load, $F(p,v,t)$ is the external load, p, v and a are the position, velocity and acceleration vectors, respectively and finally the simulation time is t.

At each time step, the forces and moments acting on each body are determined. Those forces and moments in the system used are weight, buoyancy, aerodynamic and hydrodynamic loading and contact forces with other objects. Then, the equations of motion, from Newton's second law, are formed for each body in the system.

OrcaFlex offers two different methods to solve solutions for time domain simulations at each time step, explicit and implicit domain integration. Explicit time domain integration is conditionally stable, meaning that the time step must be small compared to the smallest natural node period, to obtain stability. In this case, OrcaFlex determines the time step and results in robust simulations. As a consequence, the computation time can be long. With implicit time domain integration however, the integration scheme is unconditionally stable for linear systems and thus stability is easier achieved. Hence, computation time is also faster. The latter is also the reason that an implicit time domain integration scheme is chosen in this research.

3.5.2. Liftdyn − Frequency domain

Liftdyn is used in *Model 2 − Waves only* to examine the wave-induced motions of the RNA. It is an in-house frequency domain tool developed by HMC in Matlab, allowing for a quick and efficient way to check the dynamics of the model.

In Liftdyn the equations of motion is as shown in Equation 3.16. This is a single matrix equation, consisting of n bodies with $6n$ equations of motion. The mass, damping and stiffness matrix are all defined with respect to the CoG of the body. The force vector F contains the forces applied on the CoG of the rigid bodies. The unknown motion vector X contains the 6 DoF motion of each body. The same hydrodynamic database is used as in OrcaFlex from which the added mass and damping values and hydrostatic properties are derived.

$$(\mathbf{M}+\mathbf{A}(\omega)) \cdot \ddot{X}(\omega,dir) + \mathbf{B}(\omega) \cdot \dot{X}(\omega,dir) + \mathbf{C} \cdot X(\omega,dir) = F(\omega,dir) \tag{3.16}$$

The equation of motion is a 2nd order linear differential equation and since they are linear, they can

be solved in the frequency domain. By assuming that the force and motion vector are harmonic with wave frequency ω, one can rewrite the equation to Equation 3.17, resulting in a simple matrix-vector equation. This equation can be solved for each wave frequency and direction to find the complex motion vector X, which contains the amplitude and phase difference of each motion.

$$\left[\mathbf{C} + i\omega\mathbf{B} - \omega^2(\mathbf{M} + \mathbf{A}(\omega))\right] \cdot X(\omega, dir) = F(\omega, dir) \tag{3.17}$$

In Liftdyn the significant response X_s is determined as shown in Equation 3.18. It yields the significant double amplitude of the response.

$$X_s(\omega, dir) = 4 \cdot \sqrt{\int_0^\infty [RAO(dir, \omega)]^2 \cdot Spec_\zeta(\omega, \omega_p)\mathrm{d}\omega} \tag{3.18}$$

Where RAO is depending on the wave direction dir and frequency ω, $Spec_\zeta$ is the wave spectrum and ω_p is the peak wave frequency.

3.6. Analysis of tower deflection at hub height

During the installation, the RNA has to be placed on top of the already installed tower. The tower is subjected to the same environmental conditions as the vessel and RNA − the monopile is exposed to waves, while the wind is applying a load on the tower. To assess the response of the tower and monopile deflection due to wind and waves, a modal analysis is performed first to determine natural periods of the structure.

The tower and monopile are assumed to be one body and is divided into a number of nodes. These nodes can deflect individually in different mode shapes. It is assumed that the monopile is fixed at the mud line and cannot deflect. As a result, the monopile and tower can be modelled as a beam with a clamped and free end. In reality, the monopile can still deflect in the seabed, depending on the soil type and the embedded length of the monopile. However, it is expected that neglecting the deflection in the sea bed does not have a significant influence on the deflection at the hub.

The mode shape of a clamped beam is as presented in Equation 3.19.

$$\varphi(z) = 1 - \cos\left(\frac{n\pi}{2L}z\right) \tag{3.19}$$

Where $\varphi(z)$ is the amplitude of the mode shape, depending on the position z along the structure (seabed to hub height), $n = 1, 2, 3...$ representing the mode shape, L is the length of the whole structure.

In this analysis the deflection at the hub height is most relevant, hence only the first mode shape is considered, e.g. $n = 1$, since this mode shape yields the largest amplitude at the top of the structure. Then, according to Rayleigh's method, the natural frequency f_n can be determined as shown in Equation 3.20.

$$f_n = \frac{1}{2\pi}\sqrt{\frac{\int_0^L EI(z)\varphi_{zz}^2(z)\mathrm{d}z}{\int_0^L m(z)\varphi^2(z)\mathrm{d}z}} = \frac{1}{2\pi}\sqrt{\frac{GK}{GM}} \tag{3.20}$$

Where $EI(z)$ is the stiffness of the structure, φ_{zz} is the second derivative of the mode shape with respect to z and $m(z)$ is the mass per unit length of the structure. The numerator and denominator in the square root are referred to the generalized stiffness GK and mass GM of the structure.

The damping of the structure has to be estimated from the critical damping, which can be calculated as shown in Equation 3.21 using the generalized mass and stiffness as determined earlier. Then, a percentage of the critical damping has to be chosen, which is typically 1% or 2%.

$$GD_{\text{critical}} = 2\sqrt{GK \cdot GM} \qquad (3.21)$$

Since no structural data of the tower is available of the GE 12 MW turbine, some derivations are made from the NREL 15 MW reference turbine, which has a hub height of 150 m and monopile diameter of 10 m. The data is scaled down to match the 138 m hub height of the turbine used in this research. Even though this would not match exactly, it is a safe assumption to make, as it is about the order of magnitude of the stiffness and mass per unit length. The results are presented in Table 3.1.

Table 3.1: Results modal analysis of the first mode shape of the monopile and tower.

Parameter	Value	
GM	$1.75 \cdot 10^5$	kg·m
GD_{critical}	$1.30 \cdot 10^6$	kg·m/s
GK	$2.42 \cdot 10^6$	kg·m/s^2
f_n	0.592	Hz
T_n	1.69	s

From the table can be seen that the natural period of the tower and monopile is 1.69 s. This is well below the frequency range of wind and waves. Nevertheless, the response of the structure due to the environment should be examined.

In the analysis only the waves are accounted for, not the wind. There are two reasons to not consider the wind – the wind is always generating a load distribution in the same direction, meaning that the structure is not expected to oscillate back and forth due to wind only. It will oscillate due to changes of wind speed and thus magnitude of the load, but these are amplitude differences are assumed to be small. For waves on the other hand, the waves travel is circular trajectories and as a result, the load distribution due to waves does change direction over each wave period and thus excites an oscillation of the structure. Second, the dominant frequency range of the wind is well below < 0.05 Hz, which is significantly further away from the natural frequency of the structure compared to the wave dominant frequency range. Therefore, the excitation due to waves is expected to be larger than the wind and thus only the waves are considered in the analysis of the response of the tower.

To determine the hydrodynamic loading on the monopile, the Morison equation is used, which is explained in section 3.4. This is valid since the monopile can be considered to be a slender structure.

In Figure 3.8 the significant responses of the tower at hub height are shown. The responses are defined as Significant Double Amplitude (SDA), which is equal to 4·std(X). The significant responses are computed for peak periods varying between 4 and 12 s, while the significant wave height is varied for 1.0 and 2.0 m. This is done to better evaluate the hub deflection for different environmental conditions. Furthermore, 1% critical damping is used. From the results can be derived that for waves with $H_s = 2.0$ and $T_p = 4.0$ s, that the tower's significant response is 0.20 m. For higher peak periods, the response decreases, because it moves further away from the natural period of 1.7 s. From these observations is concluded that the tower hub deflection is not taken into account in this research.

Figure 3.8: Significant response as SDA of the fore-aft deflection of the tower at hub height for different T_p, H_s = 1.0 and 2.0 m and damping as 1% of the critical damping of the structure.

4

Model 1 – Wind Only

This chapter deals with the first model that is built to run time domain simulations in OrcaFlex for the wind only case. The purpose of first looking into the motions of the RNA due to the wind only, is to understand the dynamic behaviour of the system due to wind by identifying what motions are excited by the wind and how these motions can be reduced as much as possible. Since the motions of the wind act directly on the RNA, these motions have to be controlled at the RNA as well if the motions have to be reduced.

First, an overview of the model is presented in section 4.1, followed by a modal analysis in section 4.2. Then, the results are shown and discussed in section 4.3, in which parameters are identified that cause excitation by the wind. Finally, conclusions are drawn and explained in section 4.4.

4.1. Model overview

For the wind only case, a model is built in OrcaFlex to run time domain simulations. An overview of the model that is used is shown in Figure 4.1, consisting of two bodies – the RNA and lift frame are modelled as one 6 degrees of freedom (DoF) rigid body and the crane block as another rigid body with 8 DoFs, as a result of the swivel and hinge. The reason that the lift frame is modelled rigidly connected to the RNA is to simplify the problem, otherwise the model would extend to a 20 DoF system, making the model more complex, without changing the dynamic behaviour of the system significantly, as the vertical slings between the lift frame and RNA are only 1.0 m.

The lift frame is connected to the crane block by three slings coupling the motion of the crane block and the RNA. Hence, this model can basically be seen as a double pendulum.

The hoist wires connected the crane block to the hoist points on the crane boom. In this case, the vessel and crane are not of importance – only the position of the crane tip and thus an Earth fixed point is used to fix the hoist wires onto. The length of the double pendulum is an important parameter for the dynamic behaviour of the system, as this influences the period of a pendulum oscillation and thus is subject to change to get a better response. A shorter pendulum has a shorter pendulum swinging period, while a longer pendulum needs more time to oscillate back and forth. A crane can boom up or down and since the RNA is hanging at a fixed height, this lowers or raises the location of the crane tip, effectively changing the pendulum length. Therefore, the height of the crane tip is a parameter that is considered to be important in this analysis. The hoist wires are modelled as two wires to provide a small stiffness in yaw rotation.

A WTG can change the pitch angle of the blades for optimal power production. By changing the

pitch angle, the orientation of the blade with respect to the wind changes and thus the lift and drag coefficients change. As a result, the lift and drag forces generated by the blades also change and thus the dynamics of the system. Therefore, the influence of the blade pitch angle on the responses of the RNA due to the wind is examined in this analysis.

The global coordinate system is also defined in Figure 4.1, where $Z = 0$ m is defined at the water line. The RNA is hanging 2.5 m above the tower, which is at a height of 138 m. Hence, the bottom of the nacelle is at $Z = 140.5$ m. The definition of the incoming wind directions is shown in Figure 4.2
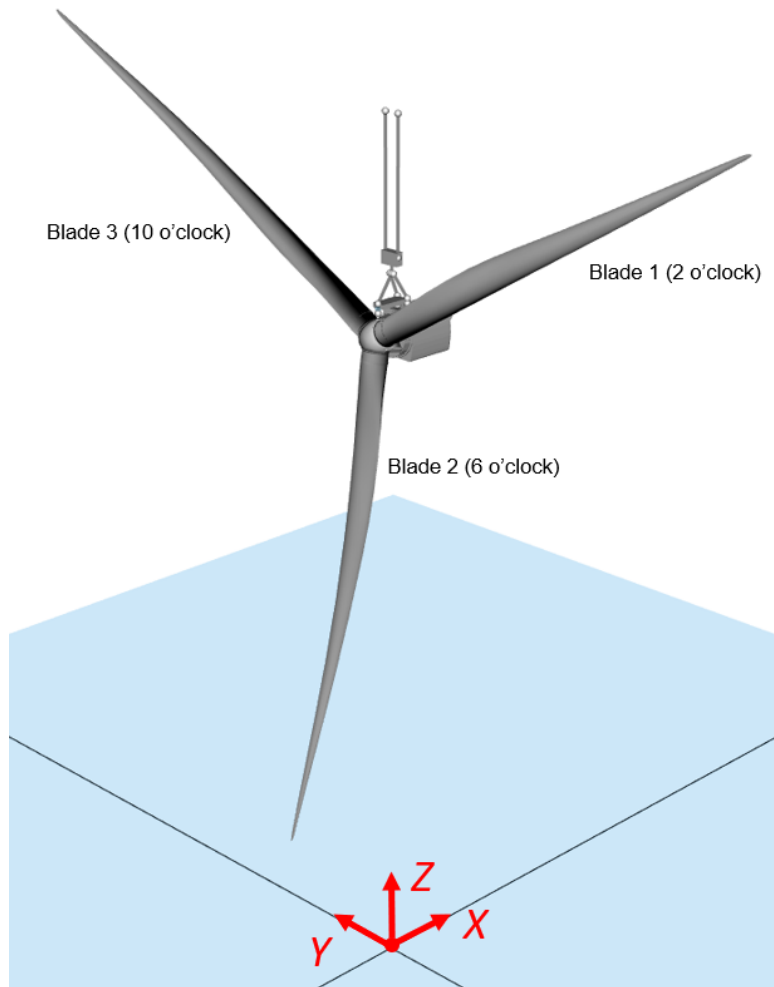
Figure 4.1: Overview of *Model 1 − Wind only*.

4.2. Mode shapes

To understand the dynamic behaviour of the RNA subjected to wind, a modal analysis is performed to identify eigenmodes and natural periods. If the RNA or pendulum is excited at a natural period, the motions can quickly become too large and thus the environmental excitation frequency and eigenmodes should be examined, which is done in this section.

The most relevant motions of the RNA suspended from the crane are pendulum motions and yawing (rotation around Z) of the RNA. These modes should be obtained and compared with the wind frequency range to see if these frequencies are close. If so, the pendulum length can be changed to change the natural frequency as well. An overview with four pendulum modes is presented in Ta-
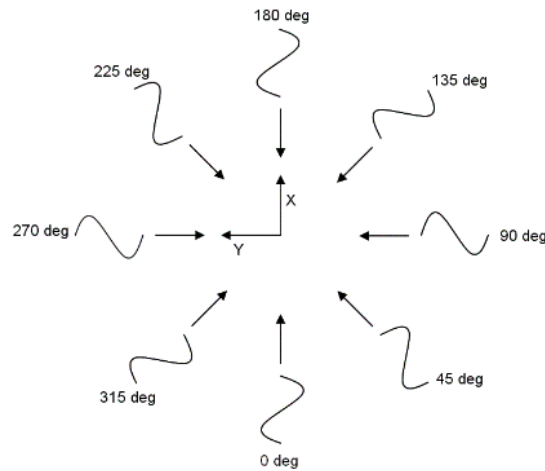
Figure 4.2: Definition of the wind direction with respect to the global coordinate system.
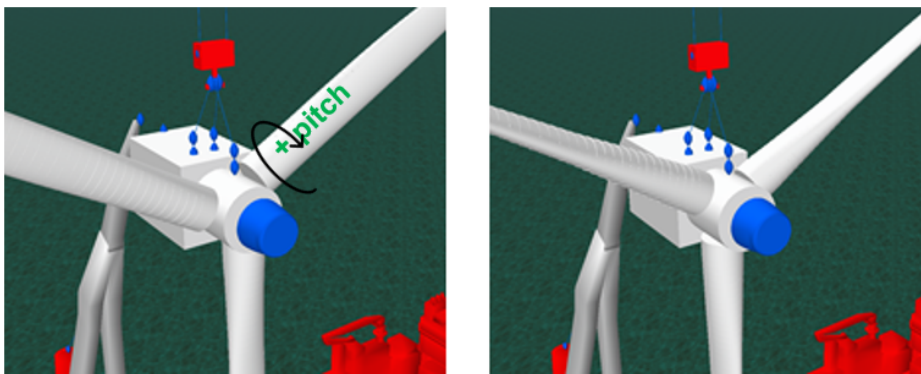
Figure 4.3: Definition of 0 deg (left) and 90 deg (right) pitch angle of the blades. For 90 deg pitch, the leading edge of the blade is at the front and the trailing edge is downwind.

ble 4.1, where a distinction is made between in phase and in anti-phase swinging of the crane block and RNA and forward or sideward swinging of the pendulum. Moreover, three different crane tip heights are used. Normally, there is no difference in forward or sideward swinging, as the pendulum is identical in both directions, however, in this case this is not true, because two hoist wires are used. Hence, the dynamic behaviour in both directions is different.

4.3. Results

In this section the results from *Model 1 − Wind only* are presented and discussed. First, analyses regarding the pitch angle of the blade is performed and thereafter the influence of the pendulum length on the dynamic behaviour is evaluated.

4.3.1. Blade pitch angle

Before determining which blade pitch angle is preferred during installation of the RNA, the forces and moments that are generated due to the wind for different conditions must be understood. As already explained in section 3.2, the load distribution and magnitude strongly depends on the wind direction and blade pitch angle, influenced by the cross-flow principle. First, the nacelle is fixed at a position to gain a better understanding of the static forces and moments for different conditions.

Table 4.1: Overview of four mode shapes and their natural periods of the RNA hanging below an Earth-fixed point. The pendulum length represents the vertical distance between the crane tip and RNA CoG. The length of the hoist wire is varied to see the effect on the natural periods. In phase of the crane block and RNA means that both bodies are swinging to the same side, while in anti-phase means that they are swinging in opposite sides. Sideward pendulum is defined as swinging in Y-direction, while a forward pendulum is in X-direction.

Crane tip height	Pendulum length	Crane block and RNA			
		In phase sideward pendulum	In phase forward pendulum	In anti-phase sideward pendulum	In anti-phase forward pendulum
200 m	53.8 m	17.1 s	16.8 s	10.4 s	6.25 s
190 m	43.8 m	14.9 s	13.9 s	9.15 s	5.91 s
180 m	33.8 m	13.7 s	11.9 s	7.19 s	4.63 s

Then, the RNA is hanging below the crane block, which is hanging below an Earth-fixed point to examine the dynamics of the system.

Static RNA

In this case the RNA is at a fixed position as where it would normally hang, but without crane block and slings. The wind direction is varied from -180 to 180 deg with steps of 15 deg, while the pitch angle of the blades is varied between 0 and 90 deg with steps of 15 deg. The effect on varying these two parameters on the aerodynamic forces and moments are analysed.

First, the loads on each blade is examined to identify the contribution of each blade to the total aerodynamic load. The results of this analysis are presented in Appendix B, providing forces and moments at the root of each blade in all directions for each blade for blade pitch angles of 0 and 90 deg and varying wind direction. Blade pitch angles between -90 and 90 deg are analysed, but are not all presented.

Next, the exact same analysis is performed, but in this case for all three blades fixed to the hub, as presented in Appendix C. Using the analysis of aerodynamic loads on each individual blade, the forces and moments acting at the RNA CoG are obtained and evaluated to see how each blade contributed to the total force and moment.

From the analyses is concluded that both 0 and 90 deg give promising results. In Figure 4.4 the same results are presented, but only for 0 and 90 deg to clearly identify differences between them. Furthermore, in Appendix C an uniform wind speed of 10 m/s is used, while in Figure 4.4 a vertical wind profile is used, as explained earlier. As a result, larger forces and moments are present. The forces and moments are reaction forces and moments and are defined in the global axis system.

The most important differences between 0 and 90 deg blade pitch are the GX and GY force and GZ moment. For a 0 deg wind direction and 0 deg pitch, the wind is hitting the rotor perpendicular to the chord of the blade, thus creating large drag forces. For 90 deg pitch this is not the case. For the results of the GY force, the wind hits the blade perpendicular for ± 90 deg wind direction and 90 deg pitch, creating large drag forces in Y-direction.

The yaw moment is important to keep the heading of the RNA the same while lifting, thus it is desired to keep the yaw moment as small as possible. For 0 deg pitch, the yaw moment does not change that much when varying wind direction and is also very small. Furthermore, a positive change in wind direction, results in a negative yaw reaction moment. This means that the yaw

moments actually tries to restore the yaw angle to 0 again. However, for the 90 deg pitch case, a positive wind direction change, results in a positive yaw moment as well and thus the nacelle yaws even more increasing the wind flow angle. Hence, this is unstable situation for wind directions between -15 and +15 deg. For wind directions beyond these angles, the yaw moment decreases again. Moreover, the curve is very steep compared to 0 deg pitch, which makes the situation even worse.
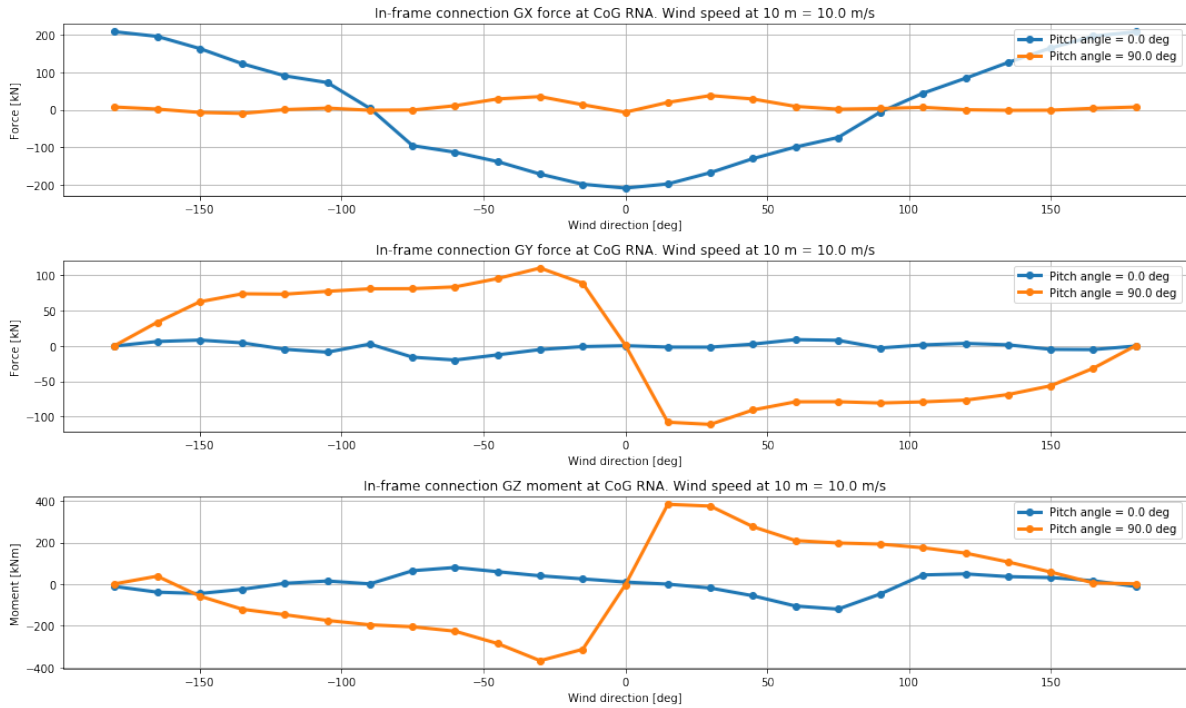
Figure 4.4: Static forces and moments (aerodynamic and gravity loads) at CoG of RNA for a wind speed of 10 m/s at 10 m with a vertical wind profile. The wind directions varies from -180 to 180 deg and for 0 and 90 deg blade pitch angle.

Dynamic RNA

Time domain simulations are performed to evaluate the dynamic behaviour of the RNA that is hanging below an Earth-fixed point with a crane block. The crane tip is at 185.0 m. Due to the two hoist wires, very little yaw stiffness in yaw direction is present in the system. From simulations is observed that the RNA is rotating in yaw with an amplitude of 500 deg, only then the hoist wires are able to yaw back the RNA. This yields meaningless results and thus a constraint is added to provide yaw stiffness that tries to keep the heading of the RNA within limits.

In Figure 4.5 1 h time series, without a 1000 s transient phase, are presented of the motion of the RNA in X, Y and yaw. A value of 5 kNm/deg is used as yaw stiffness and applied at the RNA CoG. One can observe that the amplitude of the yaw motion of the 90 deg pitch case is significantly larger than the 0 deg pitch case. This is because even though both yaw moments in the static case for 0 deg wind direction (Figure 4.4) are similar, a small deviation from this wind direction (due to a yaw response) results in a large change in yaw moment for 90 deg pitch. Therefore, the yaw will oscillate significantly more than with 0 deg pitch. Moreover, the slope of the 90 deg pitch curve between -15 and 15 deg wind direction is approximately 25 kNm/deg and thus the applied yaw stiffness of 5 kNm/deg is not sufficient to solve the instability in yaw motion.

As a result of these large yaw amplitudes, the motion in X and Y are also affected and are larger than for 0 deg pitch. Note that the response in X is larger than in Y, that is because a wind direction of 0 deg is towards X-direction and hence the RNA is more excited in X. This can also be observed in the magnitudes of the GX and GY force for this wind direction in Figure 4.4.
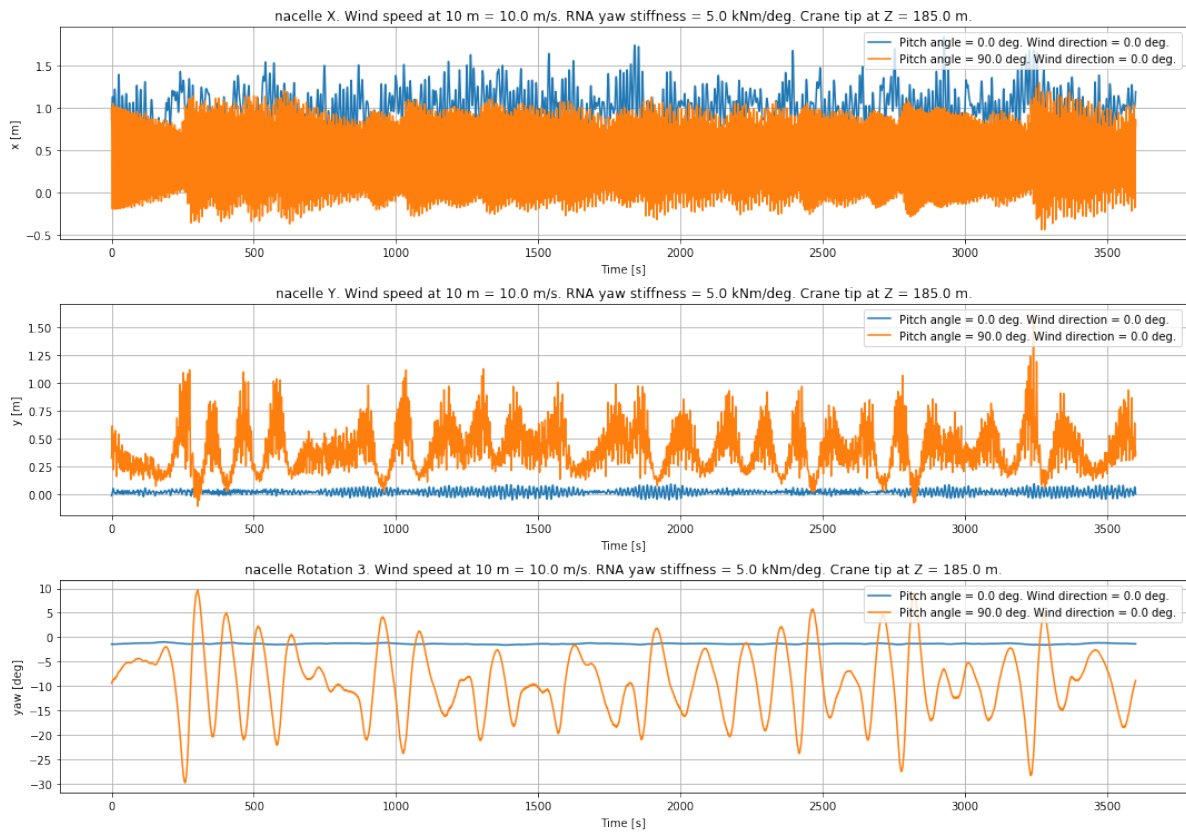
Figure 4.5: 1 h time series of the motion of the CoG RNA in X, Y and yaw for a wind speed of 10 m/s at 10 m, wind direction of 90 deg, Frøya wind spectrum, RNA yaw stiffness of 5 kNm/deg and with the crane tip at 185 m. This is simulated for both 0 and 90 deg blade pitch angle to evaluate the dynamic response in both cases.

The steep increment in yaw moment at 0 deg wind direction is only an issue for that wind direction. Therefore, in Figure 4.7, the same time series are presented, but with a wind direction of 90 deg (in Y-direction). As a result of this wind direction change, the RNA motion is excited in Y-direction, which can be seen in the magnitude of the responses in X and Y. Furthermore, the amplitude of the yaw motion of the 90 deg blade pitch is reduced compared to the 0 deg wind direction case. This can again be derived from the static aerodynamic loads – the change of yaw moment around a wind direction of 90 deg is less steep and thus the yaw moment fluctuates less, resulting in smaller yaw motions. Nevertheless, the magnitude of the yaw moment is larger than for the 0 deg blade pitch case and as a result still has a larger yaw motion response.

Conclusion
From this analysis can be concluded that a blade pitch angle of 0 deg yields the most favourable results compared to 90 deg blade pitch angle. More yaw stiffness is required to keep constrain the yaw motion in case of a 90 deg blade pitch angle, which is not favourable. Therefore, it is decided that blade pitch angle of 0 deg is chosen in further research. Note that the same analyses are performed for pitch angles between -90 and 90 deg, but only 0 and 90 deg are shown here.

4.3.2. Pendulum length

With the obtained blade pitch angle, the next step is to determine the effect of the pendulum length on the dynamic behaviour of the RNA subjected to wind. Then, the magnitude of the response due to wind only can be determined and a decision have to be made to include the response due to
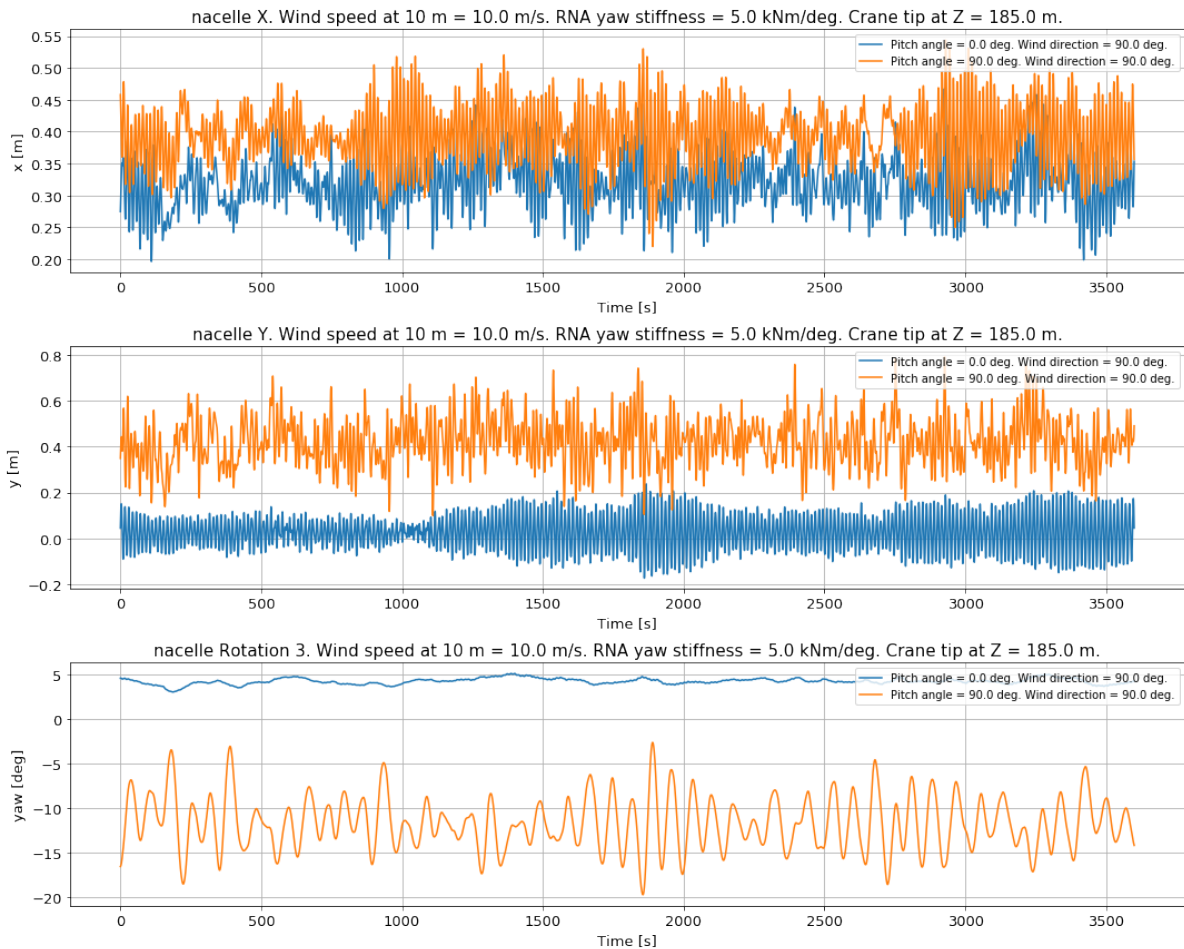
Figure 4.6: 1 h time series of the motion of the CoG RNA in X, Y and yaw for a wind speed of 10 m/s at 10 m, wind direction of 90 deg, Frøya wind spectrum, RNA yaw stiffness of 5 kNm/deg and with the crane tip at 185 m. This is simulated for both 0 and 90 deg blade pitch angle to evaluate the dynamic response in both cases.

wind, when also looking to the response due to waves. This is important, because the motions due to wind have to be controlled directly on the load, while for waves this can be compensated in the crane. Generally, the pendulum length is based on the wave frequencies, as the pendulum periods are often in the wave frequency range. Nevertheless, the excitation due to wind is examined.

Again time domain simulations are performed in OrcaFlex with a wind speed of 10 m/s at 10 m, Frøya wind spectrum, 0 deg blade pitch angle, RNA yaw stiffness of 5 kNm/deg. The varying parameters are the wind direction (0, 90, 180, 270) deg and crane tip height (200,195,190,185,180) m, which results in pendulum lengths ranging between 34 and 54 m.

PSD analysis

In Table 4.1 an overview is provided with the natural periods of the pendulum eigenmodes of the system for different pendulum lengths. It is important to understand at which frequencies the motions are oscillating and whether this is at an eigenmode or not. For this purpose, a power spectral density (PSD) is performed, which describes the distribution of the energy of the RNA motion into frequency components. PSD plots are made from time domain simulations, in this case 3 h to get more confident results.

An estimation of a single pendulum swinging period can be obtained according to Equation 4.1. From this can be derived that a longer pendulum results in a longer swinging period. Since the
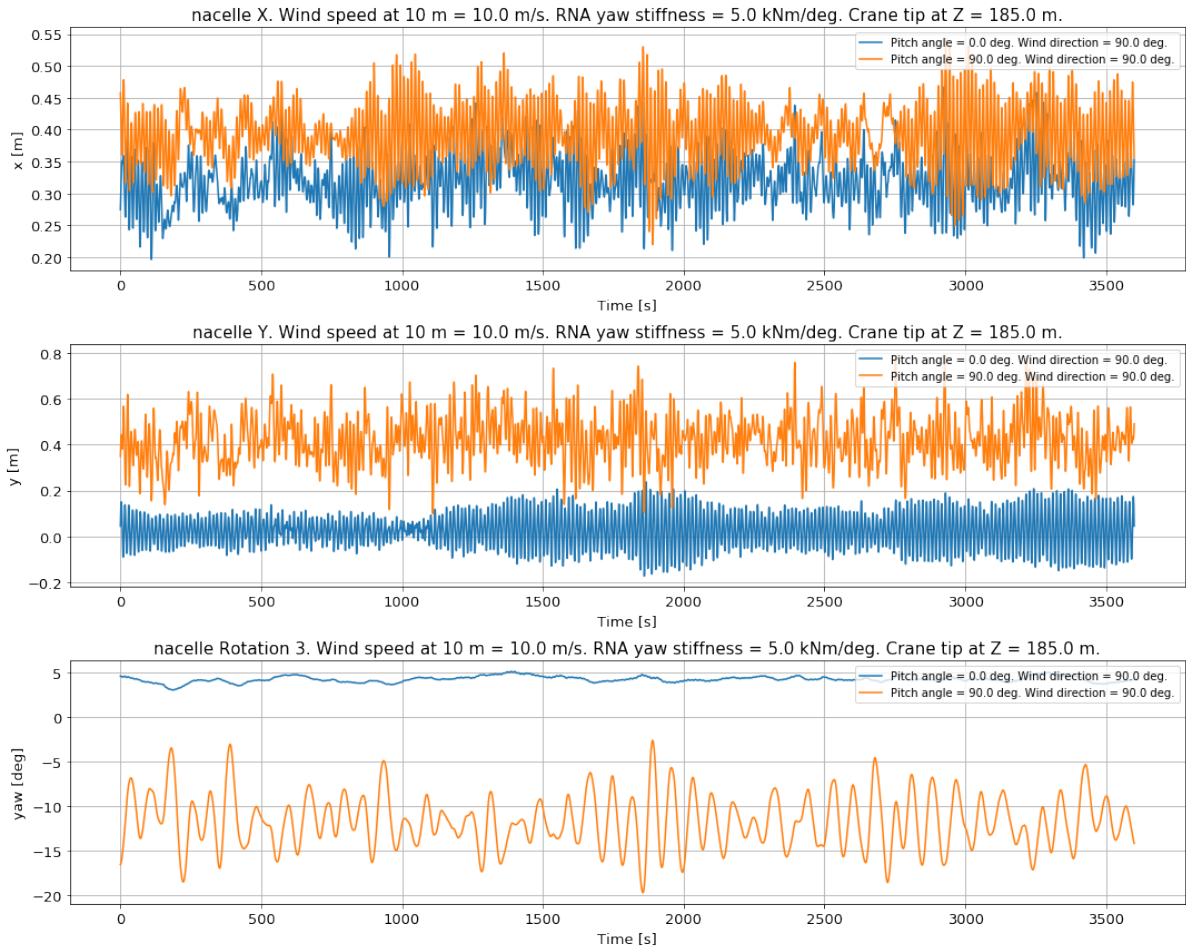
Figure 4.7: 1 h time series of the motion of the CoG RNA in X, Y and yaw for a wind speed of 10 m/s at 10 m, wind direction of 90 deg, Frøya wind spectrum, RNA yaw stiffness of 5 kNm/deg and with the crane tip at 185 m. This is simulated for both 0 and 90 deg blade pitch angle to evaluate the dynamic response in both cases.

wind spectrum is dominant in the low frequency range, this means that a longer pendulum is more excited by the wind than a shorter pendulum. Therefore, the response of the RNA with a crane tip height of 200 m should be larger compared to the response of a lower crane tip height.

$$T_n \approx 2\pi \cdot \sqrt{\frac{L}{g}} \tag{4.1}$$

In Figures 4.8 and 4.9 PSD plots are presented for 0 and 90 deg wind direction and 200, 190 and 180 m crane tip height for the RNA motions in X, Y and yaw. When looking first at 0 deg wind direction, one can observe that motion in X-direction is larger than in Y, due to the wind coming from X. Furthermore, the RNA is oscillating at its own natural frequencies, as derived in Table 4.1. The peaks shift to higher frequencies for smaller crane tip height, because the natural periods decrease accordingly. The small peak at the low frequency in X is due to a yaw eigen period of around 125 s, which originates from the added yaw rotational stiffness of the RNA. Moreover, the response for a longer pendulum is larger in X. In Y the pendulum length does not have an effect on the response, as the motion in Y is not really excited.

Next, the PSD plots for the 90 deg wind direction are analysed and as a result of this wind direction, the RNA response is excited in Y-direction, which can be seen when looking at the magnitude of

the spectral density. The peaks in Y are again at the natural frequencies of the system. The response in X is again excited at natural frequencies of the pendulum and also of the yaw eigen period. The reason that yaw affects the response in X, but not in Y, is because the RNA does not rotate exactly around the CoG, but with a slight offset. Therefore, when yawing the RNA, it also moves in X.
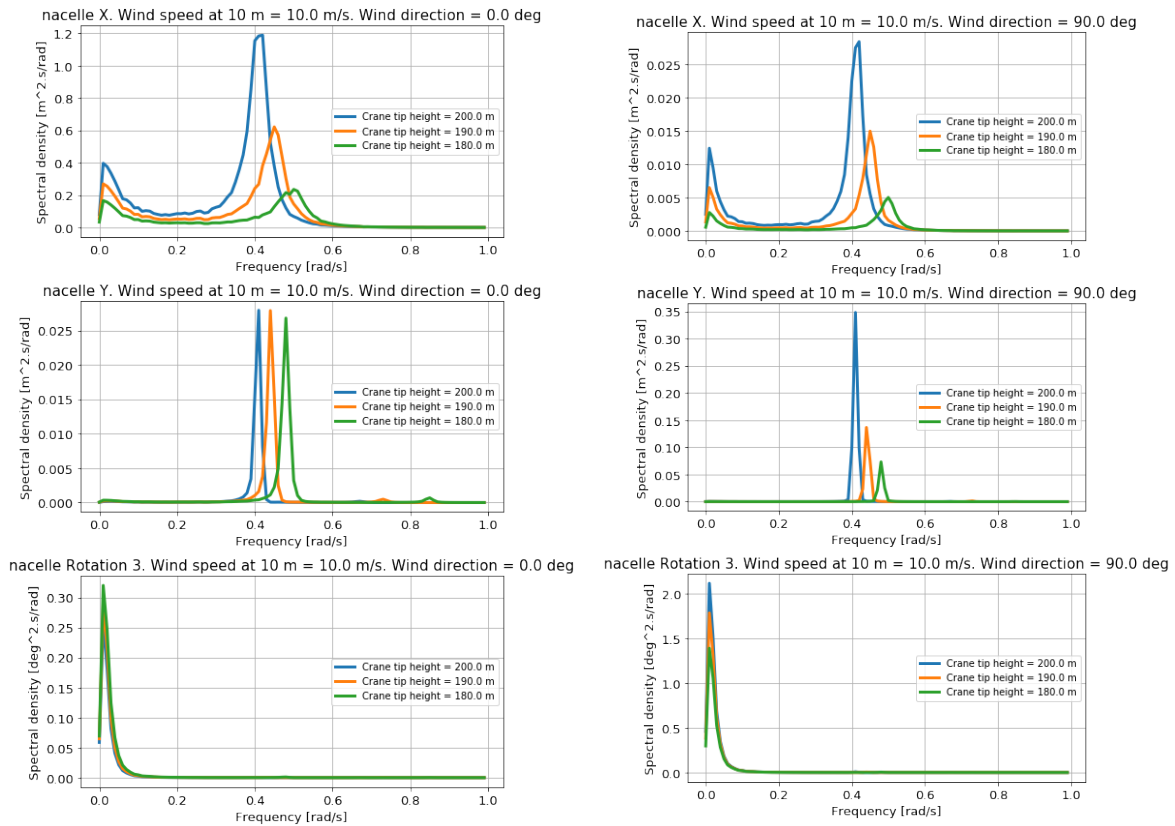
Figure 4.8: PSD plots of RNA at CoG for motion in X, Y and yaw for a wind speed of 10 m/s at 10 m, a wind direction of 0 deg and blade pitch angle of 0 deg. Three different crane tip heights are used.

Figure 4.9: PSD plots of RNA at CoG for motion in X, Y and yaw for a wind speed of 10 m/s at 10 m, a wind direction of 90 deg and blade pitch angle of 0 deg. Three different crane tip heights are used.

4.3.3. RNA responses

With the defined blade pitch angle of 0 deg, and the analysis regarding the effect of the pendulum length on the response, the next step is to get a clear overview of the response for different wind speeds and wind directions. This is done by showing station keeping plots of the RNA response in the horizontal plane, e.g. in X and Y, which are derived from 1 h time series by drawing a line around the maximum amplitudes. For the simulations, this was in a form of an ellipse. The station keeping plots allow for a quick method to analyse and compare in which direction the RNA moves and with what amplitude for varying wind conditions. Finally, significant responses are compared. In all simulations a yaw stiffness of 15 kNm/deg is applied to the RNA to fix the heading.

Effect wind speed on RNA response
First, the wind speed is varied between 4 m/s and 12 m/s to observe how the response differs with increasing wind speed. In this case the wind direction is set to 0 deg and crane tip height to 185 m. In Figure 4.10 the station keeping plot is presented of the RNA in global coordinates. The wind direction is also indicated in the figure.

Several effects of increasing wind speed can be identified from the figure. First, one can observe

that the response is larger for a higher wind speed, due to the larger aerodynamic loads. Second, the static position of the RNA is more 'pushed' backwards (towards positive X) due to the increased wind loads and third, the RNAs response is mainly in the direction of the wind, as observed earlier.

From the time series, the significant responses as SDA are determined as well for the different wind speeds and wind direction, as presented in Table 4.2. From these responses, an approximate relation is established between the significant response of the RNA and wind speed as defined in Equation 4.2. This relation fits the significant responses for 0 and 180 deg wind direction accurately, while for -90 and 90 deg, the relation deviates from the ratio. Still, it serves as a quick estimation on what the responses are for other wind speeds.

$$\frac{X_1 \text{ for } V_w = V_1 \text{ m/s}}{X_2 \text{ for } V_w = V_2 \text{ m/s}} \approx \left(\frac{V_w = V_1 \text{ m/s}}{V_w = V_2 \text{ m/s}}\right)^2 \tag{4.2}$$

Where X represents the significant response in SDA for each wind speed.
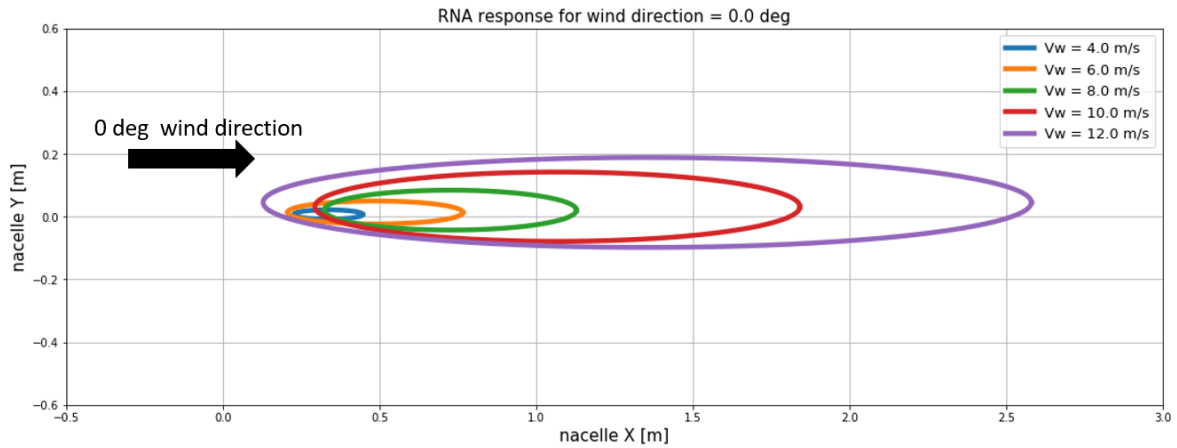
Figure 4.10: Station keeping plot of the RNA in X and Y for 0 deg wind direction and varying wind speed. The drawn lines represent the maximum amplitudes that occur during 1 h time simulations.

Table 4.2: Significant responses as SDA (4·std(X)) of the RNA CoG in X with varying wind direction and varying wind speed. Note that only the significant response in the main direction is given. For 0 and 180 deg wind, this is the response in X, for -90 and 90 deg wind, this is Y. Crane tip height of 185 m. 0 deg blade pitch angle.

	Significant response as SDA of RNA CoG			
Wind direction	0 deg	180 deg	-90 deg	90 deg
$V_{w,10m}$ [m/s]	X [m]	X [m]	Y [m]	Y [m]
2	0.032	0.032	0.002	0.004
4	0.135	0.135	0.006	0.013
6	0.310	0.310	0.018	0.046
8	0.566	0.566	0.033	0.145
10	0.880	0.879	0.058	0.172
12	1.28	1.28	0.079	0.238

Effect wind direction on RNA response

With the obtained results on the effect of wind speed on the RNA responses, the influence of chang-

ing wind direction on the RNA is examined next. In the PSD analysis regarding the pendulum length is already determined that the RNA moves in the direction of the wind and that the magnitude differs per wind direction. This is shown in more detail in this section. Again station keeping plots are used to provide a clear overview of different wind directions, as shown in Figure 4.11 of the RNA response in global X and Y. The wind directions used are 0, -90, 90 and 180 deg and a wind speed at 10 m of 10 m/s.

The responses from the wind from front and aft (0 and 180 deg) look familiar, while this is also the case for the two sides (-90 and 90 deg). The difference in the amplitude is significant. The reason that the difference is so significant is because for wind from the side, the drag forces are considerably smaller, as the frontal area is smaller. This is a result of the chosen blade pitch angle. The responses for both -90 and 90 deg are different, because for -90 deg, the wind hits the leading edge of the blade, while for 90 deg wind, the trailing edge is hit first. Consequently, the lift coefficient C_l from the airfoils is different (the drag coefficient is approximately the same) and thus, different loads are generated. Time series of the forces and moments in X, Y and Z due to aerodynamic loads and gravity of the rotor at the hub are provided in Appendix D, showing the difference in the magnitude of the loads for the different wind directions.
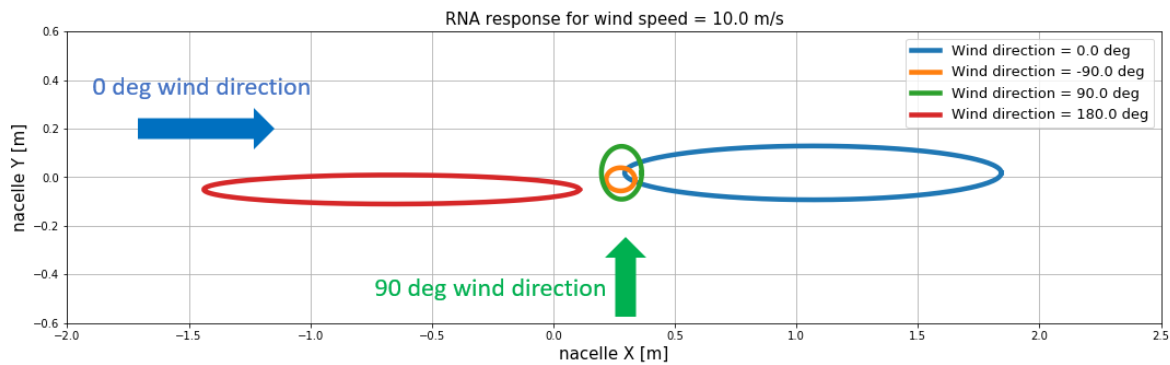
Figure 4.11: Station keeping plot of the RNA in X and Y for 10 m/s wind speed at 10 m and varying wind directions. The drawn lines represent the maximum amplitudes that occur during 1 h time simulations.

Statistics of RNA response
After identifying and understanding the effect of wind speed and direction on the responses of the RNA, statistic values are presented in this section that allow for an easy way to compare the input parameters on the responses.

In Figure 4.12 the significant responses as SDA of the RNA motion in X, Y and yaw are plotted against the pendulum length. Furthermore, 4 different wind directions are shown, a wind speed of 10 m/s at 10 m is used and a 0 deg blade pitch is used.

In all cases, the response in X and Y increase for a longer pendulum length, as explained earlier. Furthermore, the magnitude of the response in X and Y depends on the wind direction as determined earlier as well. The small response for the -90 deg wind direction is clearly visible. A final remark has to be made on the yaw response, which does not depend on the pendulum length. The yaw eigen period is around 125 s and only varies ± 2 s.

4.4. Conclusion

The purpose of this model is to look into the behaviour and response of the RNA hanging below the crane block, which is suspended from an Earth-fixed point, representing the crane tip, focusing on
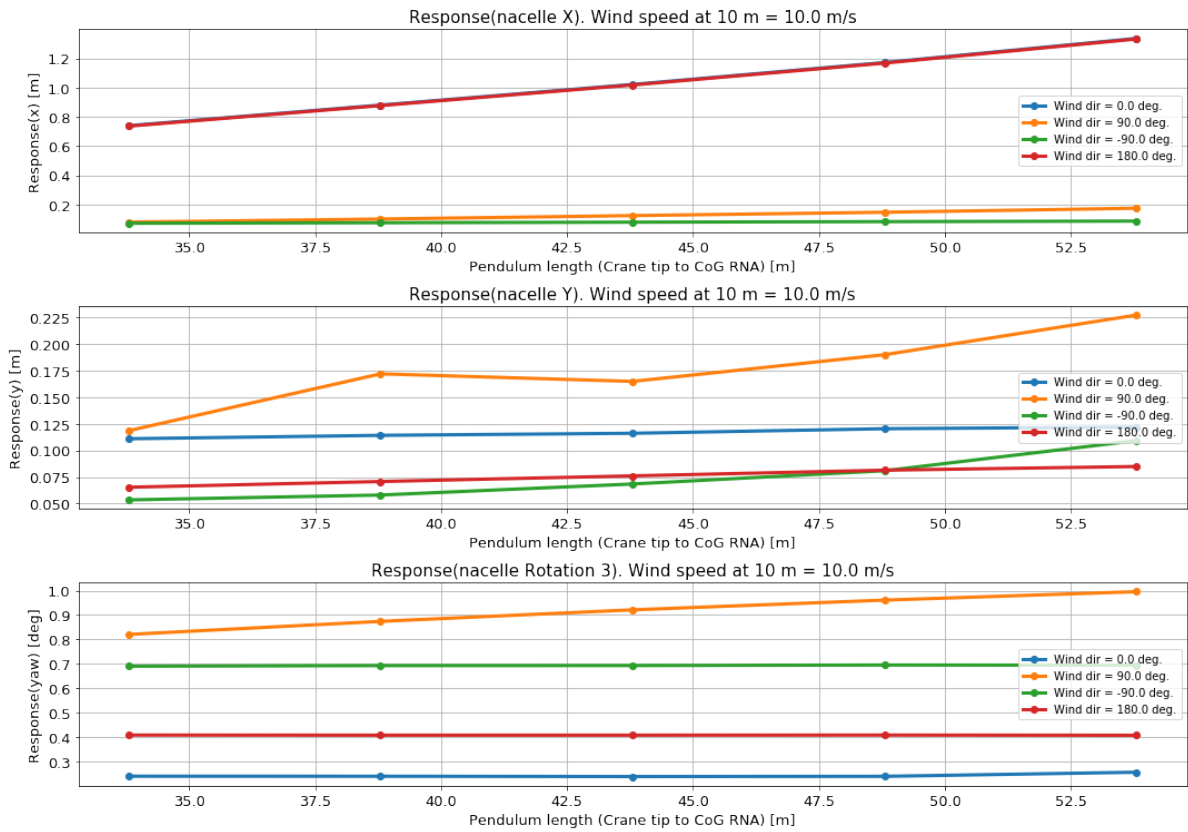
Figure 4.12: Significant response as SDA (4·std(X)) of the RNA motions in X, Y and yaw for different pendulum lengths. The wind direction is varied between 0, -90, 90, 180 deg, the wind speed is 10 m/s at 10 m height and a blade pitch angle of 0 deg is used.

the response due to the wind only and to determine whether the wind must be included to simulate and control the RNA responses.

First, it is determined that a blade pitch angle of 0 deg results in the smallest motions. Then, the influence of the length of the hoist wires is examined, from which is concluded that longer hoist wires are more excited by the wind, because the wind is dominant in the low frequency range. Furthermore, it is derived that a small yaw stiffness is required to fix the heading of the RNA.

It is determined in this model, that by choosing the optimal blade pitch angle and hoist wire length, the RNA responses due the wind only, can already by reduced by a significant amount. Still, the significant RNA responses are up to 1.25 m for wind from the front and 10 m/s wind speed at 10 m and thus cannot be disregarded. While the wind speed is a given input and cannot be changed, this is not the case for the wind direction, as the RNAs heading can be changed. This is however, limited, because the RNA is hanging in the crane. Nevertheless, it can be concluded that the wind should be included to accurately model the RNA response.

<div align="right">

5

</div>

Model 2 – Waves Only

The next step to analyse the dynamic behaviour of the RNA suspended from the crane is to examine the motions due to waves only. The model is analysed in the frequency domain. This is performed in Liftdyn. From this tool the motions of the RNA for different conditions is evaluated, such as wave conditions and crane configurations to understand how the system behaves in different conditions.

The same approach is used as for the wind only case, first an overview of the model used in the analysis is provided in section 5.1, followed by a modal analysis to gain insight in the dynamic behaviour in section 5.2. Finally, the results are presented in section 5.3 and parameters that influence the behaviour of the RNA are identified and conclusions are drawn in section 5.4.

5.1. Model overview

This section provides an overview of *Model 2* of this research, where wind is not included, but only waves. The Earth-fixed point where the RNA was suspended from *Model 1* is now replaced by the installation vessel with a crane. An important difference is that the rotor is replaced by a simple rigid body with equal mass, CoG and radii of gyration. Even though the rotor would move through the air due to the wave-induced motions, the aerodynamic loads generated by the rotor is assumed to be negligible.

Another change is made in this model compared to *Model 1*, which is a simplified crane block. Where in *Model 1* a crane block is used with a hinge and swivel, this is not the case in this model. The essence of Liftdyn lies in having a have simple model that is easy to understand that allows for a quick method to determine the responses of your system. Therefore, the crane block is modelled as a 6 DoF rigid body with the same properties as the crane block with a swivel and hinge.

A 9.0 m draft is used for the vessel, which is based on the weight of the RNA. The vessel can change its draft by ballasting water by using its ballasting tanks. These tanks make sure that the vessel remains horizontal by checking the trim and heel. Basically, the result of ballasting the vessel is changing the vessel's CoG and mass and this depends on the slew angle, radius of the crane and mass of the load.

The global coordinate system used the model is shown in Figure 5.1. The global origin is at Mean Sea Level (MSL) at the stern, keel of the vessel. The local coordinate system of the vessel is also at stern, keel, but $z = 0$ m is at the bottom of the vessel. Hence, the vessel is at $Z = -9$ m. The crane slew in the figure is 0 deg and the angle increases positive in clockwise direction when looking at $X - Y$ plane from above, so a crane slew angle of 90 deg points to starboard. The definition of the direction of the incoming waves is presented in Figure 5.2.
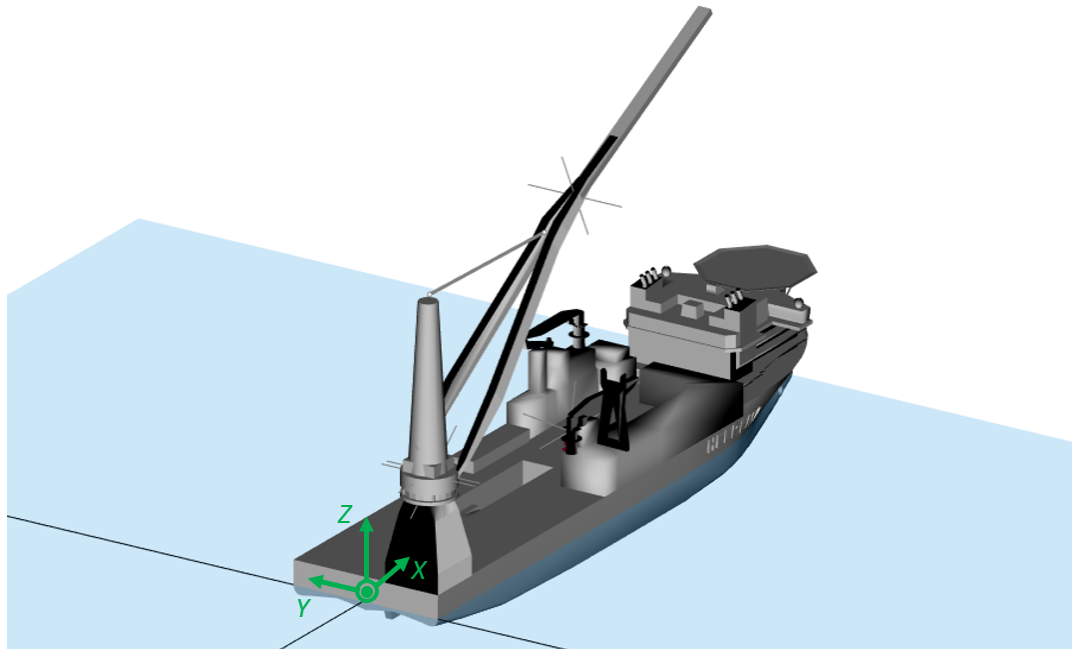
Figure 5.1: The global coordinate system used in *Model 2 − Waves only*, which is defined at MSL and stern, centerline of the vessel.
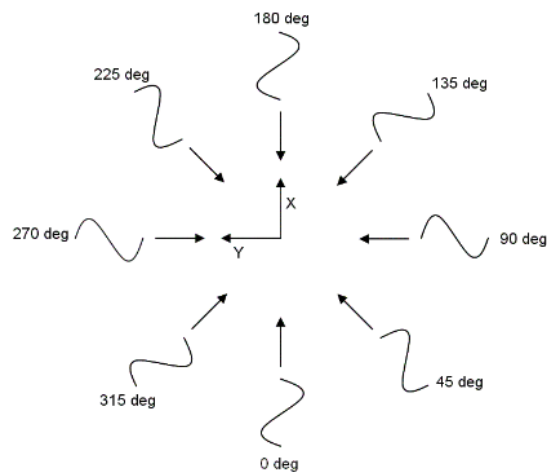
Figure 5.2: Definition of the waves direction with respect to the global coordinate system.

5.2. Mode shapes

A modal analysis is performed to gain a better understanding of the dynamic behaviour of the system. Whereas in *Model 1*, the RNA and crane block were modelled, now a third 6 DoF body is added, the vessel. Note that the crane is rigidly attached to the vessel and is also considered as a rigid body. The position of the crane can be changed, but is then fixed to the vessel.

In Liftdyn the mode shapes are determined by solving the eigenvalue problem as shown in Equation 5.1. Since the added mass matrix is frequency dependent, the natural frequencies depend on the chosen frequency. In Liftdyn the selected frequency is the median of the frequency range of which the added mass is known. In this case, this is at 1.0 rad/s, as the hydrodynamic database contains the added mass and damping values between 0.025 and 2.0 rad/s.

Table 5.1: Mode shapes of vessel without crane in Liftdyn.

Mode shape		Natural period [s]	Natural frequency [rad/s]
1	Yaw	246	0.0255
2	Sway	206	0.0305
3	Surge	170	0.0370
4	Roll	11.1	0.566
5	Heave	9.55	0.658
6	Pitch	9.16	0.686

$$\left[-\omega^2 \left(\mathbf{M} + \mathbf{A}(\omega)\right) + \mathbf{K}\right] \cdot \hat{X} = 0 \tag{5.1}$$

Where ω is the wave frequency, $\mathbf{M}$ is the mass matrix, $\mathbf{A}$ is the frequency dependent added mass matrix and $\mathbf{K}$ is the stiffness matrix, containing the hydrostatic terms and restoring terms from the DP system.

The mode shapes of the vessel without crane boom are presented in Table 5.1. The vessel's roll, heave and pitch are within the frequency range of waves.

Then, the same modal analysis as in *Model 1* can be performed to identify the mode shapes of the RNA and crane block. Those depend again mainly on the length of the hoist wire making the pendulum shorter or longer and are thus equal to the mode shapes obtained in *Model 1*. However, the motion of the vessel and the RNA are coupled, meaning that the motions influence each other. Mainly the roll and pitch motion of the vessel affect the motion of the RNA, especially since the crane boom is located at the stern, port side of the vessel. Furthermore, the slew angle of the crane changes the response of the RNA, as that determines due to what kind of vessel motions, the RNA motion is induced. Therefore, the mode shapes of the total coupled system cannot be obtained, as the crane configuration is not set yet.

5.3. Results

This section discusses the results of the waves only case. First, the vessel and RNA responses are obtained for varying wave directions. Then, the effect of crane slew and radius on the response of the RNA is examined. The significant responses are determined as shown in Equation 3.18.

5.3.1. RNA response

RAOs of the vessel in all 6 DoF are obtained from internal documents (HMC). From the RAOs, the response of the vessel can be determined as explained in section 3.5. The same approach is used to obtain the RNA responses at the CoG for all 6 DoF, which are shown in Figure 5.3. Three wave directions are shown, 180 deg (head seas), 135 deg (quartering seas) and 90 deg (beam seas). From these responses is concluded that 180 deg waves results in the smallest motions of the RNA. With this wave direction, the vessel pitch motion is excited. At a wave peak period of 11.0 s, the pitch response is 5 times larger than at a 7.0 s wave, while for roll response, this factor is 3. The vessel pitch and roll directly affect the crane tip motion and that in turn excites the RNA response.

The magnitude of the significant response of the RNA due to wave-induced motions, is also con-

siderably larger, when comparing to the RNA significant responses due to the wind. For a wave condition of $H_s = 1.0$ m and $T_p = 11.0$ s, the significant response of the RNA in X is 7 m, while for wind-induced motions, it is up to 1.25 m for a wind speed of 10 m/s.

Significant response as SDA for Hs = 1.0 m
JONSWAP with gamma = 1.0 - cos^2 spreading
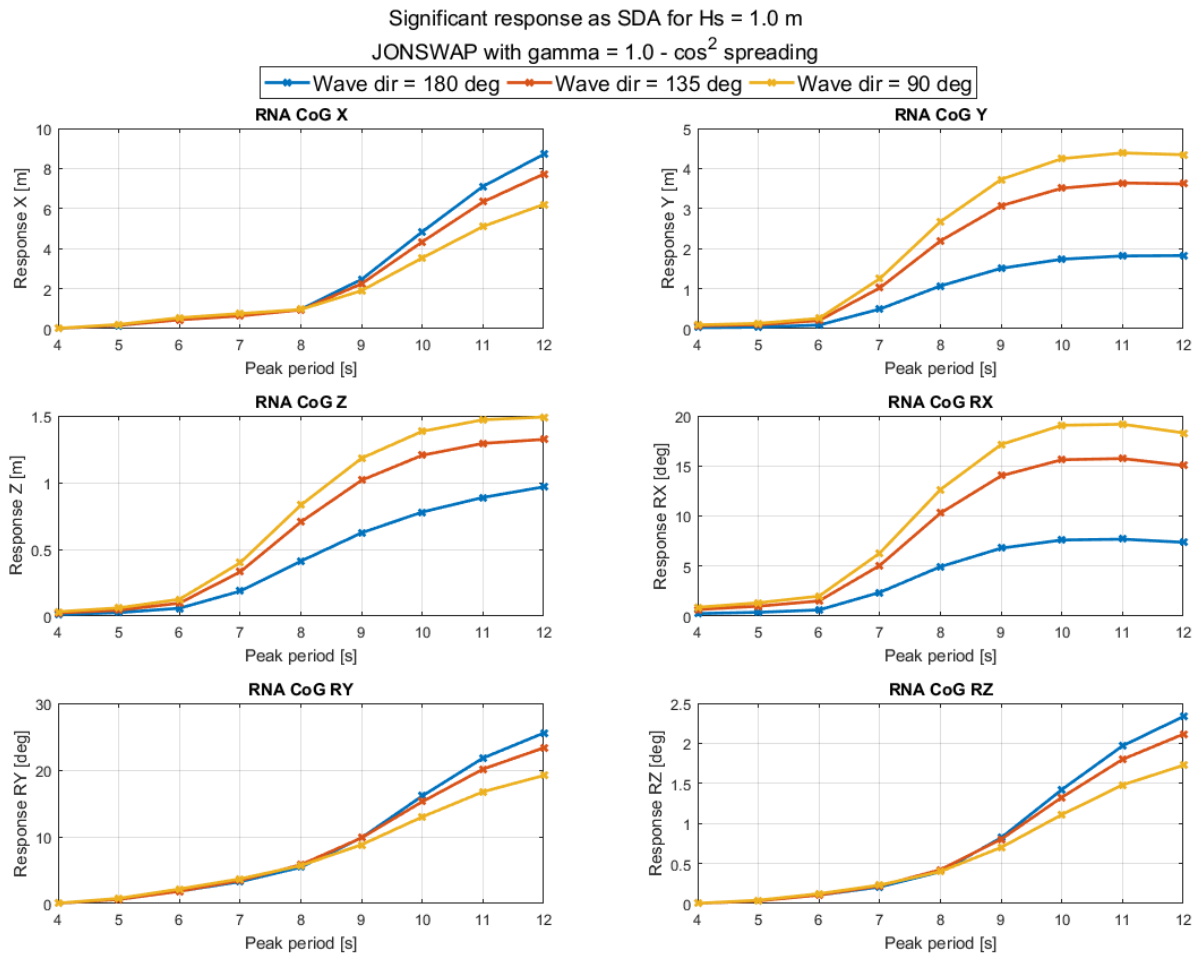
Figure 5.3: Significant response as SDA (4·std(X)) of RNA motions with $H_s = 1.0$ m and varying T_p. Wave spreading is used with spreading exponent 2. Crane tip is at 180 m, slew angle 270 deg.

5.3.2. Crane slew

The crane slew determines the position of the crane with respect to the vessel. The angle is defined as 0 deg for the crane pointing to bow, 90 deg to starboard and 270 deg to port side. In Figures 5.5 and 5.6 the definition of crane position is also visualised. Note that the RNA rotates along with the crane, so that the backside of the nacelle is pointing towards the crane boom. As explained in the modal analysis, the position of the crane affects the behaviour of the RNA, which is examined in this section.

Two different crane slew angles are used: 90 and 270 deg. Note that because the crane mast is not located at the centerline, the position of the RNA with respect to the vessel centerline for the 270 deg slew case is smaller than 90 deg slew, while having the same crane tip height. Due to the shift in location of the RNA in both cases, the static equilibrium of the system changes as well. When setting the crane slew, the vessel is ballasted again to have even keel and trim. As a result, the vessel CoG changes to the opposite direction where the crane is pointing. When the crane is at 90 deg slew, the ballast tanks at the port side of the vessel have to be filled and the vessel CoG shifts accordingly to

the port side.

Furthermore, the natural periods of the 90 and 270 deg slew case stay approximately the same − the natural period changes less than 0.25 s.

In Figure 5.4 the significant responses as SDA are presented. A wave direction of 180 deg is used, with a JONSWAP wave spectrum with $H_s = 1.0$ m and varying T_p, without spreading. From the figure can be observed that for RNA motion in X, RY and RZ are similar. The yaw motion is not excited by the waves and is thus very small, only 1 deg double amplitude per meter H_s for a 10 s wave. The motion in X and RY is excited by the pitch motion of the vessel (RY) and the slew angle is not affecting that response, but the magnitude of RY is significant due to 180 deg waves. The motion in Y and RX on the other hand, are excited by the roll motion of the vessel and that does have an effect on the RNA response. Since for 90 deg slew the vessel CoG is further from the centerline than for the 270 deg case, the roll motion of the vessel is larger and as a result, the RNA motion is more excited.
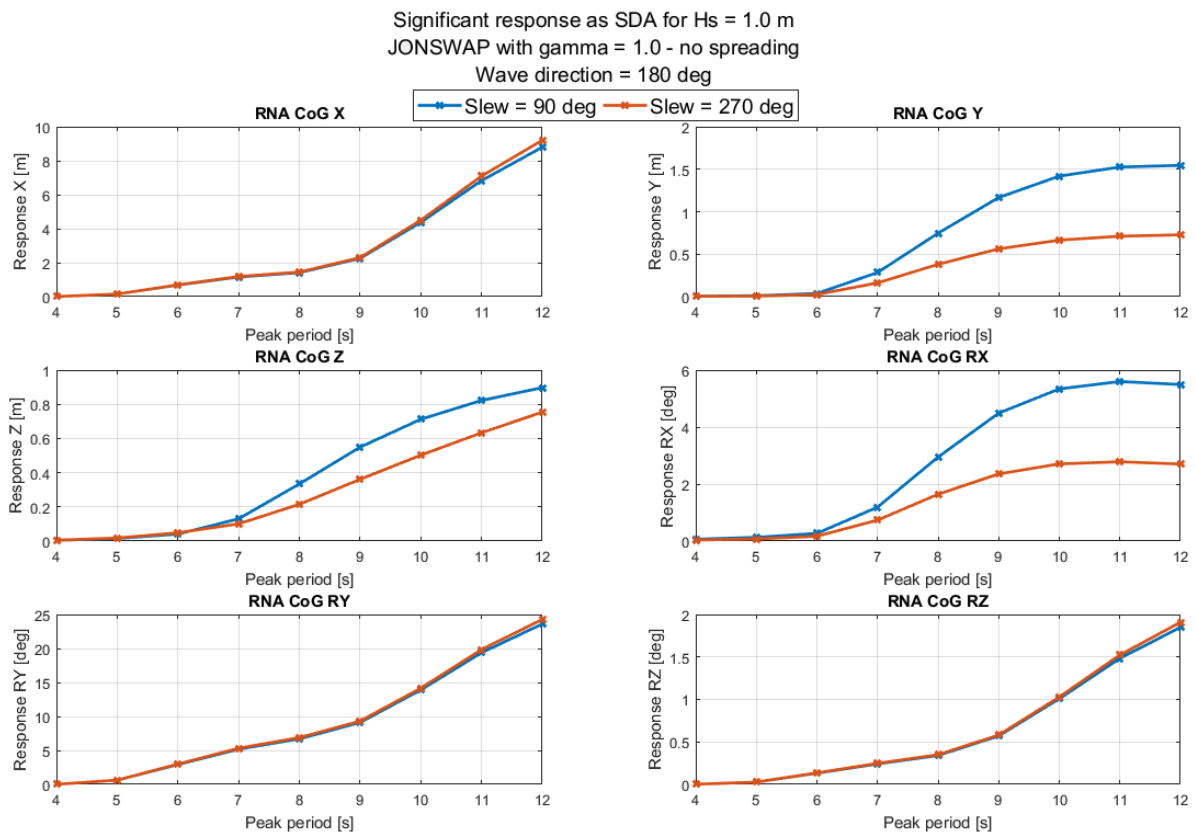
Figure 5.4: Significant responses as SDA ($4 \cdot \text{std}(X)$) of the motion of the RNA without any constraints in all 6 DoF, defined in global coordinate system. The crane slew angle is varied between 90 deg (pointing starboard) and 270 deg (pointing port side). The crane tip is set to a height of 185 m.

5.3.3. Crane radius

The crane radius is defined as the horizontal distance between the crane block and hinge of the crane boom on the vessel. By increasing the crane radius, the crane boom has to boom down to get the reach required. Since the nacelle is fixed at a height, 2.5 m above the tower, which is at 138 m, this means that changing the radius of the crane, the crane is boomed up or down. As a result, the crane tip is raised or lowered and thus the pendulum length changes. This is also what is looked into in *Model 1* by changing the height of the points where the hoist wires are connected to.
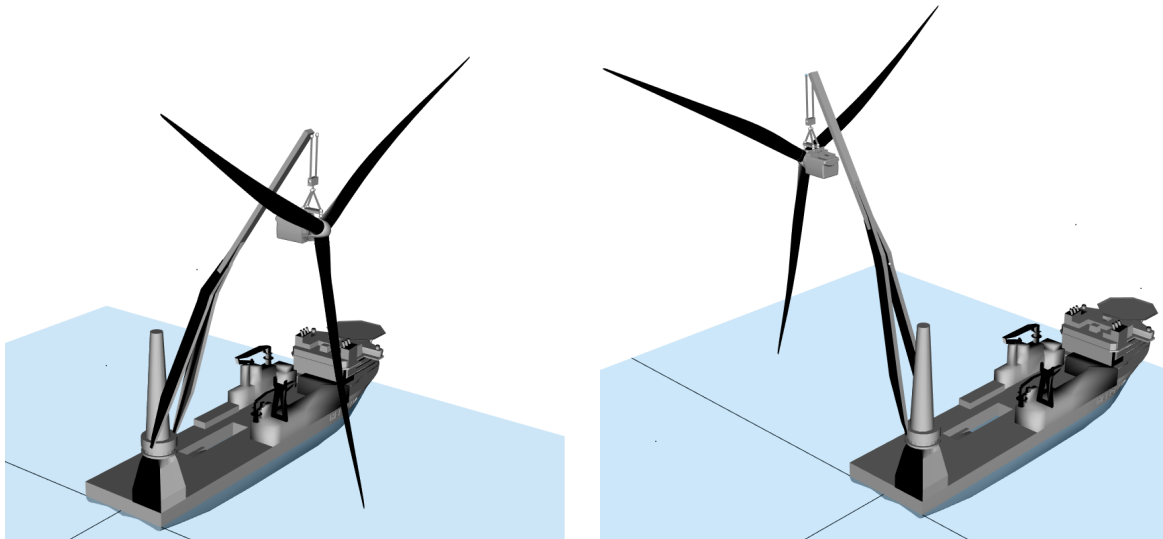
Figure 5.5: Slew angle of 90 deg and crane radius of 52 m. Crane tip height is 190 m.

Figure 5.6: Slew angle of 270 deg and crane radius of 64 m. Crane tip height is 185 m.

In Figures 5.5 and 5.6 two situations are shown with two different crane radii, 52 m and 64 m, resulting in crane tip heights of 190 m and 185 m, respectively. One can observe that the hoist wires are shorter in the 64 m crane radius case and thus the pendulum period is shorter as well, changing the behaviour of the system.

In the analysis a third crane radius is added of 74 m, resulting in a crane tip height of 180 m. The responses with the varying crane radii are determined in Liftdyn and the results are presented in Figure 5.7. When observing the magnitudes of the responses, the motions in X and RY are large, this is the sideward pendulum of the RNA, that is swinging in the direction of the waves, due to the pitch of the vessel. Since no spreading is used, the response in Y and thus RX is very small, as the vessel roll is very small as well. For the 180 m crane tip height, the response in RY is significantly smaller for the peak periods between 6 and 9 s and consequently the same thing happens in X due to a different pendulum length and thus natural period. From this can be concluded that the response depends on the wave period and thus the crane radius best for the operation depends on the wave climate.

5.4. Conclusion

The purpose of the waves only model is to look into the dynamic behaviour of the RNA, when the vessel is subjected to waves. It is identified that the vessel response heavily depends on the wave conditions (wave height, period and direction). It can be concluded that the vessel response yields the most favourable motions of the RNA for head seas (180 deg) on the vessel. In that case, the pitch motion of the vessel is excited and that excites the crane tip motion and that in turn excites the sideward pendulum of the RNA.

Furthermore, analyses is performed on the crane configuration, slew angle and crane radius. It is observed that with a slew angle of 270 deg (crane pointing to port side) yields the smallest motions of the RNA. This means that in case of wind waves, where wind and waves come from the same direction, the rotor experiences a wind from the side, which is a wind direction of -90 deg, as defined in the coordinate system in *Model 1*. This is the wind direction that yields a significant response of below 0.10 m for 10 m/s wind speed at 10 m. When comparing the magnitudes of the significant
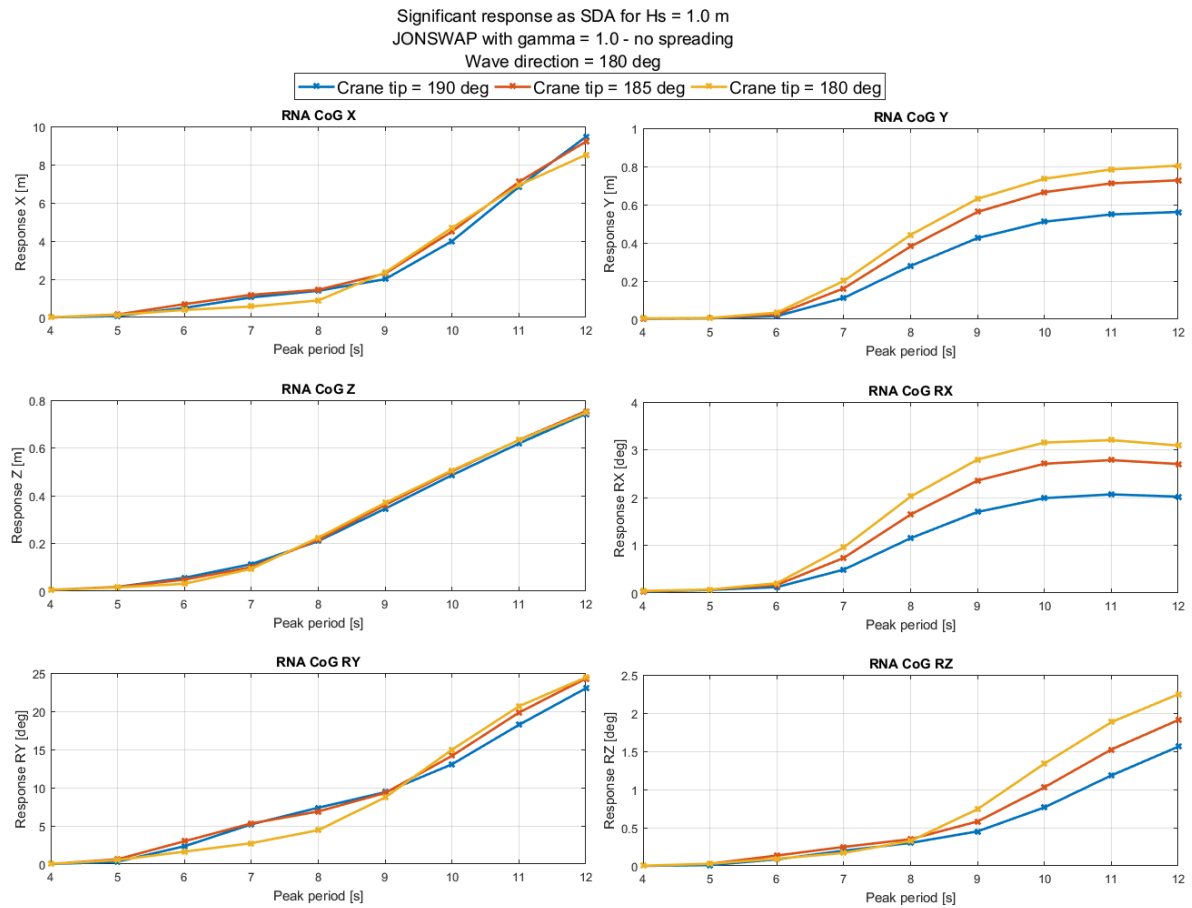
Figure 5.7: Significant responses of the RNA in SDA ($4 \cdot \text{std}(X)$) without any constraints in all 6 DoF, defined in global coordinate system. The crane radius is varied between 52, 64 and 74 m, resulting in crane tip heights of 190, 185 and 180 m.

responses for wind and wave-induced motions, one can conclude that the wave-induced motions are governing, as the significant response is up to 7 m for 11.0 s peak period waves. In the next model, the wind and waves are coupled in OrcaFlex in time domain simulations, to further elaborate on this conclusion.

6

Model 3 – Wind & Waves

After analysing the wind and waves only cases in the previous two chapters and understanding the behaviour, the next step is to add the wind and waves together in the coupled model in OrcaFlex to run time domain simulations. In both the wind and waves only case, it is identified that the direction of how the RNA pendulum is swinging in the crane depends mainly on the direction of the wind or waves. In this chapter the conditions of the incoming wind and waves are varied to see how this affects the response of the RNA.

First, an overview of the coupled model in OrcaFlex is shown in section 6.1. Then, a modal analysis is performed in section 6.2 and compared with Liftdyn mode shapes. A short analysis on the vessel DP system in performed in section 6.3. Finally, the results and conclusions are presented and discussed in sections 6.5 and 6.6.

6.1. Model overview

The same model is used as in the waves only case, but since the wind is accounted for, the rotor has to be modelled again, to incorporate the aerodynamic effects due to the wind on the rotor. Therefore, the body resembling the rotor in *Model 2 – Waves only* is replaced by the rotor again from the wind only case.

The model used in OrcaFlex is presented in Figure 6.1, which also shows the global coordinate system. Note that the same coordinate system is used as in *Model 2*. The same wind and wave direction definition is used as in previous models, but is shown in Figure 6.2 again for clarity. However, do note that in *Model 1*, the RNA orientation with respect to the global coordinate system was different. In this model the RNA is pointing towards positive Y, while in *Model 1* this was towards negative X. Hence, the wind direction used in *Model 1* represents a different wind direction with respect to the RNA. Furthermore, the RNA significant responses are reported as local significant response of the RNA and not in the global coordinate system. This is done to better identify what the RNA motions exactly are. If the RNA is slightly yawed and shows a local roll response, this also contributes to the global pitch response. The local axis system of the nacelle is shown in Figure 6.3.

6.2. Mode shapes

The mode shapes from *Model 2* do not change when modelling the rotor blades, because the mode shapes depend on rigid body motions and the mass, CoG and radii of gyration do not change.

Figure 6.1: Overview of *Model 3 - Wind & Waves*. The global coordinate system is shown as well, which has its origin at MSL, stern, centerline of the vessel.
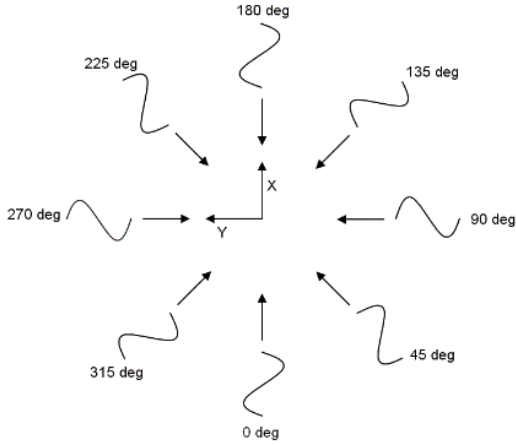
Figure 6.2: Wind and wave direction definition in the global coordinate system.
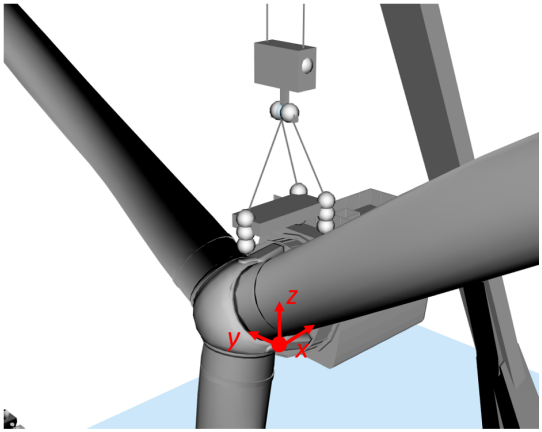
Figure 6.3: Local axis system of the nacelle.

There is however, a difference in determining mode shapes of the vessel in Liftdyn and OrcaFlex. As explained, in Liftdyn the natural periods are determined at the median of the given frequency range of the hydrodynamic database, because the added mass is frequency dependent. In OrcaFlex, the added mass matrix is only accounted for, when it is constant. If not, the added mass is not included in the modal analysis. As the vessel's added mass is frequency dependent, it is hence not included. As a result, the natural periods from modal analysis in Liftdyn and OrcaFlex are not the same. It is however, of importance that the same vessel and its properties are used in this model as in *Model 2*. The natural periods can be compared by performing a free decay test in OrcaFlex − the vessel is given an initial displacement or rotation and is released at $t = 0$ s. Note that this is only the vessel, no RNA or crane boom. In Table 6.1 the results are presented. Note that the natural periods can deviate from these values, as it depends on loading condition, position of the crane and crane load.

Table 6.1: Mode shape comparison of the vessel in Liftdyn and OrcaFlex. The OrcaFlex natural periods are derived from a free decay test. Note that the natural periods can deviate from these values, depending on loading condition, position of the crane and crane load.

Mode shape		Liftdyn T_n	OrcaFlex T_n
1	Yaw	246 s	243 s
2	Sway	206 s	208 s
3	Surge	170 s	168 s
4	Roll	11.1 s	11.4 s
5	Heave	9.55 s	9.30 s
6	Pitch	9.16 s	9.20 s

6.3. Vessel DP system

In Table 2.1 the stiffness and damping values of the DP system of the vessel were presented. However, after adding the wind, a yaw instability of the vessel was encountered in the model. For a 270 deg wind direction, the wind is acting perpendicular to the rotor plane, creating large drag forces of the rotor, which can be up to 200 kN for a wind speed of 10 m/s at 10 m. Since the crane is located at the stern of the vessel, this drag load creates a large yaw moment around the vessel CoG. With the wind spectrum being dominant in the low frequency range, where the yaw natural period of the vessel is as well, the consequence is that the yaw motion of the vessel is excited. This issue is solved by adding more yaw stiffness to decrease the yaw natural period to around 100 s. With the yaw natural period of around 250 s, this means that the 'new' yaw stiffness must be 2.5^2 times larger. Thus, the yaw stiffness becomes $21.82 \cdot 10^3$ kNm/deg. The yaw damping of the DP system, which was defined as 50% of the critical damping is also updated to $38.34 \cdot 10^3$ kNm.s/deg.

6.4. Load cases

Simulations are performed to evaluate the effect of the wind speed using two sets of wave conditions. The first H_s T_p combination is 2.0 m and 6.5 s; this is a wave climate with reasonable short waves, but with high amplitude. It is expected that the RNA responses are less excited by the this wave peak period, due to small vessel responses as concluded from *Model 2*. Hence, the wave height is increased. The second combination is a H_s and T_p of 1.0 m and 11.0 s. With these wave conditions, it is expected that the RNA response is excited due to the wave peak period that excites the vessel pitch response. Additionally, the wind speed is varied between 0, 5 and 9 m/s. In this way, the contribution of the wind can be evaluated. The crane tip is set at 180 m. The wind and waves are coming from the same direction, representing wind waves. Furthermore, spreading of the waves is

used with a spreading exponent of 2.0 and the directional spreading spectrum is discretised into 11 directions, as explained in section 3.3.

6.5. Results

In this section the results are presented and discussed for the coupled simulations of wind and waves. The wind and wave conditions are varied to see how the response of the RNA changes.

6.5.1. Vessel response

In this section the vessel response for the two wave cases are examined. This is done to gain a better understanding how the vessel response affects the RNA response.

In *Model 2* is concluded that for higher wave peak periods (> 8 s), the vessel pitch response is excited. The same conclusion can be drawn for the vessel roll response.

To gain a better insight on how the vessel response affects the RNA response, the crane tip motion is shown in Figure 6.4. One can clearly observe that for $H_s = 1.0$ m and $T_p = 11.0$ s, the crane tip motion is significantly higher, which is a result of the vessel pitch response that is dominant. When looking at the magnitude of the crane tip motion for $H_s = 2.0$ and $T_p = 6.5$ s, one can say that if the RNA exactly follows the crane tip motion, the significant responses of the RNA are relatively small. This is a valuable input requirement for a method for mitigating the RNA horizontal motions. On the other hand, for larger wave peak periods, the RNA should not follow the crane tip − the RNA should follow the opposing motion of the crane tip. Again, this is valuable input for reducing the RNA motions.

6.5.2. RNA responses

In Table 6.2 the significant responses as SDA are presented for the different environmental conditions. Note that the responses of the RNA are given in the local coordinate system of the body. To get a better overview on how the RNA is moving, station keeping plots of the nacelle significant response in x and y are plotted in Figure 6.5. These elliptical shapes are borders around the maximum amplitudes of the motions and allow for a quick method to analyse the RNA response for different environmental conditions, rather than an accurate comparison. Furthermore, 1 h time series of all DoF of the RNA at CoG are presented in Appendix E.

From the results can be observed that the RNA responses for wave case 1 are significantly smaller than wave case 2. This is also what is concluded from Figure 5.7 in *Model 2*, because both the roll and pitch response of the vessel is larger for longer peak periods, affecting the RNA response. Furthermore, in all cases the RNA is excited in the y and Rx motion, which corresponds to the sideward pendulum of the RNA. The sideward pendulum is excited because of the wind and wave direction. The magnitude of the response is large, so mitigation of the horizontal motions is required. In Figure 6.5 is clearly visualised how the motion of the RNA is beyond the limits. One can also observe that the waves are the main contributor to the RNA response, the effect of increasing wind speed is small.

For wave case 1, the significant response as SDA in x is very small and equal for 0 and 5 m/s wind speed. However, when the wind is increased to 9 m/s, the significant response doubles, while it remains the same for the significant response in y. This means that the wind is exciting the motion of the RNA in x. Moreover, the wind decreases the yaw significant response of the RNA for increasing wind speed, for both wave cases. This is due to the increased restoring yaw moment from the wind. Note that a yaw stiffness of 15 kNm/deg is applied at the RNA relative to the crane boom.
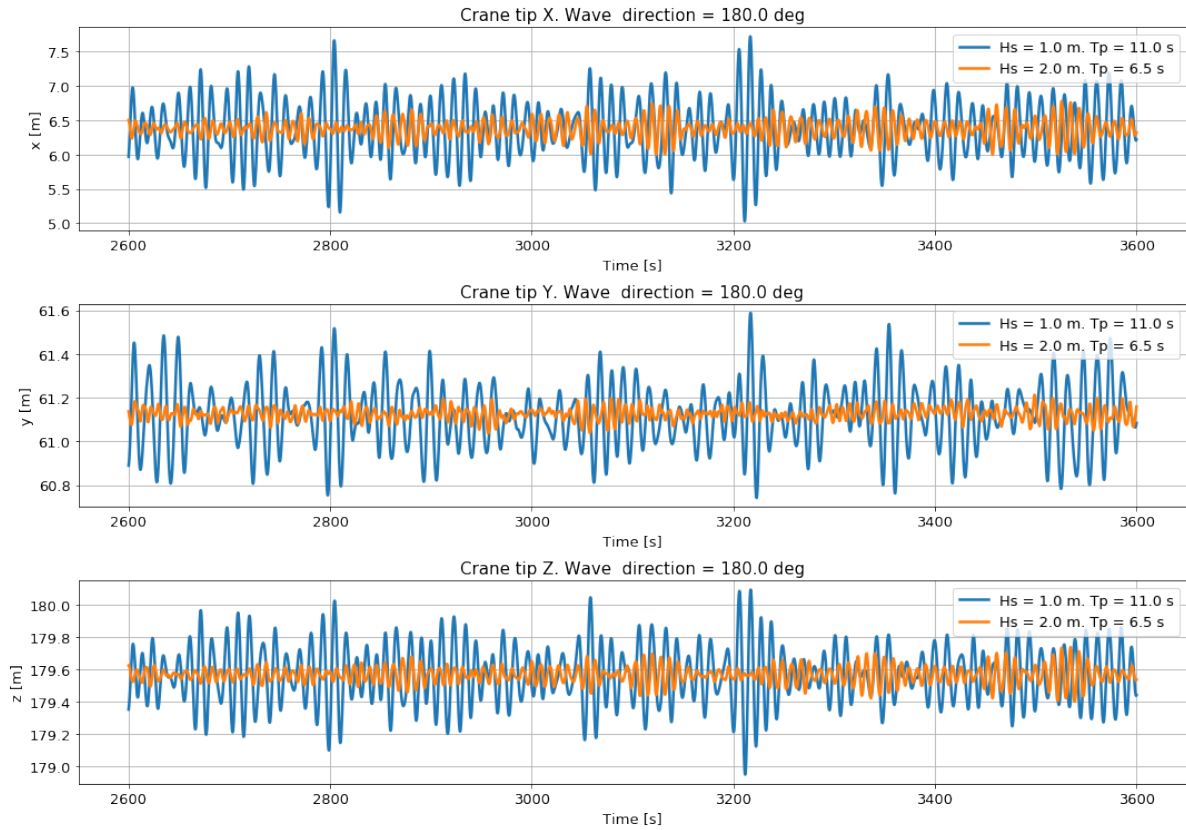
Figure 6.4: Crane tip motion in X, Y and Z for the two different wave conditions with the free hanging RNA. With wind speed at 10 m = 9.0 m/s.

Table 6.2: Significant responses as SDA (4·std(X)) of the RNA for different wind and wave conditions. Both the wind and wave direction is 180 deg. Note that the RNA responses are given in the local body coordinate system.

Waves H_s and T_p	Wind $V_{w,10m}$	Significant response as SDA of RNA				
		x [m]	y [m]	Rx [deg]	Ry [deg]	Rz [deg]
1. $H_s = 2.0$ m, $T_p = 6.5$ s	0 m/s	0.30	2.3	8.1	1.9	4.4
	5 m/s	0.30	2.2	8.0	1.4	3.8
	9 m/s	0.60	2.2	7.8	1.3	3.1
2. $H_s = 1.0$ m, $T_p = 11.0$ s	0 m/s	1.4	8.5	30	5.0	7.9
	5 m/s	1.1	7.6	27	3.4	5.9
	9 m/s	1.1	6.8	25	2.6	5.3

6.5.3. PSD analysis

A PSD analysis is performed to evaluate at what frequencies the responses are oscillating, the results are presented in Figures 6.6 and 6.7. The RNA responses in x, y, Rx and Ry are shown, because in x and Ry the effect of wind speed is visible and y and Rx correspond to the governing sideward pendulum motion.

When looking at the PSD plots for x and Ry, one can see that for 0 m/s wind speed for both wave cases, there is only one excitation peak, which is around 10.0 s (= 0.65 rad/s) for wave case 1 and 10.5 s (= 0.6 rad/s) for wave case 2. These two excitation ranges correspond to a forward pendulum mode shape coupled with vessel pitch of 9.5 s (= 0.66 rad/s). When the wind speed increases, these peaks

(a) $H_s = 2.0$ m, $T_p = 6.5$ s and varying wind speed.

(b) $H_s = 1.0$ m, $T_p = 11.0$ s and varying wind speed.
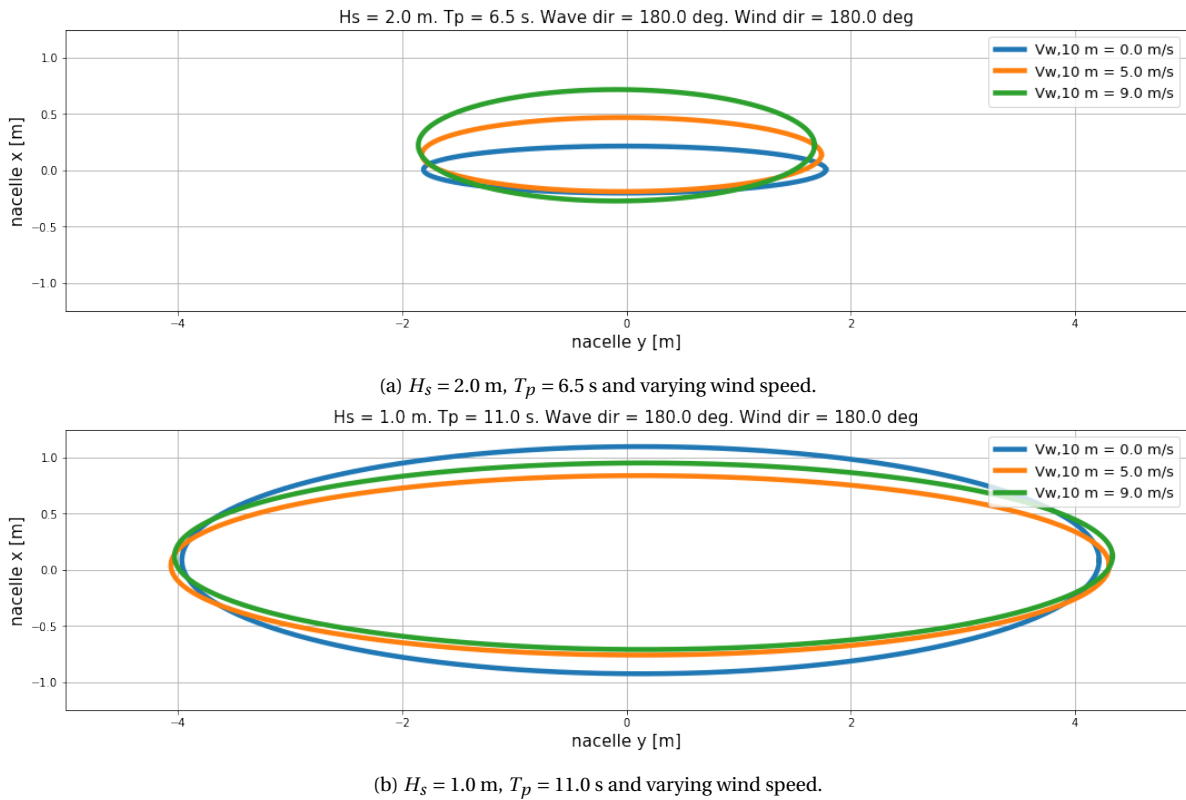
Figure 6.5: Station keeping plot of the RNA in x and y position for varying wind speeds. The drawn lines represent the maximum amplitudes that occur during 1 h time simulations.

are decreasing, while a peak < 0.1 rad/s is growing, corresponding to a yaw eigen period of both the vessel and RNA that is excited by the wind. One can thus conclude that the x and Ry response of the RNA is governed by the waves without wind, but the wind is becoming more dominant with increasing wind speed.

The PSD plots for y and Rx of the nacelle are identical for wave case 1, which is oscillating around 8.0 s (= 0.8 rad/s). This is a sideward pendulum mode shape with RNA and crane block in anti-phase coupled with vessel pitch. The motion in y and Rx are coupled, because the RNA is both rolling and moving to the side at the same time. However, when looking at the PSD plot for wave case 2, the peaks are shifted to around 14.0 s (= 0.45 rad/s) which is also an sideward pendulum mode shape, but with RNA and crane block swinging in phase. As expected, the different peak period excites other mode shapes.

Furthermore, the peaks of y and Rx do not shift to other frequencies with increasing wind speed, hence no other modes are excited by the wind, which was the case for x and Ry. Therefore, the wind is actually damping the sideward pendulum of the RNA. With a sideward pendulum, the RNA is moving into and away from the wind direction, changing the relative velocity of the wind and RNA continuously. As a result, the aerodynamic loads change as well − when the RNA is moving into the wind, the relative velocity increases, creating a larger drag force and thus the pendulum is slowed down more. When swinging to the other side, the relative velocity decreases and a smaller drag force is generated. This is aerodynamic damping. The reason that the aerodynamic damping increases with wind speed is because the aerodynamic loading scales with V_w^2, thus the damping force is larger for higher wind speeds.
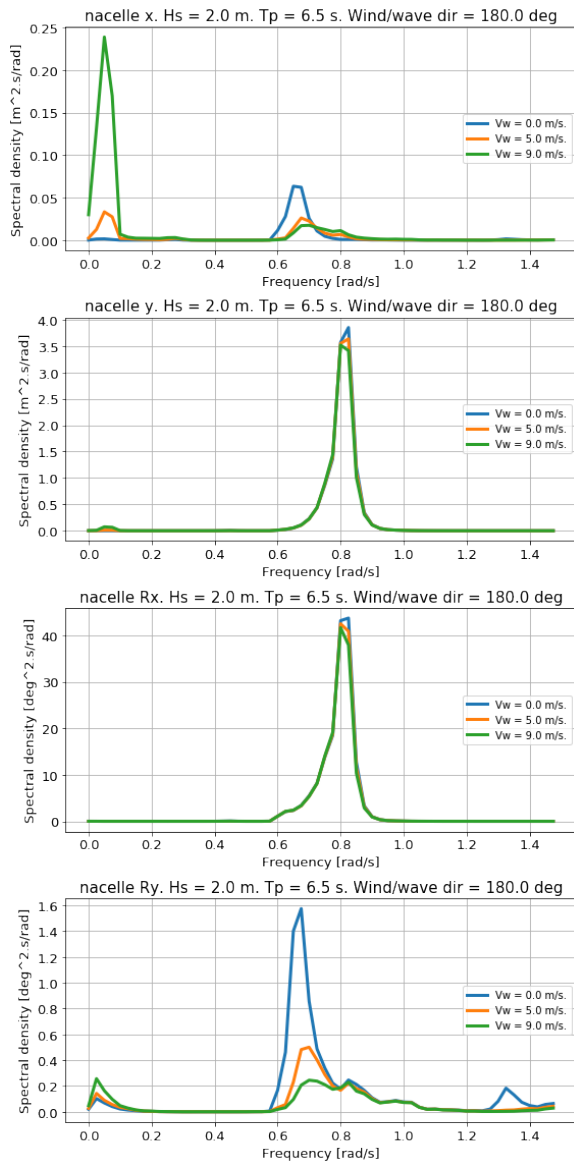
Figure 6.6: PSD plots of RNA at CoG for motion in x, y, roll Rx and pitch Ry for $H_s = 2.0$ m, $T_p = 6.5$ s and varying wind speed.
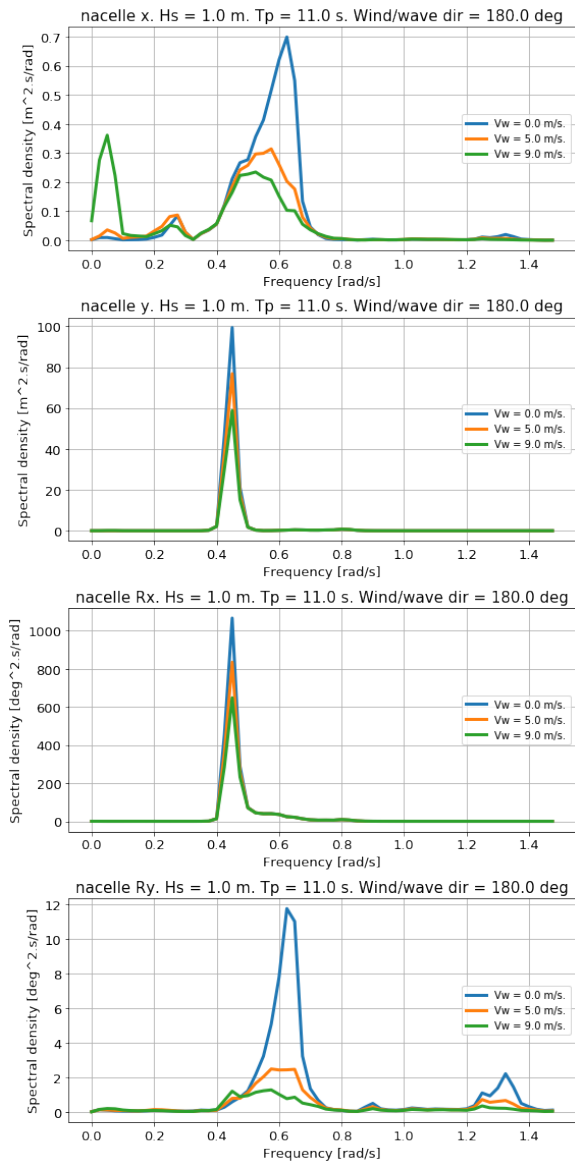
Figure 6.7: PSD plots of RNA at CoG for motion in x, y, roll Rx and pitch Ry for $H_s = 1.0$ m, $T_p = 11.0$ s and varying wind speed.

6.6. Conclusion

Time domain simulations have been performed with two different wave conditions and three different wind speeds. This is done to clearly identify how the wind speed influences the response of the RNA due to waves, which was expected to be governing. Furthermore, only wind and waves from 180 deg direction are used to simulate wind waves. If swell waves are considered, the wind can come from another direction, which is not done in this model.

The two wave conditions excite different mode shapes, as expected, which are mainly the sideward pendulums, in phase and in anti-phase of the RNA and crane block, coupled with vessel pitch motion. The wind speed is not changing the complete behaviour of the system, especially not the sideward pendulum of the RNA. It does change the forward pendulum with increasing wind speed. Furthermore, the effect of aerodynamic damping of the rotor is visible. In *Model 1* is also concluded that the response of the RNA due to wind is not significant for the wind direction used in this case.

Thus, the small effect of the wind on the responses were expected to be small.

Overall, it can be concluded that main requirement to control the motion of the RNA is to reduce the sideward pendulum. Moreover, for shorter wave peak periods, the relative motion of the RNA and crane boom should be as small as possible, as the crane tip motion is small. This serves as valuable input for the development of a concept that has to reduce the RNA motions. For higher wave peak periods, the RNA should not follow the crane tip motion, because those motions are too large.

<div style="text-align: right; font-size: 4em;">7</div>

Case Study: Tugger Line Control

Extensive analyses are performed in *Models 1*, *2* and *3* on modelling and understanding the dynamic behaviour of the RNA during installation. It is also shown that, depending on the environmental conditions, the RNA responses are such that it can be difficult to land the RNA on top of the tower. Therefore, the RNA response has to be controlled by restraining its motions. This can be done by using tugger lines, a generally used method in the offshore industry because of its simplicity and versatility, which are wires that run on winches and can be payed in or payed out, changing the tension of the wire. In this chapter, a case study is performed to evaluate if the model is suitable to assess the effectiveness on reducing horizontal motions of the RNA. This is done by implementing a tugger line system. The coupled wind and waves model from Chapter 6 is used.

First, different tugger winch modes are explained in section 7.1 and the model overview is presented in section 7.2. Then, the modelling of an ideal tugger line system is explained and implemented in the model in section 7.3. The effect on the response of the RNA is evaluated and results are presented. Next, the ideal tugger line system is translated into a physical representation to show that the model can be used for further analysis of motion control of the RNA in section 7.4. Finally, the conclusion of the case study is established in section 7.5 and future implementations of tugger line systems in the model is discussed in section 7.6.

7.1. Tugger winch modes

The winches on which the tugger lines run, can be operated in different modes – on brake, constant tension and damping – and are briefly discussed in this section. In all cases, the tugger lines are connected to the RNA at one side and to the crane boom at the other side. In reality, the lines run via sheaves through the crane boom back to crane house. In the model, the tugger lines provide stiffness or damping in the relative motion between the crane boom and RNA.

If the winch is put on brake, the tugger line is fixed to a length and is not payed in or out by the winch. Pretension can be applied to the lines, to make sure that with the fluctuation of the tension during the operation, the tension on the lines remains positive, to avoid slack lines and possibly snapping of the lines. Basically, with this winch mode, the tugger line is modelled as a spring with the stiffness being dependent on material properties.

The second winch mode is the constant tension. With this mode the winch is set to a specified tension and remains at this tension by paying in and out the winch accordingly. In theory, this means that this does not have an effect on the dynamics of the system, as it is a static force. In practice

Figure 7.1: Overview of *Model 3 - Wind & Waves*. The global coordinate system is shown as well, which has its origin at MSL, stern, centerline of the vessel.

however, the winch cannot follow the desired pay in or out velocity exactly and thus fluctuates a bit, resulting in damping of the motion. This deviation from reality can be modelled in OrcaFlex by defining winch deadband, winch stiffness effects and damping and drag forces that are proportional to velocity and velocity squared, respectively.

Damping winches changes the tension on the lines based on the pay in or out velocity of the line. When the load moves away from the winch, the tension is increased to pull back the load, while the tension is decreased when the load moves towards the winch. In this way damping of the motion is applied.

7.2. Model overview

The same coordinate system is used as in *Model 3* in Chapter 6 and is shown here again. Figure 7.1 presents the global coordinate system, Figure 7.2 defines the wind and wave direction in the global coordinate system and Figure 7.3 shows the local coordinate system of the RNA.

7.3. Tugger lines as constraints

When connecting tugger lines between the RNA and crane boom, a spring damper is added to the system, providing stiffness or damping in the relative motion between the RNA and crane boom. By connecting these lines in such a way, certain DoFs can be constrained, while other DoFs can still be free. In order to get a clear understanding of what the effect is on adding a tugger line on the RNA, an ideal tugger line system is used, that can provide stiffness or damping in each DoF as desired. A real tugger line connected between the RNA and crane boom that is connected for example in X, also provides stiffness in Y if the RNA moves in Y. Therefore, it is more straightforward to understand if a stiffness or damping is provided in a DoF. This can be achieved by making use of constraints in OrcaFlex, which are objects in OrcaFlex that provide an enhanced and versatile method to connect objects in the model. It is important to note that these constraints define stiffness or damping
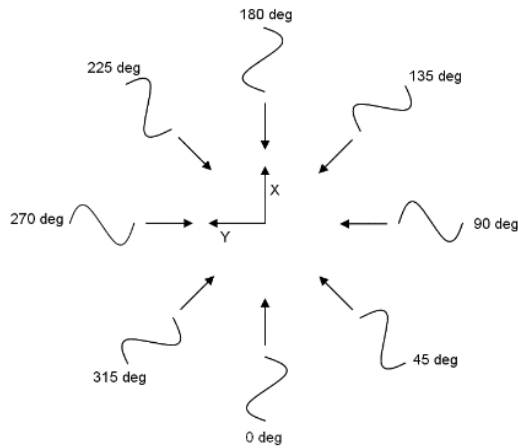
Figure 7.2: Wind and wave direction definition in the global coordinate system.
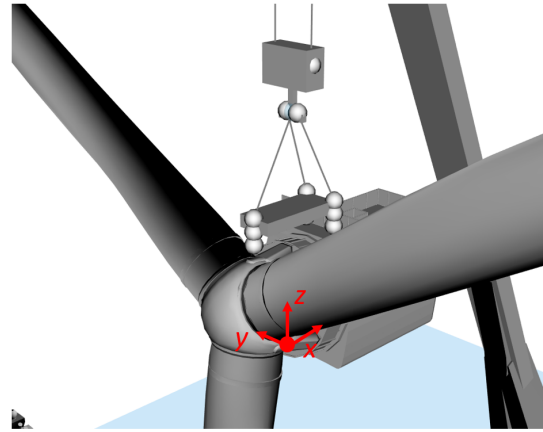
Figure 7.3: Local axis system of the nacelle.

between two objects in the global coordinate system. Moreover, constraints provide stiffness and damping in both in positive and negative displacement, thus it is important to consider this when translating it to tugger lines, as they can only provide tension.

In this section constraints are added in the model to assess what the effect is on the dynamics and if it works as expected, focusing on reducing the sideward pendulum. First, stiffness in the translational direction in the horizontal motions is added and then the addition of rotational stiffness is also examined. Different load cases are used to analyse the effect. The same environmental load cases are used as in Chapter 6, to clearly evaluate the effect of the applied stiffness. Two sets of different wave conditions (wave case 1: $H_s = 2.0$ m, $T_p = 6.5$ s and wave case 2: $H_s = 1.0$ m, $T_p = 11.0$ s), one wind speed (9 m/s at 10 m) and varying stiffness values for the constraints.

The results are presented in the following order: 1. An overview of the significant responses per DoF of the RNA for the different load cases, 2. The reaction forces in the constraint representing the tension in the tugger lines and 3. PSD analysis to analyse the distribution of the energy of the RNA motion into frequency components. The analyses are briefly described below.

The reaction forces in the constraint represent in the tension in the tugger line. While the constraint provides both tension and compression, a tugger line can only provide tension. Therefore, it is important that the reaction force is always positive, to avoid slack lines. The simulations are performed without taking this into account, thus the forces oscillate around 0 kN, resulting in positive and negative forces. Then, the minimum amplitude is added to the time series to ensure that the force is always positive, which is allowed because of the linear relation between force and displacement. In this way, slack lines are avoided. Note however, that due to this pretension at the start of the simulation, the RNA would get an offset, which is not considered here. It is assumed that the offset of the RNA with the pretension is small due to restoring gravity forces of the relatively heavy RNA. Normally, during an operation, the load variation is determined beforehand. The pretension of the tugger winch is set to a value, which is equal to minimum load amplitude plus ∼ 2 mT, to ensure that slack lines do not occur.

The reason that it is interesting to perform a PSD analysis is because adding stiffness to the system means that the dynamic behaviour changes and thus the mode shapes as well. By adding stiffness, the natural period lowers. In this way, a stiffness can be added to change the natural period to avoid frequencies, for example wave frequencies.

7.3.1. Translational stiffness constraint

In this section, simulations are performed focusing on constraining the translational motion of the RNA, with emphasis on the sideward pendulum, that is the RNA global response in X and RNA local response in y if the RNAs heading is kept constant. A translational stiffness is added to the RNA. The constraint is placed at the RNA CoG and moves along with the crane boom, thus if the RNA moves with respect to the crane boom, the defined stiffness or damping in the constraint for the chosen DoFs is applying restoring or damping forces if the RNA moves in those DoFs.

A stiffness is applied in X to control the sideward pendulum motion of the RNA. The value is varied between 1000, 3000, 5000 kN/m. Moreover, a stiffness of 1000 kN/m is applied in Y and a yaw stiffness of 15 kNm/deg. A wind speed of 9 m/s at 10 m is used and the wind and waves come both from 180 deg. Also, the crane tip at 180 m is used, the blade pitch angle is 0 deg and wave spreading with a spreading exponent of 2 is used.

RNA responses

The results are presented in Table 7.1, where an overview of the used stiffness values is shown as well. The responses are reported with respect to the CoG of the RNA.

By first looking at wave case 1, one can observe that the effect of adding stiffness significantly reduce the significant responses as SDA. Whereas without stiffness the nacelle would move 2.2 m in y, this is now below 1 m and is smaller for larger stiffness. The stiffness also prevents the nacelle roll motion Rx, by decreasing the significant response to approximately 1 deg. The roll response Rx increases with increasing stiffness, while y decreases. This means that while the RNA approximately stays in position in the horizontal plane, the roll is still large, meaning it is rolling around its own CoG, with having a small response in the translational direction. The significant x response of the nacelle does not change for different stiffness values in X, as that is applied in a different direction. The significant yaw response Rz is very small.

When looking at wave case 2, the same results are observed, but still with higher significant response. From y and Rx can be concluded that the RNA is still moving a lot in a sideward pendulum motion, which is due to a sideward pendulum mode shape coupled with vessel pitch motion.

For both load cases can be concluded that a 3000 kN/m stiffness in X seems the most promising, as it shows a significant difference in motion reduction with 1000 kN/m and a small difference with 5000 kN/m.

Table 7.1: Significant responses as SDA (4·std(X)) of RNA CoG for different environmental conditions and stiffness values. Both the wind and wave direction is 180 deg. Wave spreading is used with spreading exponent 2. Note that the RNA responses are given in the local body coordinate system.

Wind & waves	**Stiffness**			**Significant response as SDA of RNA**				
$V_{w,10m}$, H_s and T_p	X	Y	RZ	x	y	Rx	Ry	Rz
	[kN/m]	[kN/m]	[kNm/deg]	[m]	[m]	[deg]	[deg]	[deg]
$V_{w,10m} = 9.0$ m/s	0	0	15	0.60	2.2	7.8	1.3	3.1
$H_s = 2.0$ m	1000	1000	15	0.19	0.91	0.90	0.34	0.16
$T_p = 6.5$ s	3000	1000	15	0.18	0.53	1.2	0.34	0.09
	5000	1000	15	0.18	0.49	1.14	0.34	0.09
$V_{w,10m} = 9.0$ m/s	0	0	15	1.1	6.8	25	2.6	5.3
$H_s = 1.0$ m	1000	1000	15	0.62	2.0	8.6	0.44	1.1
$T_p = 11.0$ s	3000	1000	15	0.62	1.5	8.1	0.42	0.93
	5000	1000	15	0.62	1.4	8.8	0.49	1.2

Forces in constraints

The same simulations as in the previous section are used to obtain the forces in the constraints. The reaction forces at the RNA CoG due to the RNA motion and the defined stiffness in X and Y are presented in Figure 7.4 for both waves cases and for a stiffness of 3000 kN/m in X. One can observe that the forces do not become negative – the minimum force is 2 mT. As already seen in the RNA responses, for the 11.0 s wave, the forces are larger, because the response is larger. The forces that serve as input for the tugger winch properties are discussed in section 7.1.

The reason that time series are presented, rather than a statistic value, is that for the tension in a tugger line the load variation and minimum and maximum value are more valuable. In this way, a better overview is presented of the tension behaviour during operation.
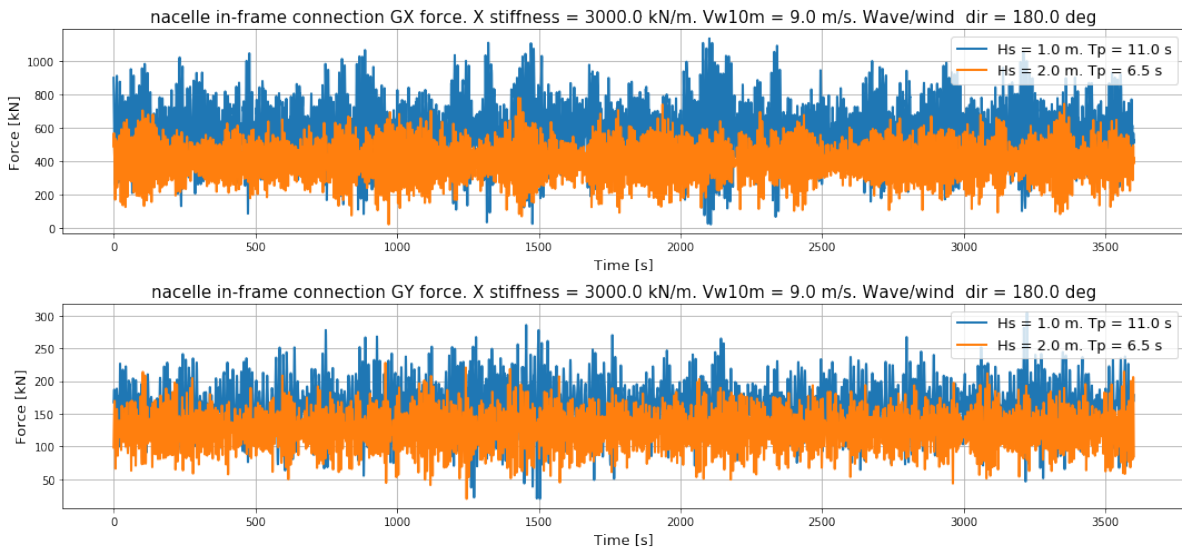
Figure 7.4: Time series of the forces in the constraint in global X and Y as a result of the stiffness defined in X of 3000 kN/m and in Y of 1000 kN/m. Both wave cases are shown. The forces do not become negative, hence slack lines do not occur.

PSD analysis

PSD plots are created to evaluate at which frequencies the responses are oscillating. Only the responses in y and Rx are presented in Figures 7.5 (wave case 1) and 7.6 (wave case 2), as their response is different per stiffness value used.

First considering the first wave case, it is clearly visible that for y the peak for 1000 kN/m at 5.0 s (= 1.25 rad/s) is gone for higher stiffness. This is a sideward pendulum mode shape coupled with vessel pitch, which is < 3 s for higher stiffness. Hence, these are not excited by the waves. Around 10.0 s (= 0.65 rad/s) there is a pure sideward pendulum mode of RNA and crane block in anti-phase, which is excited for both 3000 and 5000 kN/m that causes the roll response. Also, the vessel pitch response is visible, which is due to the relatively broad range of frequencies that is excited. This is also observed from the vessel pitch RAOs (HMC).

For wave case 2 in Figure 7.6, the nacelle y response is at the same frequencies for all stiffness values, but is less damped for 1000 kN/m. The nacelle roll response Rx is also occurring at the same frequency, which is the pure sideward pendulum of the RNA in anti-phase with the crane block at around 10.0 s (= 0.65 rad/s) that causes the significant roll response. This mode shape is excited more than for the first wave case, because the wave peak period is closer.

Conclusion

From this analysis can be concluded that adding stiffness in the translational directions of the RNA

does have a positive effect on the RNA responses, decreasing the motion significantly by adding restoring forces and changing natural periods of the system. It is observed that the difference in the significant response between 1000 and 3000 kN/m is large, while this is not the case between 3000 and 5000 kN/m. Hence, 3000 kN/m is selected to be the stiffness in X for further analysis. However, for long waves the RNA sideward pendulum is still excited, which is due to the vessel pitch response and pure pendulum mode shape of the RNA and crane block in anti-phase.

By adding stiffness in translational direction in X and Y, it is tried to prevent the RNA from swinging in a pendulum motion. Nevertheless, the the RNA roll response Rx is excited. Hence, in the next set of simulations, rotational stiffness is added.
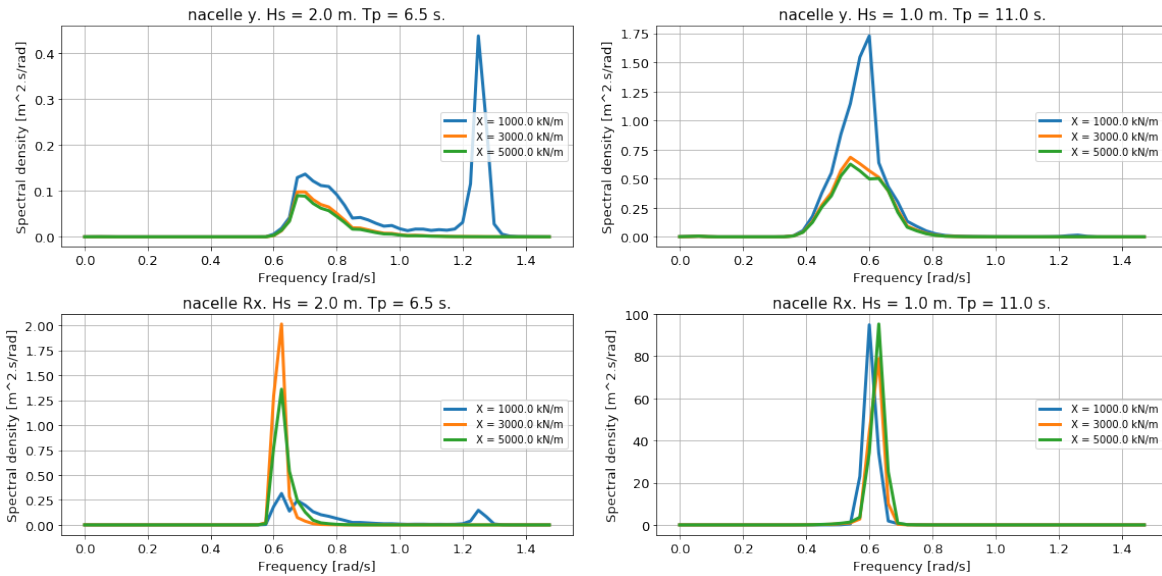
Figure 7.5: PSD plots of RNA at CoG for motion in y and roll Rx for $H_s = 2.0$ m, $T_p = 6.5$ s and varying applied stiffness global X to the RNA. Wind/wave direction = 180 deg, wind speed at 10 m = 9 m/s.

Figure 7.6: PSD plots of RNA at CoG for motion in y and roll Rx for $H_s = 1.0$ m, $T_p = 11.0$ s and varying applied stiffness in global X to the RNA. Wind/wave direction = 180 deg, wind speed at 10 m = 9 m/s.

7.3.2. Rotational stiffness constraint

In the previous section is identified that by adding translational stiffness in the horizontal plane $X - Y$, the sideward pendulum motion is reduced. However, the roll response Rx of the RNA is still excited. In this section, roll stiffness is added to the RNA. Hence, the stiffness is defined as kNm/deg. Again, the constraint provides rotational stiffness in the relative motion between the crane boom and RNA. Furthermore, as constraints are defined in the relative response between two objects in the global coordinate system, the roll stiffness is defined in RY, which applies stiffness to the RNA Rx response.

The applied rotational stiffness is varied between 5, 15, 30, 100 and 250 kNm/deg. The reason that this wide range of values are chosen, is because from simulations is observed that the effect on the significant response is different for both wave cases, because the natural periods change. This is also discussed in more detail in this section. Furthermore, a stiffness of 3000 kN/m in X is used, as concluded from the previous section, a stiffness of 1000 kN/m in Y and a yaw stiffness RZ of 15 kNm/deg to constrain the heading of the RNA. The same wind and wave cases are used.

RNA responses

In Table 7.2 the values are presented with varying stiffness for RNA roll Rx, which is applied in global

RY.

When first looking at the first wave case (H_s = 2.0 m and T_p = 6.5 s), one can observe that the RNA responses stay approximately the same for all DoFs, except for Rx, which is the purpose of making use of an 'ideal' tugger line system. First, the significant roll response decreases when increasing the roll stiffness. However, for stiffness above 30 kNm/deg, the significant response increases again, which can be due to a mode shape that is excited more. For the 30 kNm/deg case, the significant responses in all DoFs are relatively small.

Considering wave case 2, another behaviour is observed. The smallest response in Rx is at 250 kNm/deg stiffness. Furthermore, all significant responses in the other DoFs stay approximately the same again. Even though the roll stiffness does reduce the RNA motion, it is still substantial. This is due to the large pitch motion of the vessel. The constraints provide stiffness in the relative motion between crane boom and RNA. Hence, if the crane boom response is large due to the vessel motion, these constraints cannot provide the required restoring forces.

Table 7.2: Significant responses as SDA of RNA (4·std(X)) for different environmental conditions and stiffness values. Both the wind and wave direction is 180 deg. Wave spreading is used with spreading exponent 2. Note that the RNA responses are given in the local body coordinate system.

Wind & waves	Stiffness				Significant response as SDA of the RNA				
$V_{w,10m}$, H_s and T_p	X	Y	RY	RZ	x	y	Rx	Ry	Rz
	[kN/m]	[kN/m]	[kNm /deg]	[kNm /deg]	[m]	[m]	[deg]	[deg]	[deg]
$V_{w,10m}$ = 9.0 m/s	3000	1000	0	15	0.18	0.53	1.2	0.34	0.09
H_s = 2.0 m	3000	1000	5	15	0.18	0.55	0.97	0.33	0.08
T_p = 6.5 s	3000	1000	15	15	0.18	0.55	0.83	0.33	0.08
	3000	1000	30	15	0.18	0.55	0.77	0.33	0.08
	3000	1000	100	15	0.18	0.54	1.7	0.34	0.11
	3000	1000	250	15	0.18	0.53	1.48	0.34	0.11
$V_{w,10m}$ = 9.0 m/s	3000	1000	0	15	0.62	1.5	8.1	0.42	1.1
H_s = 1.0 m	3000	1000	5	15	0.63	1.6	7.2	0.38	0.80
T_p = 11.0 s	3000	1000	15	15	0.63	1.6	6.9	0.38	0.77
	3000	1000	30	15	0.63	1.6	6.9	0.39	0.88
	3000	1000	100	15	0.61	1.5	6.3	0.36	0.76
	3000	1000	250	15	0.61	1.5	5.0	0.34	0.52

Forces in constraints

Time series of the forces and moment in the constraint in X, Y and RY at the RNA CoG due to the defined stiffness are presented in Figure 7.7. For both wave cases, the roll stiffness that result in the smallest stiffness is shown. Again, the forces and moment are all above 0 kN or kNm to avoid slack lines. The forces that serve as input for the tugger winch properties are discussed in section 7.1.

One can observe that while the differences of the forces in X and Y are small, this is not the case for the moment. There are two reasons for this. First, the significant RNA response in Rx is larger for H_s = 1.0 m and T_p = 11.0 s, and second, the constraint is stiffer. As a result, a larger restoring moment is created.

A tugger line can only provide tension, not a restoring moment. Hence, the restoring moment that

a tugger line needs to provide is done by giving it an offset with the point of rotation, in this case the RNA CoG. Then, the restoring moment is equal to the tension multiplied by the arm. More is discussed on this in section 7.4.
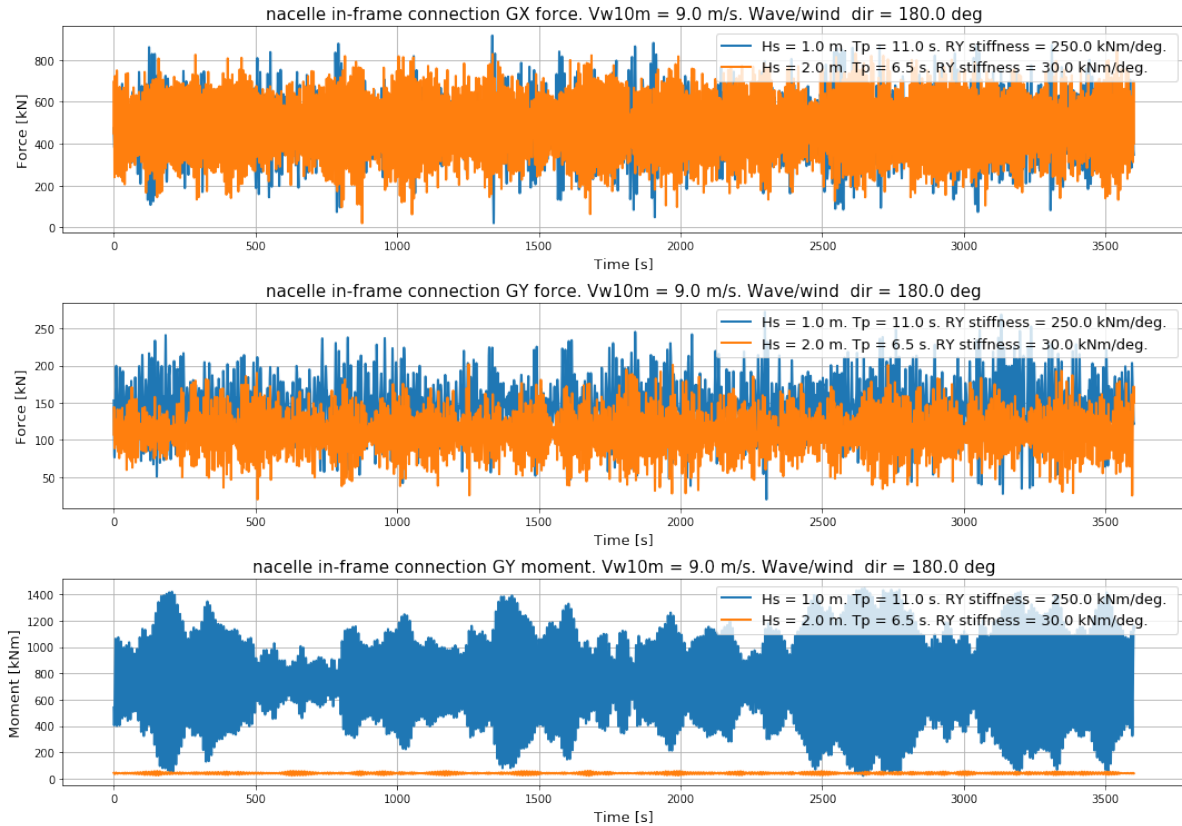
Figure 7.7: Time series of the forces and moment in the constraint in global X, Y and RY as a result of the stiffness defined in X of 3000 kN/m, in Y of 1000 kN/m and roll stiffness of 30 kNm/deg for $T_p = 11.0$ m and 250 kNm/deg for $T_p = 6.5$. Both wave cases are shown. The forces and moment do not become negative, hence slack lines do not occur.

PSD analysis

PSD plots are created to gain an insight at what frequencies the RNA is oscillating. In this case, only the roll response Rx is shown, because the other responses do not change with the varying roll stiffness. The plots of both wave cases are presented in Figures 7.8 and 7.9.

The defined roll stiffness has a small effect on changing the mode shapes of the system, as it only affects the sideward pendulum. For 0 kNm/deg roll stiffness, the natural period is 10.1 s (= 0.62 rad/s) and reduces to 9.5 s (= 0.66 rad/s) when increasing the roll stiffness. As a result, the same mode is excited for both wave cases, which is the sideward pendulum mode swinging in anti-phase with the crane block. The damping of the mode differs for both wave cases, due to the shift in natural period.

Conclusion

From the analysis of the responses, internal forces and moments and the distribution of the frequency components, can be concluded that for the different wave cases a different roll stiffness is required to reduce the significant responses. Whereas a stiffness of 30 kNm/deg is needed for $H_s = 2.0$ and $T_p = 6.5$ s, an increased stiffness of 250 kNm/deg is required for $H_s = 1.0$ and $T_p = 11.0$ s, due to the shift in natural period and the different wave frequency. Nevertheless, for the second wave case, the sideward pendulum response remains too large. It has to be noted however, that in Figure 5.7 from *Model 2 – Waves only* is shown that the crane tip should be increased to get a smaller
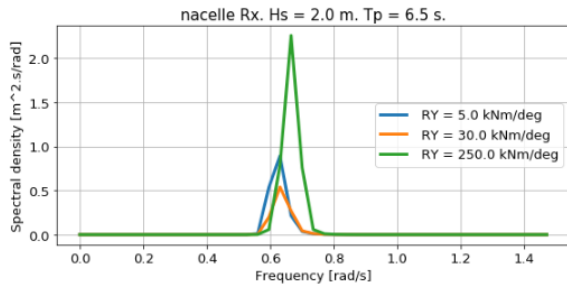
Figure 7.8: PSD plot of RNA response in roll Rx for H_s = 2.0 m, T_p = 6.5 s and varying rotational stiffness in global RY to the RNA. Wind/wave direction = 180 deg, wind speed = 9 m/s.
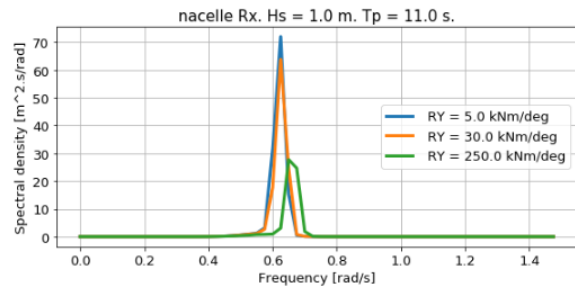
Figure 7.9: PSD plot of RNA response in roll Rx for H_s = 1.0 m, T_p = 11.0 s and varying rotational stiffness in global RY to the RNA. Wind/wave direction = 180 deg, wind speed = 9 m/s.

RNA roll response RY for higher peak periods. In this analysis the crane tip is set to 180 m, in order to get a more straightforward comparison of results. However, it is expected that the difference in the significant response is still small. Hence, a more advanced method is required to reduce the sideward pendulum motion for longer peak periods, that should focus letting the RNA follow the opposing motion of the crane tip.

7.3.3. Conclusion constraints

In this section the effect of constraints on the RNA response is evaluated. From the analyses that are performed, some requirements in terms of stiffness provided by the tugger line system can be defined as shown below. The maximum allowed tension in the tugger line depends on the configuration (orientation and number of lines) and thus no conclusions can be drawn in this section. This is done in the next section.

- Translational stiffness in X of 3000 kN/m;

- Translational stiffness in Y of 1000 kN/m;

- Rotational stiffness in RY of 30 kNm/deg (T_p = 6.5 s) / 250 kNm/deg (T_p = 11.0 s);

- Rotational stiffness in RZ of 15 kNm/deg.

7.4. Tugger line configuration

In the previous section requirements are defined for the stiffness that has to be provided by the tugger lines. It is shown that the ideal tugger lines do work as expected and also reduce the RNA motion. As explained earlier, it is however modelled as an ideal tugger line system and this should be translated into a physical system. In this section an example is shown on how the constraint requirements can be converted into a tugger line configuration and how that affects the assumption of having an ideal constraint.

7.4.1. Translational tugger lines

First, the tugger lines that represent the stiffness in X and Y are shown as discussed in subsection 7.3.1. The stiffness of the tugger lines depends on the material properties, which can be chosen, such as different strains of steel in the wire or from synthetic materials. The stiffness constraints are applied at the RNA CoG. This is done to give direct control on the translational motion of the RNA.

If there is an offset with the CoG, a moment and thus a rotation is induced. Hence, the tuggers are placed directly through the CoG as well. The attachment points of the tugger lines on the RNA has to be chosen as well. In this case, it is assumed that the lines can only be fixed at the corners of the backside of the nacelle.

In Figure 7.10 the tugger lines in the $X - Y$ plane are visualised. By having the lines through the CoG and at the corner of the backside, the orientation of the lines is limited to this configuration. The angle between the two lines is approximately 40 deg. The tugger lines are attached to the crane boom at the other side. In the figure, these points are floating in space, but in reality this can be fixed by having a horizontal beam fixed to the crane boom with sheaves on which the lines run.

As a result of the limited configuration, a stiffness of 3000 kN/m in X and 1000 kN/m in Y is not achieved. It could be achieved if the tuggers are attached at the side of the nacelle and with an increased angle in between them. However, an increased angle also means that the beam connecting the tugger lines with the crane boom must be longer. From a structural point of view, this can be limiting as well. Therefore, by choosing the current configuration, the stiffness in Y must increase, to ensure that X still provides a 3000 kN/m stiffness, which is the limiting response of the RNA.
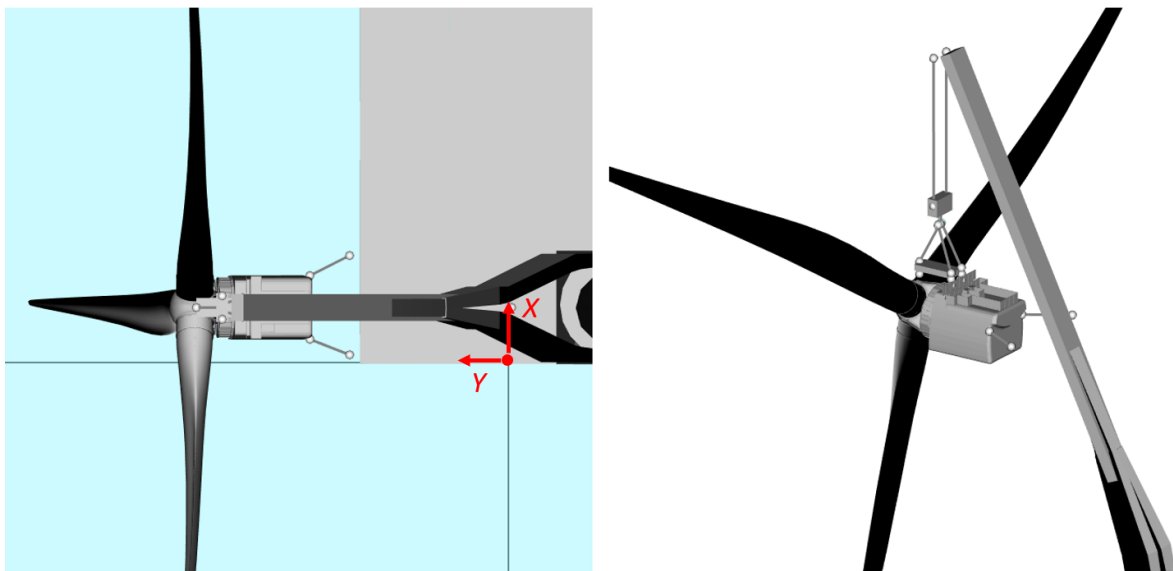
Figure 7.10: Visualisation of the two tugger lines in the horizontal plane. They are attached at the corners of the backside of the nacelle and go through the RNA CoG. At the other side they are connected to the crane boom.

7.4.2. Rotational tugger lines

After adding the tugger lines in the horizontal plane, the next step is to add tugger lines that can control the roll motion of the RNA. A restoring roll moment can be achieved by having a vertical force with an offset to the CoG. This requirement can be translated into different methods to add the restoring roll moment. One example is shown in this section.

Vertical tugger lines connected between the main deck and to the bottom at the side of the nacelle are shown in Figure 7.11 that provide the required roll stiffness. The roll stiffness however, is defined in kNm/deg and needs to be translated to two tugger lines in kN/m. The way how this is converted in shown in the free body diagram in Figure 7.12, representing the front view of the nacelle. The two tugger lines connected to the bottom provide a tension and compression force due to the rotation and hence, a restoring roll moment is created. If the roll stiffness in kNm/deg is known, the stiffness

of the tugger lines k can be determined. Note that the vertical tugger lines also provide stiffness in Z-direction and thus other DoFs are also affected.

The requirement on the yaw stiffness of 15 kNm/deg is achieved by the tugger lines in the horizontal plane. In static position the lines act through the CoG, but this is no longer the case if the nacelle yaws. Hence, a restoring moment is created. This is verified by running simulations.
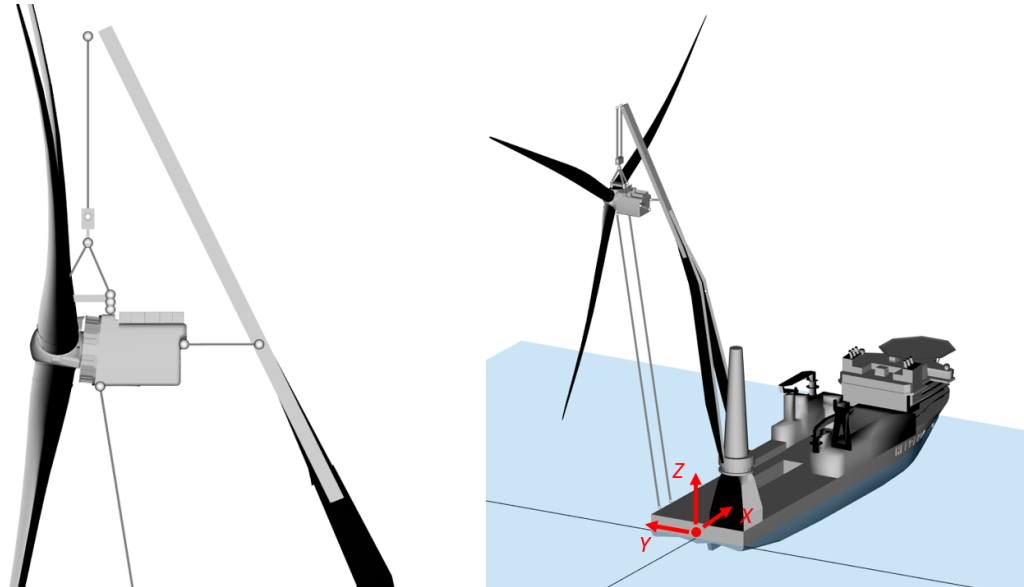
Figure 7.11: Visualisation of the two tugger lines to provide roll stiffness. They are attached at the bottom of the nacelle and go through the RNA CoG. At the other side they are connected to the vessel.
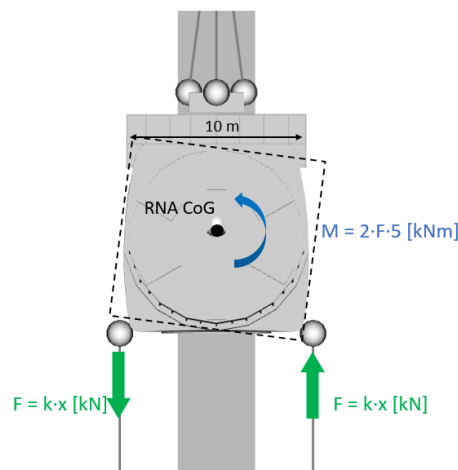
Figure 7.12: Front view of the nacelle that is rotated by 1 deg. The two tugger lines that are attached at the bottom provide tension and compression due to the rotation and hence create a restoring roll moment. Note that the tugger lines have pretension, so the direction of the force remain the same, but for clarity only the difference in tension is shown.

7.4.3. Tugger winches

The tugger lines run that are connected to the RNA, run to the tugger winches. In this case study, four tugger lines are used. Generally, the winches are placed at the base of the crane and run via sheaves to the location. In this case study, the two horizontal tugger lines run via a sheave at the

height of the RNA and at the side of the crane boom, back to the base of the crane. The two vertical tugger lines run straight back to the main deck. This is done to provide a larger vertical component of the tugger line, rather than straight back to the crane base. This is one example of where the tugger winches can be placed. Choosing the location depends on more factors, such as operational constraints from slewing of the tower and equipment that is stored on deck. Moreover, with the tugger winches placed on deck at port side, the RNA can only be installed over port side as well, adding operational limits.

In the simulations, the reaction forces in the constraints are examined. This represents the tension in the tugger lines that the winches have to provide. For the first wave case ($H_s = 2.0$ m, $T_p = 6.5$ s), the combined tension in X and Y is not exceeding 600 kN, which is a reasonable amount, noting that this have to be provided by two winches. For the second wave case $H_s = 1.0$ m, $T_p = 11.0$ s) however, as the responses are larger, the tension is also larger, being up to 1000 kN, so each winch has to provide a 50 mT tension. This is a significant amount and it depends on the available winches if this can be achieved.

7.5. Conclusion case study

In this chapter a case study is performed regarding controlling the motion of the RNA due to wind and waves, focusing on reducing the sideward pendulum. This is done using constraints in OrcaFlex, by adding stiffness in certain DoFs. Time domain simulations are performed to examine the effect on reducing the RNA responses. This is done by looking into the RNA responses, internal forces and moments of the constraints and PSD analyses for different stiffness values of the constraint. From these simulations is concluded that constraints do work as expected and can reduce the sideward pendulum of the RNA. However, constraints serve as an ideal representation of tugger lines, as they can add stiffness or damping to a single DoF, while tugger lines work in multiple DoFs and the orientation changes if the RNA moves.

To show how requirements of the constraints in the model can be translated into a physical tugger line configuration, the case study also contains an example of how the determined requirements for the constraint are translated into an actual tugger line system. This is done by four tugger lines that restrain the horizontal, translational response of the RNA and the roll response of the RNA. By doing this, it is demonstrated how the tugger lines also affect other DoFs, making it more complicated to understand the effect on the dynamic behaviour of the RNA.

Only one tugger line configuration is used. The constraints can be translated into numerous of other tugger line configurations, with different attachment points (on nacelle, lift frame, crane block), different orientation and different tugger winch modes.

Overall, in this case study is demonstrated how one can approach the problem of mitigating the horizontal motions of the RNA, by adding a method to reduce the motions, looking into how the effect of the method on the RNA responses and vary the input parameters for the method. Furthermore, by performing a PSD analysis, one can gain an insight on at what frequencies the system is oscillating and one can look at the internal forces of the constraint, that serve as an input requirement of the tugger winches. This same approach can be used when implementing other methods to reduce the RNA motions in the model.

7.6. Future implementations in the model

In the case study one tugger line configuration is shown. Numerous other methods exist to mitigate the horizontal motions of the RNA. In this section is discussed what can be implemented in the

model in the future.

First of all, the configuration of the tugger lines can be adjusted. That can vary in number of lines, orientation of the lines, attachment points of the lines on the RNA, lift frame or crane block. Furthermore, how the tugger lines run back to the winches can be varied, by adding sheaves.

Secondly, there are different tugger winch modes as explained in this chapter, while only the winch on brake is considered in this case study. The damping winch mode is expected to give similar results as with a damping constraint, since it works according to the same principle as a stiffness constraint, except that it applies a damping force rather than a restoring force. Furthermore, the constant tension winch that deviates from a perfect constant tension and thus applied damping, can be modelled in OrcaFlex using detailed winches, but not using constraints. Another interesting method to control the tension applied by the winch, is by using active tension control. This can be done by adding an external Python function, containing the controller scheme to control the winch wire payout or tension. To verify that this is possible in the model, a PID controller (Proportional, Integral, Differential) has been implemented. However, testing and verification of the results is considered to be outside of the scope and is thus not investigated further. Nevertheless, it is shown that active control of the tugger winches can be used for further research regarding mitigating the horizontal motions of the RNA.

Finally, for further implementations it is important on what motions should be focused to reduce the RNA horizontal motions. As discussed throughout the results of all models, it is concluded that the RNA response mainly depends on the wave peak period, as that excites the pitch motion of the vessel. Furthermore, the wave-induced motions are governing. Whereas for low wave peak periods, the RNA should follow the crane tip, this is not the case for high wave peak periods, where the crane tip motions are large. In the case study, stiffness is added in the relative motion between the RNA and crane tip. Even though it helped reducing the motions for long wave peak periods, it would not be enough, as the crane tip motions remain too high. Therefore, with this generic tugger line configuration it would not be possible to install the RNA and the control method should focus on opposing the crane tip motion. In OrcaFlex this can be done by actively changing the orientation and tension of the tugger lines, based on accelerations of the RNA or vessel that serve as input for the controller.

8
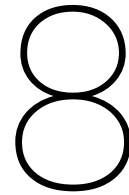
Conclusions & Recommendations

This chapter provides the conclusions from the results of these models, as presented in section 8.1. Furthermore, recommendations are given regarding future work on this subject in section 8.2.

8.1. Conclusions

To examine the dynamic behaviour of the RNA during the installation using a floating vessel, three different models have been developed that assess the response due to the wind only, due to the waves only and due to coupled wind and waves.

Model 1 − Wind only is performed in OrcaFlex using time domain simulations. The purpose of this model is to understand the behaviour of the RNA due to wind and how parameters affect the response. The RNA is hanging below an Earth fixed point, representing the crane tip. The vessel is not modelled. The aerodynamic loads on the blades in static position of the RNA for different wind conditions are verified. The cross-flow principle is used to compute the aerodynamic loads acting on the blade segments, which are used for rigid body motion analysis of the blades. A spatially uniform, but varying in height and time varying wind field is used. From this model, the following conclusions are drawn:

- It is determined that the smallest motions are occurring with a blade pitch angle of 0 deg, which is defined as the leading edge of the blade pointing to clockwise positive direction. Different wind directions are analysed to determine this. Furthermore, for this blade pitch angle, a restoring yaw moment is observed to keep the RNAs heading fixed.

- It is determined that by making the hoist wires longer, while the RNA is at a fixed height, the pendulum length and thus pendulum period increase and the RNA is excited more by the wind. By increasing the crane tip height from 180 to 200 m, the significant responses in translational direction ($4 \cdot \text{std}(X)$) are 1.2 to 2.5 times larger, depending on the wind speed and direction, as that determines the magnitude and direction of the aerodynamic load. Therefore, from the perspective of the wind-induced motions, it is concluded that a low as possible crane tip height result in the smallest responses.

- A yaw stiffness of 15 kNm/deg is required to keep the RNA heading within 1.0 deg for wind speeds up to 12 m/s and wind from front of the RNA.

- The dominant RNA response is a resonant pendulum motion in the direction of the wind and a slow yaw motion. The significant response as double amplitude in translational direction

68

remains below 0.25 m for a wind speed of 10 m/s and wind from the side. This is considered to be small. For wind from the front and 10 m/s wind speed, the significant response can be up to 1.25 m. This is considered to be large. Therefore, it is concluded that it is relevant to take the wind into account. Furthermore, this means that if the wave-induced motions can be fully compensated by a motion compensation concept, these wind-induced motions remain and thus have to be accounted for.

Model 2 – Waves only is performed in Liftdyn using a frequency domain analysis. The purpose of this model is to gain insight on the motions of the RNA as a result of wave-induced vessel motions. The vessel and crane are added to the model and irregular waves are used. From this model, the following conclusions are established:

- The vessel response is the smallest for head sea, exciting the vessel pitch response, as a mono-hull vessel is sensitive to roll. For head sea, the vessel pitch response is dominating.

- The slew angle of the crane is determined to be set to port side. The sideward pendulum motion of the RNA is up to 2 times smaller for longer wave peak periods, compared to the crane pointing to starboard. As a result of this slew angle and with head sea, the main RNA response due to vessel pitch motions, is a sideward pendulum, swinging into the direction of the waves

- The crane tip height resulting in the smallest RNA response, depends on the wave peak period. For short wave peak periods (< 8 s), the crane tip should be set to 180 m, as that decreases the RNA sideward pendulum response up to 2 times, compared to a crane tip height of 190 m. For this crane tip height, the wind-induced motions are also minimised.

  For long wave peak periods (> 8 s), the crane tip should be set to 190 m, as that decreases the RNA sideward pendulum response up to 1.2 times, compared to a 180 m crane tip height. For this crane tip height, the wind-induced motions are not minimised. Therefore, a trade-off has to be made in the coupled wind and waves model.

- The RNA sideward pendulum response depends on the wave peak period, as that determines which motions are excited. For short wave peak periods, a pure pendulum mode shape is excited. For wave peak periods above 8 s, the vessel pitch motion is significantly more excited. As a result, the crane tip motion and RNA sideward pendulum are large. The wave-induced significant responses of the RNA are up to 7 m, which are 6 times larger than wind-induced significant responses.

Model 3 – Wind & Waves is performed in OrcaFlex using time domain simulations. The goal is to evaluate how the RNA behaves when it is subjected to both wind and waves in the coupled system of the vessel and RNA. The vessel and RNA responses in OrcaFlex are verified with responses from Liftdyn. The following conclusions are drawn from this model:

- The RNA responses due to the wind and waves are both a sideward pendulum motion, using wind and waves from the same direction. The wave-induced pendulum motion is governing compared to motions due to the wind, as expected from the results from *Models 1* and *2*. The pendulum motion is excited by vessel pitch, but depending on the wave peak period, the magnitude is different. For short wave peak periods (< 8 s), the vessel pitch is relatively small and coupled with a pure pendulum mode shape. For long wave peak periods (> 8 s), the vessel pitch response is large and also coupled with a pure pendulum mode shape. The effect of increasing wind speed on the RNA response is negligible. Note that the used wind direction, is the one that results in the smallest motions, as concluded from *Model 1*.

- For short wave peak periods, the crane tip motion is small, because the vessel pitch response is small. This means that if the RNA follows the crane tip, the RNA responses are small as well. For long wave peak periods, this is the other way around, because the vessel pitch motions are excited. The RNA should not follow the crane tip motions, because those are too large. This serves as valuable input for developing a method to reduce RNA motions.

Finally, a case study is performed to assess the applicability of implementing an idealised tugger line system, taking into account only the stiffness and damping effects of the tugger lines for specific DoFs. In reality, a tugger line system is used to mitigate the horizontal motions. The case study is performed in the coupled wind and waves model. The following conclusions are established:

- For short wave peak periods (< 8 s), it is concluded that adding a translational stiffness constraint between the relative motion of the RNA and crane boom, is an effective way to mitigate horizontal motions.

- For long wave peak periods (> 8 s), it is concluded that adding a translational stiffness constraint between the relative motion of the RNA and crane boom, does mitigate the horizontal motions, but large motions remain, more specifically the RNA roll response. This is due to a pure pendulum mode shape of the RNA and crane block in anti-phase that is excited, in which the RNA is rolling around its CoG, coupled with the vessel pitch response.

- By adding roll stiffness between the relative motion of the RNA and crane boom, the RNA roll response is reduced. For both short and long wave peak periods, the RNA roll response is reduced up to a factor 1.6.

- By adding the constraints in the model and translating them to a tugger line configuration, it is demonstrated that the model can be used for implementing and evaluating methods to mitigate the RNA horizontal motions and to assess the workability of the operation. Furthermore, an approach is defined on what steps to undertake from modelling the motion compensation method and evaluating the responses that serve as input requirement for the concept.

8.2. Recommendations

Based on the research that is performed and the conclusions that are drawn, recommendations are given in this section. The recommendations are divided into to two categories, focusing on future work on implementing methods to compensate RNA motions in the model, and on improving the accuracy and validity of the model.

In the case study, simulations are performed with constraints, representing an ideal tugger line system, to prove that the model can be used to implement methods to reduce the RNA motion. For further research focusing on the improvement on the workability of the installation, the following recommendations are given:

- Only a limited amount of environmental conditions have been used in the simulations to assess the RNA response. In all cases, the wind and waves were coming from the same direction, representing wind waves, and this wind direction also led to the smallest wind-induced motions. The number of different environmental load cases should be increased by varying the wind and wave direction, significant wave height, peak period and wind speed, to determine if other modes can be excited as well.

- The tugger line configuration that is presented in the case study is connected to the RNA to reduce the sideward pendulum by providing stiffness. Various alternatives exist on this con-

figuration, that require more in depth analysis and simulations. Parameters to look at are the stiffness, damping and pretension on the lines. Furthermore, the attachment points of the lines, which can be the nacelle, lift frame or crane block and where on the crane boom or vessel deck the lines are connected to. Moreover, active control of the tension of the tugger lines can be implemented in the model as well or active control on changing the orientation of the tugger lines.

- Damping can be added to the system, by putting the tugger winch in damping or constant tension winch. Moreover, non-linear stiffness or damping can be given as input to the winch in the OrcaFlex model. Furthermore, the performance of the winch drive can be modelled by adding deadband, stiffness, inertia, damping and drag to get more realistic results.

- In this research is determined that the RNA response depends heavily on the wave peak period. Therefore, the peak period serves as essential input for a design of a method to compensate these motions, because that determines what modes are excited. However, the wave conditions at a wind farm location cannot be chosen, leaving two options for the concept. 1. The concept should focus on only one range of wave peak periods that excite the same modes. As a consequence, the workability of the operation is reduced. 2. The concept should be capable of compensating the modes that can be excited by both short and long peak period waves, making the concept more complex. Recommendations on both approaches are discussed below:

    1. If it is decided to design the concept for short wave peak periods (< 8.0 s), the concept can focus on the modes that are excited by these kind of waves. Furthermore, as concluded earlier, the RNA must follow the crane tip motion. This means that if there is a relative motion between the RNA and crane boom, the RNA should be 'pulled' back in place. A tugger line configuration connected between the RNA and crane boom fits this purpose, as that only provides stiffness or damping in the relative motion of the RNA and crane boom.

    2. If the requirement of the concept has to be able to compensate RNA motions for longer peak periods as well, the concept what is explained at 1, must be extended. However, with large the crane tip motion, the RNA should follow the opposing motion of the crane tip. This is fundamentally another problem and requires an in depth analysis on how to solve this issue, focusing on opposing the crane tip motion. This can be done by actively controlling the tension of the tugger lines or by actively changing the orientation of the tugger lines. If this problem can be solved, the workability of the operation can be significantly improved. In addition to focusing on opposing the crane tip motions to control the RNA, the wind-induced motions also need to be considered, which are motions that originate directly from the RNA.

- With the crane pointing to port side and the main RNA motion being the sideward pendulum, the RNA does not move towards the crane, but in side lead direction. Therefore, it is hard to add tugger lines to restrain that motion. If the crane slew angle is adjusted, the direction of the swinging motion of the RNA can be changed to move in offlead direction. This can help to get an improved control of the RNA motion. As a consequence, the dynamic behaviour of the RNA due to waves change as well. Therefore, this requires a more detailed analysis on assessing the effect of changing the crane slew angle.

For improving the accuracy and validity of the model, the following recommendations are given:

- The wind field in OrcaFlex can be considered as a 2D grid. For each local point in this 2D grid, the local wind direction is equal to the global wind direction. Hence, on local scale, the wind

direction cannot change. Furthermore, the wind speed only changes in time and in height. As a result, the wind speed does not change on local scale at a particular height. This could represent wind gusts or a turbulent wind field. By taking into account these two effects, the response of the RNA could be modelled more accurately.

- The cross-flow principle is used to determine aerodynamic loads on the blades for wind with an inflow angle in the horizontal plane, in which spanwise flow is neglected. The validation of this assumption for large inflow angles is questionable and should be assessed and corrected.

- Massless slings, hoist wires and tugger lines are used in the model to simplify the model, assuming that the effect of adding the mass is negligible. By adding the masses in the model and comparison of results, this assumption can be verified.

- An analysis is performed on the magnitude of the deflection of the tower at hub height, in which it is concluded that deflection is relatively small and thus is neglected during this research. The tower deflection should be included during detailed simulations of landing the RNA on the tower, to include impact velocities and forces more accurately.

Bibliography

De Leeuw, K. (2019). Single lift blade alignment for large offshore wind turbines. Master's thesis, Delft University of Technology.

DNV (2010). DNV-RP-C205 Environmental Conditions and Environmental Loads. (October).

Eurogate (). Umschlag von on-und offshore windenergieanlagen. URL http://www1.eurogate. de/Leistungen/Windenergie. Accessed on 11-11-2019.

Faltinsen, O. M. (1990), *Sea Loads on Ships and Offshore Structures*. Cambridge University Press.

Fred. Olsen Wind Carrier (2017). Wikinger Offshore Wind Farm Installation - Full Length. URL https://www.youtube.com/watch?v=rwOBl5AeKWQ. Accessed on 30-12-2019.

Fred. Olsen Windcarrier (). URL https://windcarrier.com/. Accessed on 11-11-2019.

Fred. Olsen Windcarrier (2013). URL https://windcarrier.com/ alstom-haliade-demonstrator-9. Accessed on 26-05-2020.

Gaunaa, M., Bergami, L., Guntur, S., and Zahle, F. (2014). First-order aerodynamic and aeroelastic behavior of a single-blade installation setup. *Journal of Physics: Conference Series*, 524(1). ISSN 17426596. doi: 10.1088/1742-6596/524/1/012073.

Gaunaa, M., Heinz, J., and Skrzypiński, W. (2016). Toward an Engineering Model for the Aerodynamic Forces Acting on Wind Turbine Blades in Quasisteady Standstill and Blade Installation Situations. *Journal of Physics: Conference Series*, 753(2). ISSN 17426596. doi: 10.1088/1742-6596/ 753/2/022007.

Hoerner, S. (1985). Fluid Dynamic Lift - Practical Information on Aerodynamic and Hydrodynamic Lift. URL http://adsabs.harvard.edu/abs/1975STIA...7632167H.

Kuijken, L. (2015). Single blade installation for large wind turbines in extreme wind conditions. Master's thesis, Delft University of Technology & Technical University of Denmark.

Morison, J., Johnson, J., and Schaaf, S. (1950). The Force Exerted by Surface Waves on Piles. *Journal of Petroleum Technology*, 2(05):149–154. ISSN 0149-2136. doi: 10.2118/950149-g.

NREL (2020). New Reference Turbine Gives Offshore Wind an Upward Draft. URL https://www. nrel.gov/news/program/2020/reference-turbine-gives-offshore-wind-updraft. html. Accessed on 01-03-2010.

Ren, Z., Jiang, Z., Gao, Z., and Skjetne, R. (2018). Active tugger line force control for single blade installation. *Wind Energy*, 21(12):1344–1358. ISSN 10991824. doi: 10.1002/we.2258.

Stehly, T., Heimiller, D., and Scott, G. (2016). Cost of Wind Energy Review. Technical report, National Renewable Energy Lab (NREL).

Timperley, J. (2017). How viable are floating offshore windfarms? URL https://www. carbonbrief.org/qa-how-viable-are-floating-offshore-windfarms. Accessed on 11-11-2019.

Wind Europe (2020). Offshore wind in Europe - Key trends and statistics 2019.

Zhao, Y. (2019). *Numerical Modeling and Dynamic Analysis of Offshore Wind Turbine Blade Installation.* PhD thesis, Norwegian University of Science and Technology.

Zhao, Y., Zhengshun, C., Gao, Z., Sandvik, P. C., and Moan, T. (2019). Numerical study on the feasibility of offshore single blade installation by floating crane vessels. *Marine Structures*, 64:442–462. ISSN 09518339. doi: 10.1016/j.marstruc.2018.12.001.

A
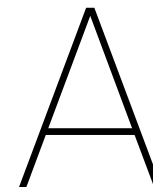
WTG Properties

This chapter contains properties regarding the WTG that is used during this research, the GE Haliade-X 12 MW. Blade properties are derived from the NREL 15 MW reference turbine and are shown below. The blade is divided into 200 segments.

Furthermore, in Table A.1 mass properties of the nacelle, rotor and lift frame are presented. The local axis system of nacelle and hub are shown in Figure A.1.

Radial position [m]	Aerodynamic twist [deg]	Chord length [m]	Thickness-to-chord ratio [%]
0	15.59455	5.2	100
0.535	15.59426	5.201177	100
1.07	15.59349	5.203028	100
1.605	15.59237	5.205435	100
2.14	15.59105	5.20828	100
2.675	15.57944	5.212345	98.07692
3.21	15.54793	5.21841	96.15385
3.745	15.49738	5.226356	94.23077
4.28	15.42863	5.236065	92.30769
4.815	15.34252	5.247418	90.38462
5.35	15.23992	5.260295	88.46154
5.885	15.12166	5.274578	86.53846
6.42	14.9886	5.290148	84.61538
6.955	14.84159	5.306886	82.69231
7.49	14.68147	5.324673	80.76923
8.025	14.5091	5.34339	78.84615
8.56	14.32533	5.362918	76.92308
9.095	14.131	5.383139	75
9.63	13.92696	5.403934	73.07692
10.165	13.71406	5.425182	71.15385
10.7	13.49315	5.446767	69.23077
11.235	13.26509	5.468568	67.30769
11.77	13.03072	5.490467	65.38462
12.305	12.79088	5.512345	63.46154

12.84	12.54643	5.534083	61.53846
13.375	12.29822	5.555562	59.61538
13.91	12.0471	5.576663	57.69231
14.445	11.79391	5.597268	55.76923
14.98	11.53951	5.617257	53.84615
15.515	11.28474	5.636511	51.92308
16.05	11.03046	5.654912	50
16.58596	10.77705	5.672371	49.26316
17.12192	10.52584	5.688734	48.52632
17.65788	10.27767	5.703883	47.78947
18.19384	10.0334	5.717697	47.05263
18.7298	9.793888	5.730057	46.31579
19.26575	9.559979	5.740844	45.57895
19.80171	9.33253	5.749937	44.84211
20.33767	9.112395	5.757218	44.10526
20.87363	8.900428	5.762567	43.36842
21.40959	8.697483	5.765864	42.63158
21.94555	8.504413	5.766989	41.89474
22.48151	8.319489	5.766763	41.15789
23.01747	8.143667	5.764719	40.42105
23.55343	7.974466	5.760921	39.68421
24.08939	7.809463	5.756097	38.94737
24.62535	7.648142	5.748702	38.21053
25.16131	7.491926	5.73613	37.47368
25.69726	7.337846	5.719999	36.73684
26.23322	7.182853	5.702341	36
26.79279	7.018571	5.681598	35.8125
27.35236	6.853673	5.657057	35.625
27.91193	6.689439	5.629751	35.4375
28.47149	6.5271	5.600883	35.25
29.03106	6.366637	5.569656	35.0625
29.59063	6.207544	5.535522	34.875
30.1502	6.050148	5.499523	34.6875
30.70976	5.894926	5.463055	34.5
31.26933	5.741604	5.425964	34.3125
31.8289	5.590071	5.387777	34.125
32.38847	5.440796	5.348821	33.9375
32.94803	5.294315	5.309538	33.75
33.5076	5.150259	5.26958	33.5625
34.06717	5.008408	5.228854	33.375
34.62674	4.869559	5.188279	33.1875
35.1863	4.734419	5.148703	33
35.72293	4.608122	5.111723	32.86818
36.25957	4.484502	5.075269	32.73636
36.7962	4.363853	5.039527	32.60455
37.33283	4.246476	5.004693	32.47273
37.86946	4.132439	4.970822	32.34091
38.40609	4.021278	4.93766	32.20909
38.94272	3.913013	4.90532	32.07727

39.47935	3.80777	4.87398	31.94545
40.01598	3.705682	4.84384	31.81364
40.55262	3.60693	4.815183	31.68182
41.08925	3.511064	4.787621	31.55
41.62588	3.417385	4.76048	31.41818
42.16251	3.32526	4.733151	31.28636
42.69914	3.234347	4.705309	31.15455
43.23577	3.145028	4.677385	31.02273
43.7724	3.057271	4.649435	30.89091
44.30903	2.971023	4.62149	30.75909
44.84567	2.886234	4.593573	30.62727
45.3823	2.802889	4.56564	30.49545
45.91893	2.72094	4.537716	30.36364
46.45556	2.640327	4.509842	30.23182
46.99219	2.560997	4.482057	30.1
47.51912	2.484402	4.454854	29.945
48.04606	2.409109	4.427716	29.79
48.57299	2.335006	4.400673	29.635
49.09992	2.261986	4.373756	29.48
49.62685	2.190021	4.346964	29.325
50.15379	2.119127	4.320281	29.17
50.68072	2.049236	4.293724	29.015
51.20765	1.980296	4.267303	28.86
51.73458	1.912333	4.241001	28.705
52.26152	1.845336	4.214814	28.55
52.78845	1.779145	4.188791	28.395
53.31538	1.713603	4.162976	28.24
53.84231	1.648617	4.137372	28.085
54.36925	1.584255	4.111956	27.93
54.89618	1.520666	4.086733	27.775
55.42311	1.457951	4.061706	27.62
55.95004	1.395977	4.036863	27.465
56.47698	1.334705	4.012202	27.31
57.00391	1.274459	3.987748	27.155
57.53084	1.215589	3.963531	27
58.06871	1.156961	3.93907	26.855
58.60658	1.099593	3.914847	26.71
59.14445	1.043296	3.89082	26.565
59.68232	0.987901	3.866945	26.42
60.22019	0.93338	3.843225	26.275
60.75805	0.879762	3.819669	26.13
61.29592	0.827016	3.796267	25.985
61.83379	0.775114	3.773004	25.84
62.37166	0.724198	3.7499	25.695
62.90953	0.674191	3.726951	25.55
63.4474	0.624733	3.704108	25.405
63.98527	0.57542	3.681316	25.26
64.52314	0.526287	3.65858	25.115
65.06101	0.477452	3.635916	24.97

65.59887	0.428799	3.613307	24.825
66.13674	0.380168	3.590733	24.68
66.67461	0.331654	3.568211	24.535
67.21248	0.283272	3.545742	24.39
67.75035	0.234812	3.523284	24.245
68.28822	0.186029	3.500787	24.1
68.81742	0.137904	3.478617	23.98889
69.34662	0.089631	3.456424	23.87778
69.87582	0.040784	3.434201	23.76667
70.40502	-0.00914	3.411934	23.65556
70.93421	-0.05998	3.389636	23.54444
71.46341	-0.11174	3.367301	23.43333
71.99261	-0.16467	3.344906	23.32222
72.52181	-0.21902	3.322421	23.21111
73.05101	-0.27447	3.299798	23.1
73.58021	-0.33138	3.277105	22.98889
74.10941	-0.39036	3.25444	22.87778
74.63861	-0.452	3.231889	22.76667
75.16781	-0.51639	3.209412	22.65556
75.69701	-0.58338	3.186993	22.54444
76.2262	-0.65291	3.164637	22.43333
76.7554	-0.72534	3.142352	22.32222
77.2846	-0.80183	3.120159	22.21111
77.8138	-0.88056	3.098011	22.1
78.343	-0.95948	3.075862	21.98889
78.8722	-1.03765	3.05369	21.87778
79.4014	-1.11615	3.031523	21.76667
79.9306	-1.19456	3.009345	21.65556
80.4598	-1.27228	2.98714	21.54444
80.989	-1.34974	2.964919	21.43333
81.51819	-1.42734	2.942694	21.32222
82.04739	-1.50314	2.920408	21.21111
82.57659	-1.5751	2.898004	21.1
83.18127	-1.65387	2.872282	21.1
83.78596	-1.73074	2.846475	21.1
84.39064	-1.80438	2.820551	21.1
84.99532	-1.87346	2.794478	21.1
85.6	-1.93666	2.768222	21.1
86.135	-1.99077	2.744823	21.1
86.67	-2.04255	2.721257	21.1
87.205	-2.08574	2.69751	21.1
87.74	-2.11415	2.673569	21.1
88.275	-2.13514	2.649438	21.1
88.81	-2.15177	2.625114	21.1
89.345	-2.16312	2.600584	21.1
89.88	-2.16864	2.575829	21.1
90.415	-2.17249	2.550836	21.1
90.95	-2.17521	2.525638	21.1
91.485	-2.17651	2.500281	21.1

92.02	-2.17562	2.474789	21.1
92.555	-2.17232	2.449137	21.1
93.09	-2.1671	2.423324	21.1
93.625	-2.16109	2.397357	21.1
94.16	-2.15308	2.37123	21.1
94.695	-2.14209	2.344942	21.1
95.23	-2.12905	2.318502	21.1
95.765	-2.11493	2.291914	21.1
96.3	-2.09866	2.265174	21.1
96.835	-2.08005	2.238282	21.1
97.37	-2.05963	2.211245	21.1
97.905	-2.03777	2.184069	21.1
98.44	-2.0138	2.156748	21.1
98.975	-1.98754	2.129282	21.1
99.51	-1.95896	2.101673	21.1
100.045	-1.92772	2.073909	21.1
100.58	-1.89313	2.045978	21.1
101.115	-1.85551	2.01792	21.1
101.65	-1.81514	1.989804	21.1
102.185	-1.7718	1.961807	21.1
102.72	-1.72515	1.93394	21.1
103.255	-1.67544	1.905901	21.1
103.79	-1.62297	1.87741	21.1
104.325	-1.56791	1.848144	21.1
104.86	-1.50976	1.817184	21.1
105.395	-1.44787	1.779922	21.1
105.93	-1.38251	1.707787	21.1
106.465	-1.31394	1.472483	21.1
107	-1.24239	0.5	21.1

Table A.1: Mass properties of the RNA.

Property	Value	
Nacelle + lift frame mass	575	mT
Nacelle + lift frame mass moment of inertia I_{xx}	13.74	mT·m^2
Nacelle + lift frame mass moment of inertia I_{yy}	18.49	mT·m^2
Nacelle + lift frame mass moment of inertia I_{zz}	14.73	mT·m^2
Hub mass	190	mT
Hub radius	3.97	m
Hub axial moment of inertia	1497	mT·m^2
Hub transverse moment of inertia	1589	mT·m^2
Blade mass	60.3	mT
Rotor mass (hub + three blades)	371	mT
Rotor mass moment of inertia I_{xx}	126·10^3	mT·m^2
Rotor mass moment of inertia I_{yy}	126·10^3	mT·m^2
Rotor mass moment of inertia I_{zz}	250·10^3	mT·m^2
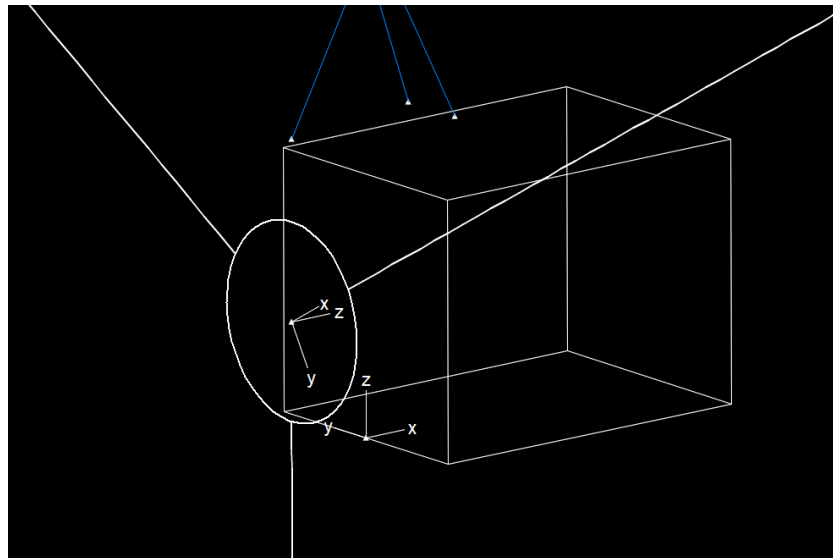
Figure A.1: Local axis origin hub and nacelle.

Aerodynamic loads on a fixed single blade

In this section the aerodynamic loads on a single blade in three different positions are determined for varying wind directions and blade pitch angles. These loads are inducing the motion of the RNA when it is suspended from the crane in the wind only case. Therefore, it is essential to understand where the loads on the blades originate from and how they respond to different conditions, such as inflow angle of the wind and blade pitch angle.

In each figure in Figures B.4 to B.5, a plot is shown for the aerodynamic forces and moments per blade in x, y and z for varying wind direction and 0 and 90 deg blade pitch angle. In these plots the differences in aerodynamic loads are clearly visible per blade.

Finally, in Figures B.6 and B.7 the aerodynamic loads of each blade and 0 and 90 deg blade pitch angle are shown to clearly see the effect of blade pitch on aerodynamic loading.

Input notes:

- Fixed single blade with radius of 107 m.

- Lift/drag coefficients from NREL 15 MW blade.

- Uniform constant wind speed of 10 m/s. Hence, it dus not vary with height.

- Varying wind direction.

- 0 and 90 deg blade pitch angle.

- The local axis system of the blade is shown in Figure B.1. Note that the wind turbine rotates around the local z-axis of the blade. The axis system moves along when the blade moves in the rotor plane. The positive direction of the local aerodynamic forces per blade is also shown in Figure B.3.

- 0 deg wind direction in same direction as global X, shown in Figure C.1. Positive wind direction is counterclockwise, when looking at RNA from above.

- Moments around x, y and z due to the aerodynamic loads defined in this chapter refer to the moments in the local origin of the blade.

- *Lx* force = force in local x-direction.

Conclusion:

- When determining the aerodynamic loads from the wind turbine blade, the cross-flow principle is considered. Using this principle, the spanwise component of the flow is neglected. This means that the aerodynamic force in spanwise direction of the blade is 0 kN, which can be seen all figures below.

- The aerodynamic loads from blade 1 and 3 are identical. This is due the cross-flow principle. Therefore, only the velocity component perpendicular to the blade is considered for blade 1 and 3, resulting in loads of the same magnitude.

  Note that for blade 2, there is no spanwise velocity component when the wind direction changes (in the horizontal plane). Hence, blade 2 generates a different load.
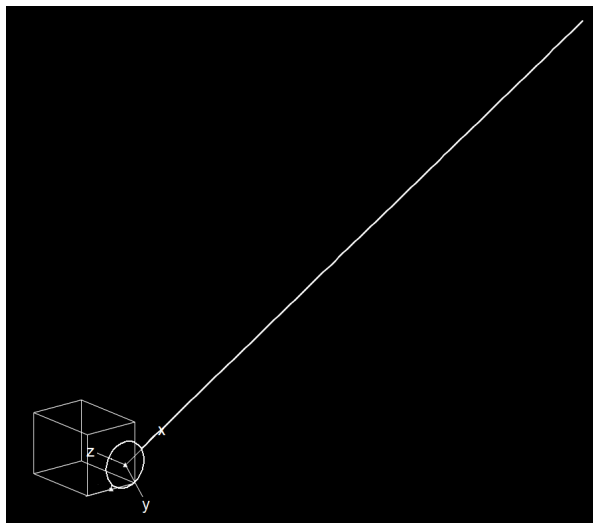
Figure B.1: Local coordinate system of the hub. The local coordinate of the wind turbine blade is at the outer border of the hub.
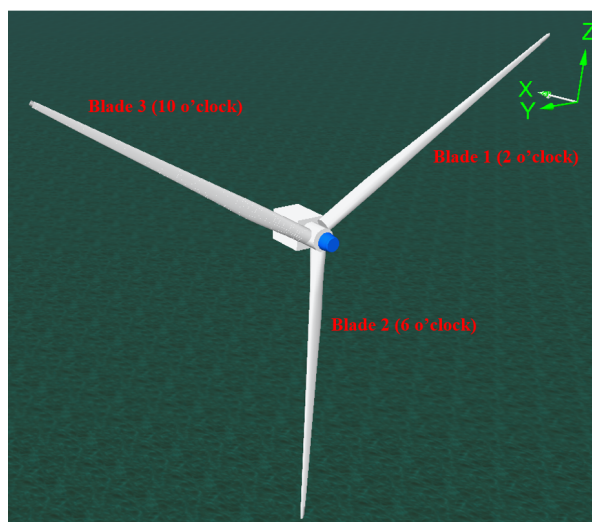
Figure B.2: Definition of the global axis system, definition of the blades and their position and the wind direction.
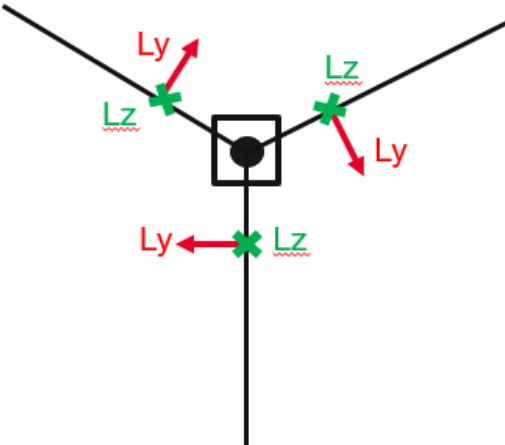
Figure B.3: Definition of direction of the *Ly* and *Lz* forces per blade.
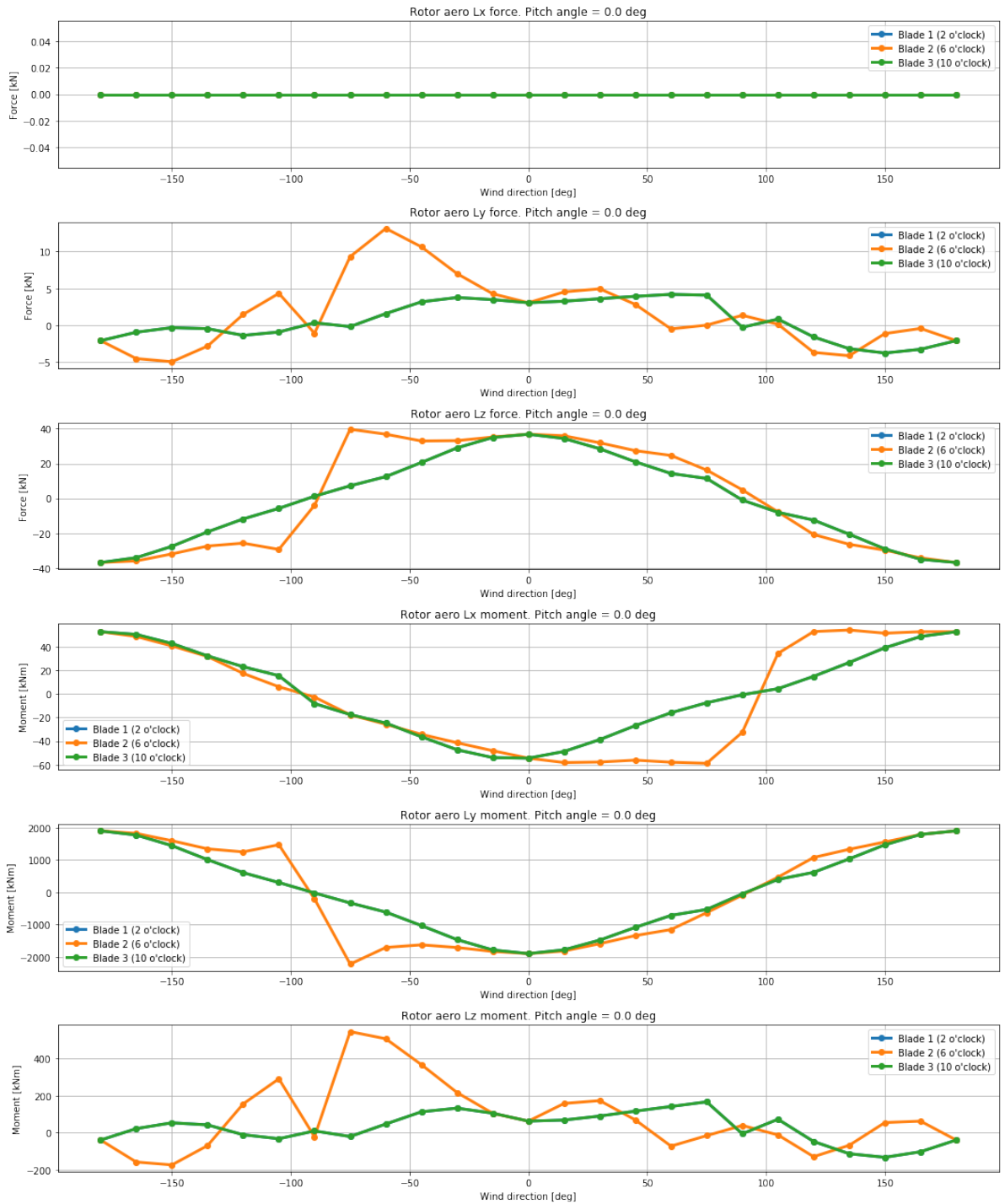
Figure B.4: Aerodynamic forces and moments on the blade for varying wind direction and 0 deg blade pitch. Note that blade 1 and 3 have identical forces. Moments are taken at the root of the blade.
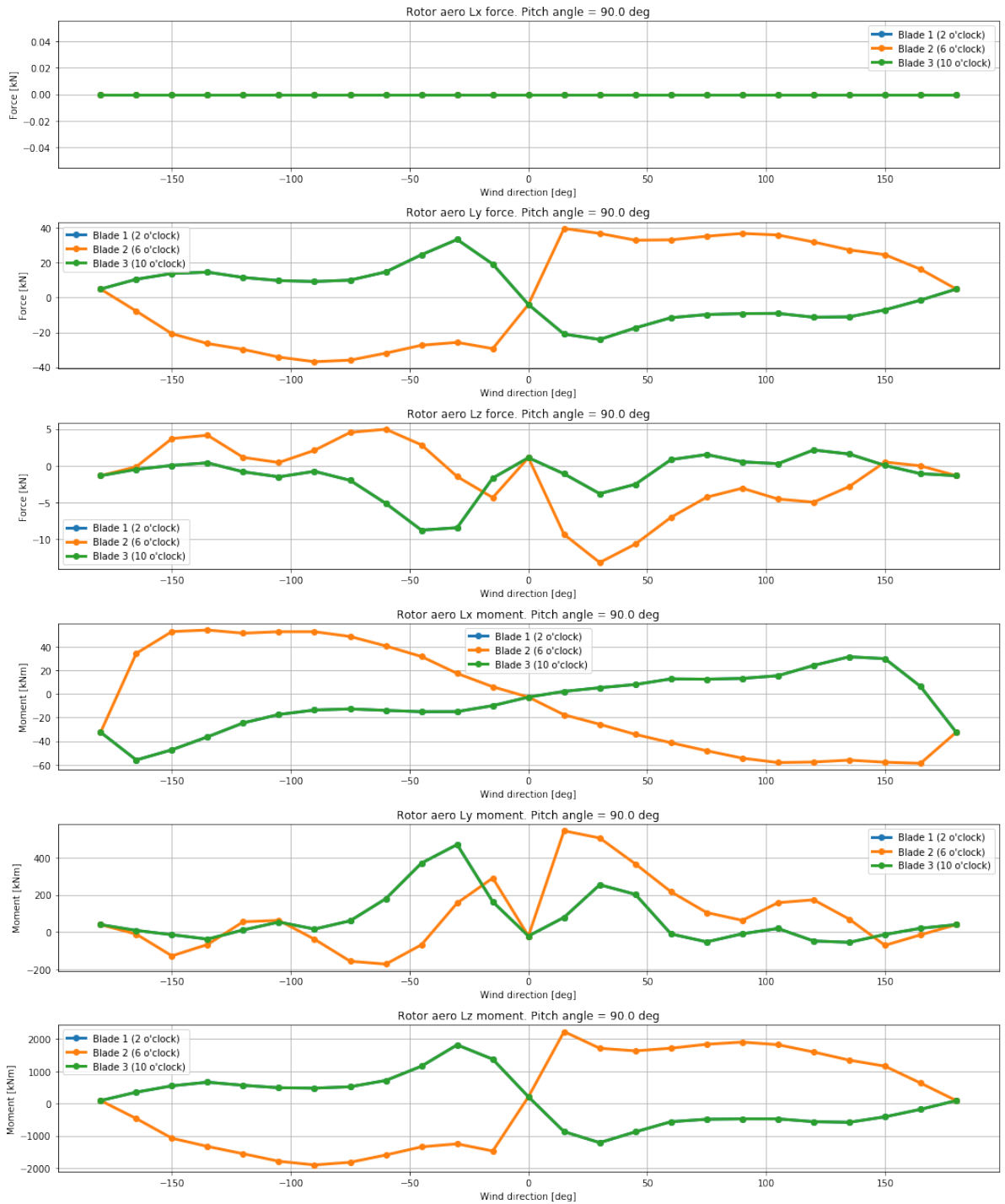
Figure B.5: Aerodynamic forces and moments on the blade for varying wind direction and 90 deg blade pitch. Note that blade 1 and 3 have identical forces. Moments are taken at the root of the blade.
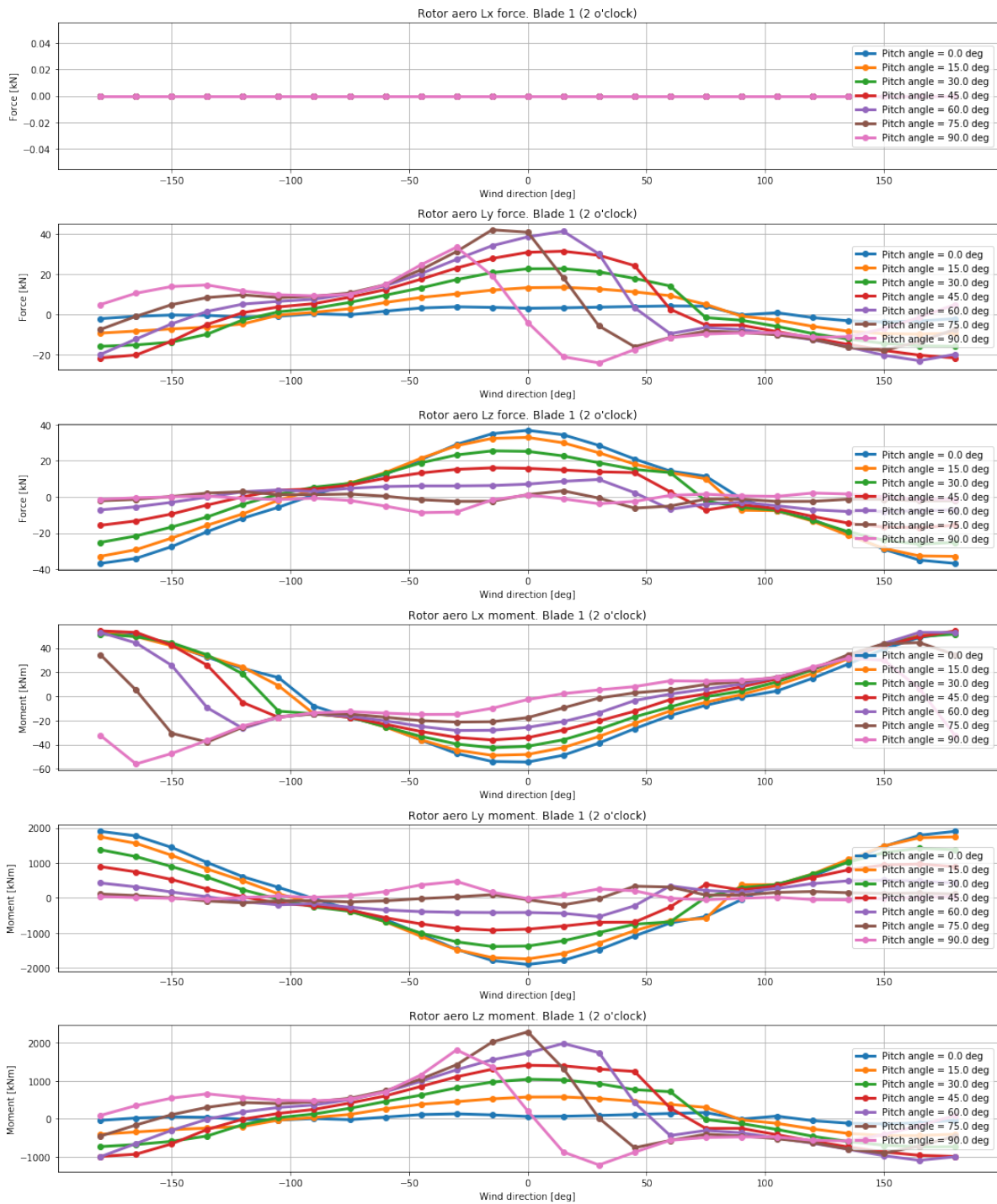
Figure B.6: Aerodynamic forces and moments for blade 1 (2 o'clock) in one overview with varying wind directions and pitch angle.
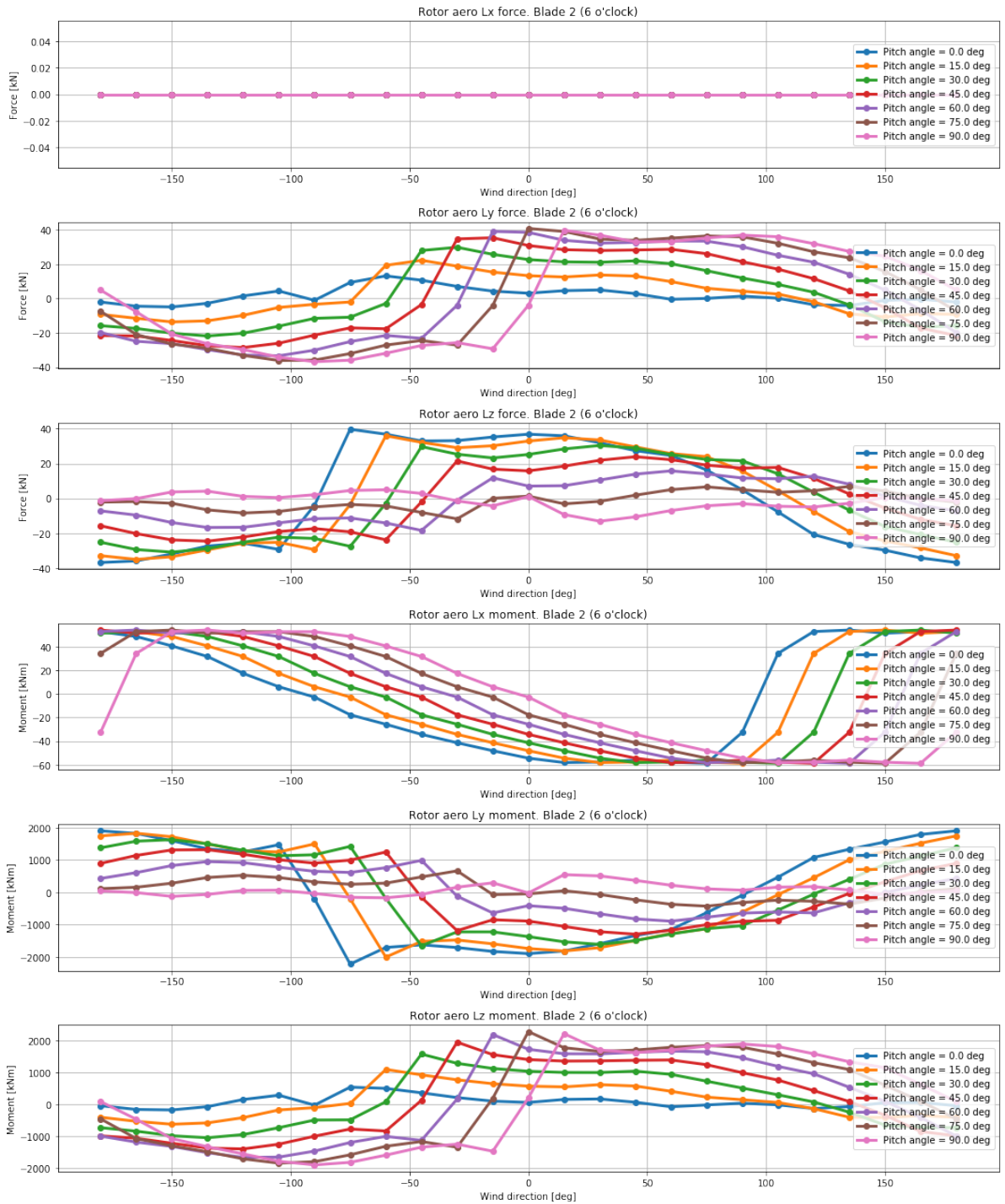
Figure B.7: Aerodynamic forces and moments for blade 2 (2 o'clock) in one overview with varying wind directions and pitch angle.
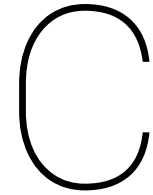
Aerodynamic loads on a fixed RNA

In this section the complete rotor nacelle assembly is considered - nacelle, hub and three blades. The forces and moments acting on the cog of the RNA due to aerodynamic loading only are looked into.

Input notes:

- RNA is fixed.

- Uniform constant wind speed of 10 m/s.

- Varying wind direction.

- Varying blade pitch angle.

- The same coordinate system is used as in the single blade case. The global coordinate system is shown again in Figure C.1.

- The results of the local aerodynamic forces and moments of all three blades are given with respect to the local coordinate system of blade 1 (2 o'clock).

- All forces and moments acting on the nacelle are given with respect to the location of the cog of the RNA. Its local position in the nacelle is $(x, y, z) = (0.234, 0.0, 5.13)$ [m]. The local origin of the nacelle is shown in Figure C.2.

- Lx force = force in local x-direction.

- GX force = force in global x-direction.

In Figure C.3 the forces and moments due to aerodynamic loading only in the RNA cog are plotted for varying wind direction and blade pitch angle. Furthermore, in Figure C.4 the same results are plotted, but then in the centre of the hub. The results in the two locations are compared and discussed below and how each blade contributes to the total forces and moments is explained.

Conclusion:

- **Connection GX force** - This is the sum of the Lz forces from the blades. In case of 0 deg pitch angle, the blade is fully rotated into the wind, thus creating large drag forces. For increasing pitch angle, the magnitude of the GX force decreases.

Equal, but opposite to the hub Connection GX force.

- **Connection GY force** - This is the sum of the Ly forces from the blades. Note that the direction of this force for each blade is different, as it is pointing in clockwise direction perpendicular to the blade spanwise direction.

  Equal, but opposite to the hub Connection GY force.

- **Connection GZ force** - This is the weight of the RNA (865 mT). Only blade 1 (2 o'clock) and 3 (10 o'clock) have a vertical component in the Ly force and they are equal in magnitude, but in opposite direction. Therefore, the total GZ force does not change for varying wind directions or pitch angles.

  GZ force at the hub is without the weight of the nacelle − only the hub and blades, and thus is smaller.

- **Connection GX moment** - This is the roll moment of the RNA induced by the Ly forces of the blades. For blade pitch angles 0 and 90 deg, this Ly force is significantly smaller compared to 75 deg blade pitch, which can be seen in Figures B.6 and B.7 and thus the roll moment for 75 deg blade pitch is also larger.

- **Connection GY moment** - This is the pitch moment of the RNA caused by several forces, the horizontal components of the Ly forces of blades 1 and 3, the Lz forces of all blades and the gravity forces of the nacelle, hub and blades.

  The values are slightly different compared to the connection GY moment at the hub, because the moments are taken at a different point.

- **Connection GZ moment** - This is the yaw moment of the RNA that is induced by the Ly forces of all blades. The yaw moment of Lz forces of blade 1 and 3 cancel each other out, while the Lz force of blade 2 does not have an offset with the GZ axis. The horizontal components of Ly of blades 1 and 2 and Ly of blade 3 have an offset in GX direction, creating the yaw moment.

  The offset in GX direction is smaller in the case where the yaw moment is determined in the centre of hub. Therefore, there yaw moment is smaller and also opposite sign.
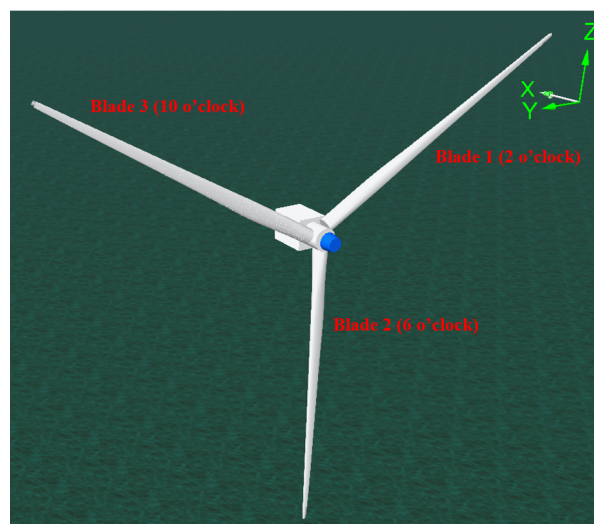
Figure C.1: Definition of the global axis system, definition of the blades and their position and the wind direction.
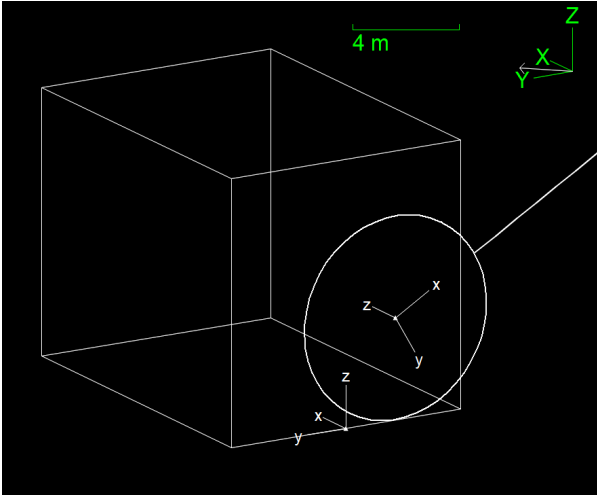
Figure C.2: Local origin of the nacelle and the hub. RNA cog is at $(x, y, z) = (0.234, 0.0, 5.13)$ [m] in local coordinates in the nacelle.
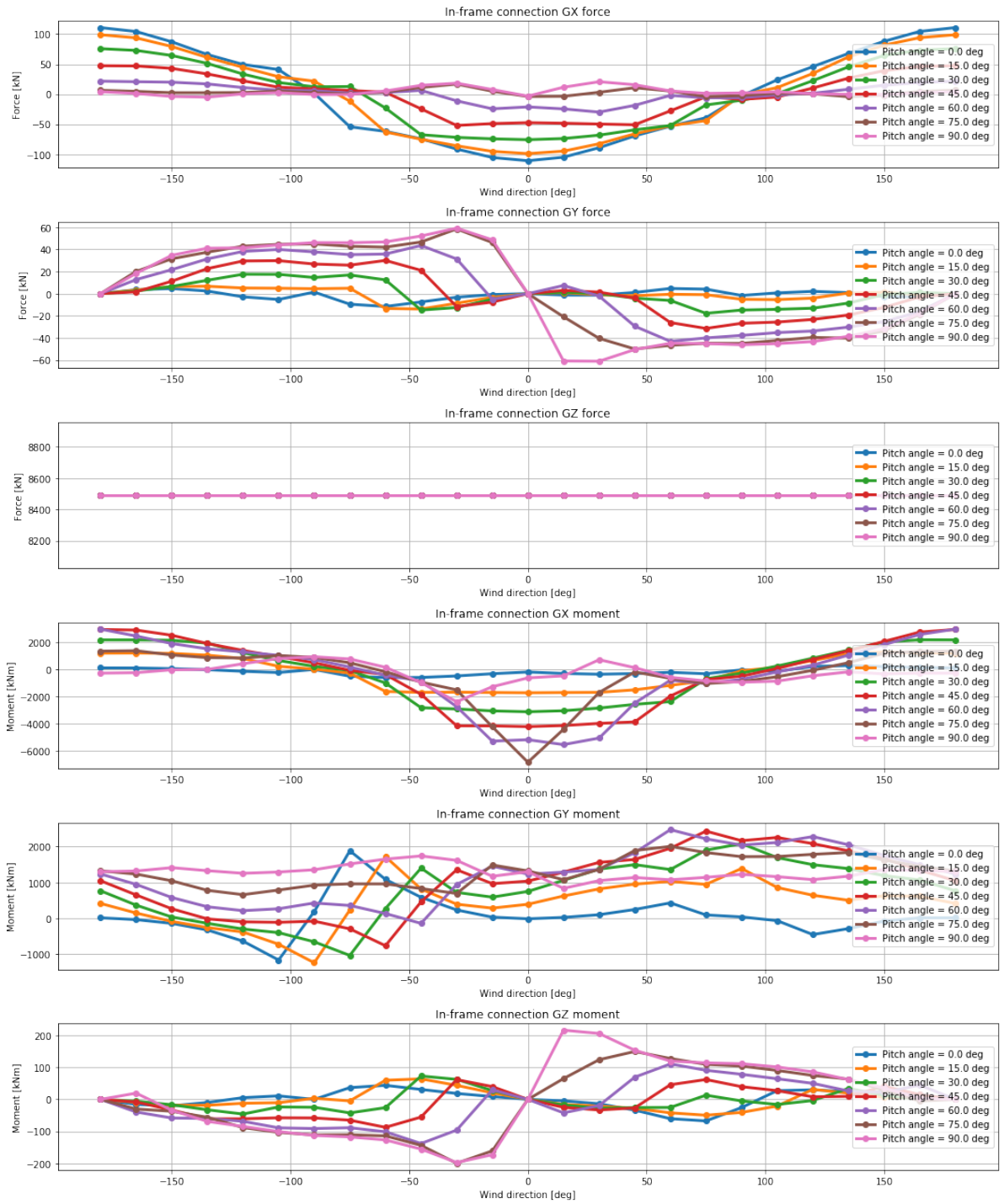
Figure C.3: Forces and moments acting on the RNA cog due to aerodynamic loading only for varying wind directions and blade pitch angles. All forces and moments are given in the global coordinate system.
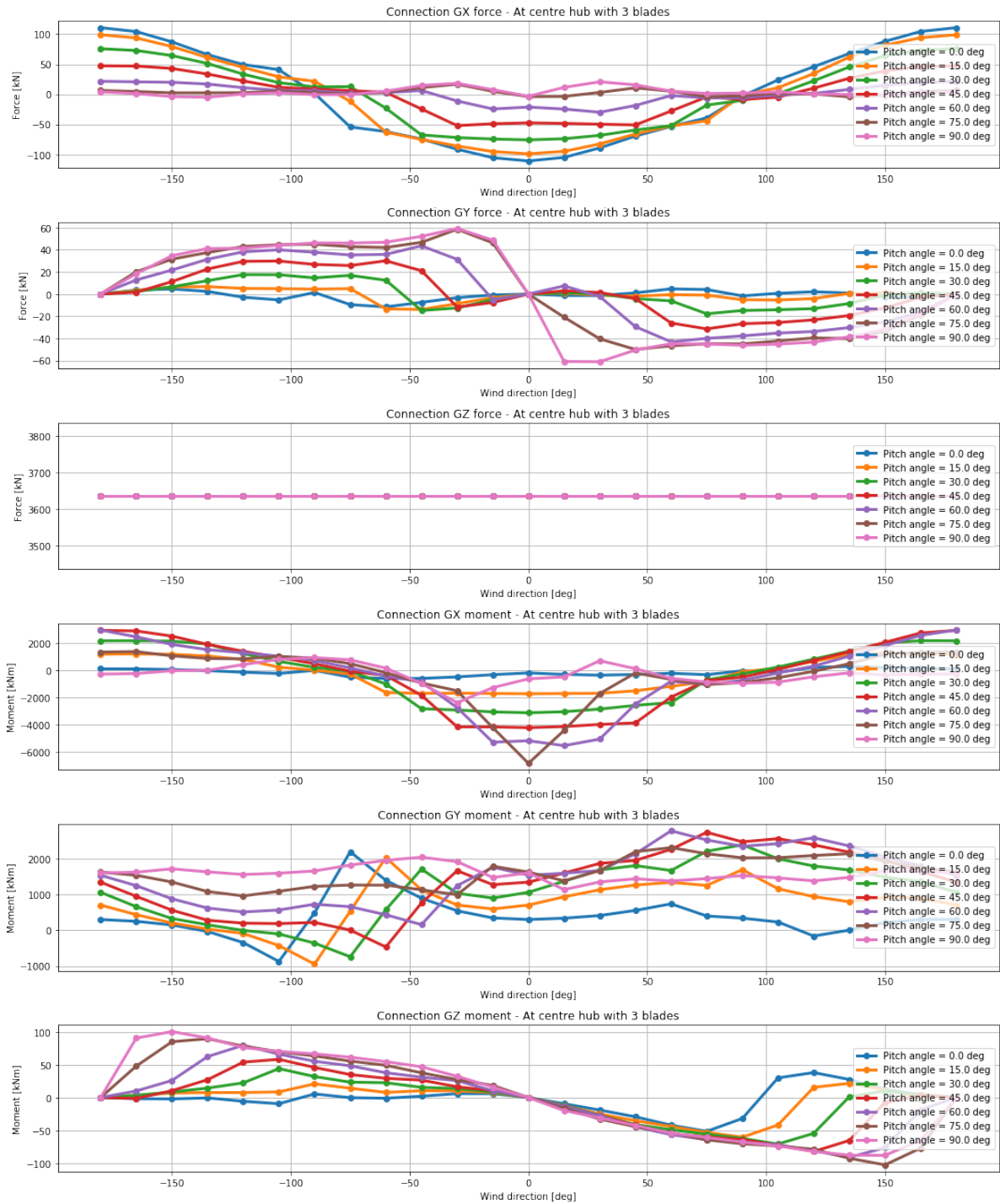
Figure C.4: Forces and moments acting in the origin of the hub due to aerodynamic loading only of three blades for varying wind directions and blade pitch angles. All forces and moments are given in the global coordinate system.

D
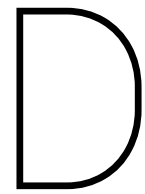
Model 1 – Wind Only Time Series

In this Appendix, time series are presented of the forces and moments in X, Y and Z, as shown below.
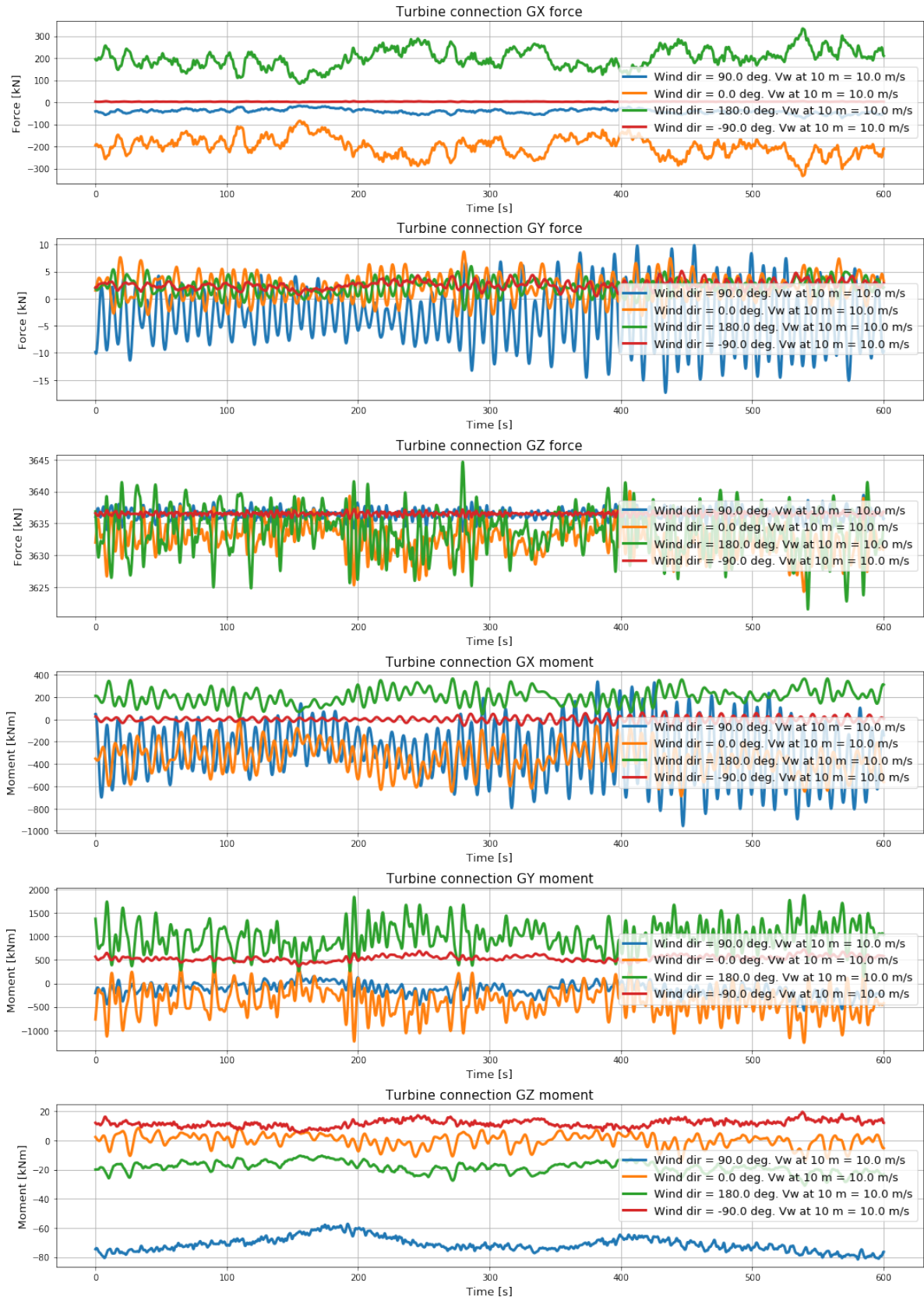
Figure D.1: Time series of the forces in X, Y and Z and moments in RX, RY and RZ for varying wind directions and a wind speed of 10 m/s at 10 m. These forces and moments are at the connection interface between the rotor and nacelle and are forces due to wind that generate aerodynamic loads and gravity loads from the rotor (hub + blades). From this can be observed that for -90 deg wind direction, the overall forces and moments are very small, due to the relative inflow of the wind on the blades. Hence, for this wind direction, the responses are small as well.
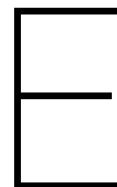
Model 3 - Wind & Waves Time Series

In this Appendix, time series are presented of the RNA responses in x, y, z, Rx, Ry and Rz for two different wave cases and varying wind speeds, as shown below.
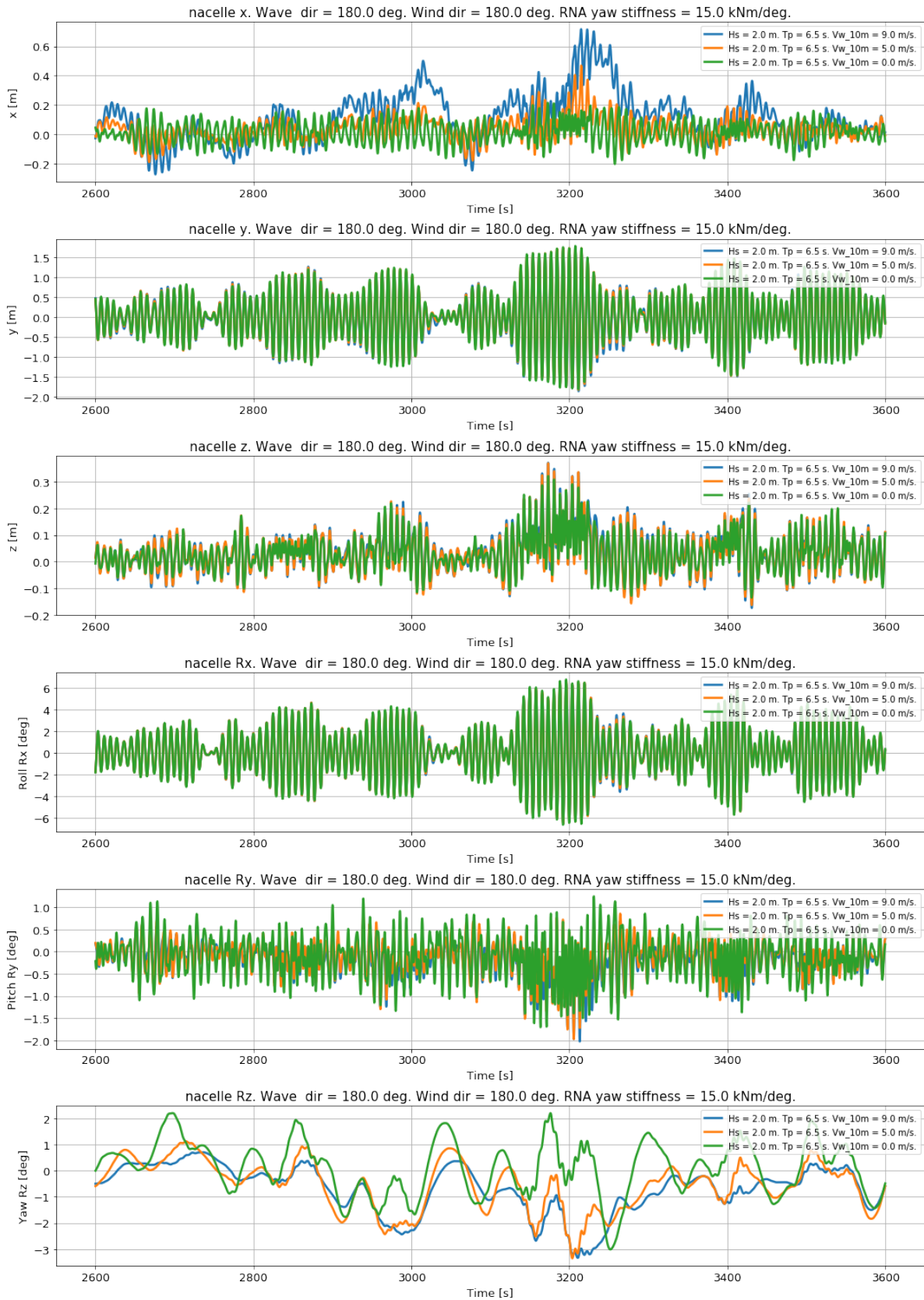
Figure E.1: Time series $H_s = 2.0$ m, $T_p = 6.5$ s, $V_w = 0, 5, 9$ m/s.
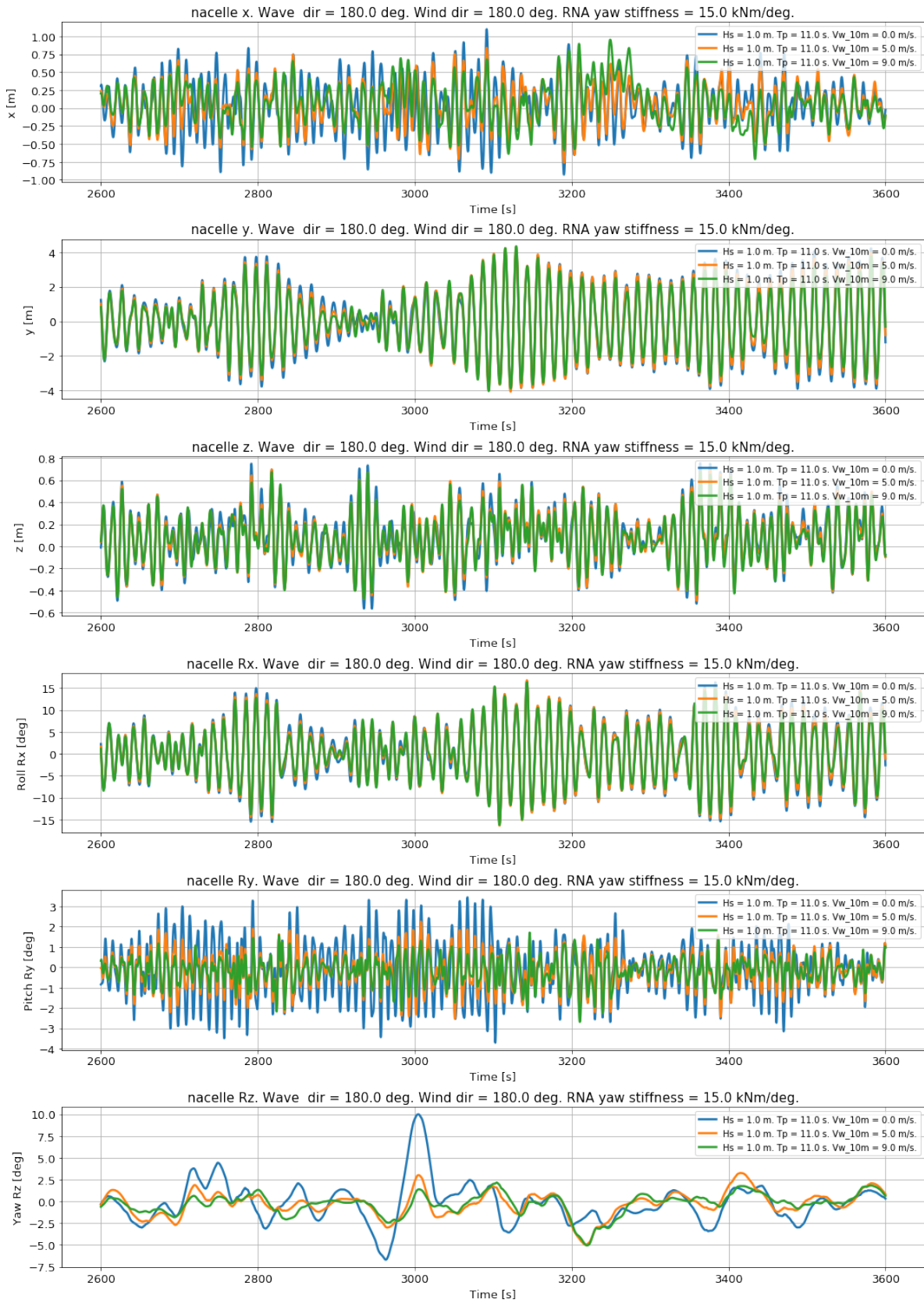
Figure E.2: Time series $H_s = 1.0$ m, $T_p = 11.0$ s, $V_w = 0, 5, 9$ m/s.